SCHLIEREN VISUALISATION OF FOCUSED ULTRASONIC IMAGES

THESIS

Submitted by

ANDREW JOHN HAYMAN

for the degree of

DOCTOR OF PHILOSOPHY

DEPARTMENT OF PHYSICS
THE CITY UNIVERSITY, LONDON

November 1977.

A B S T R A C T

Direct ultrasonic visualisation of defects (DUVD) is a method of producing an instantaneous optical image of acoustic discontinuities inside a material. The material is insonified with repetitive ultrasonic pulses, reflected pulses are focused by a sonic lens system into a transparent medium, and the acoustic image is visualised using a stroboscopic schlieren system. This thesis describes further development of the technique, with the main aims of improving the sensitivity and resolution beyond those apparent in previous crude demonstrations.

A theoretical analysis of schlieren visualisation of ultrasonic pulses leads to the identification of the most sensitive visualising media - liquids with up to ten times more sensitivity, theoretically, than water. The sensitivity of selected liquids is measured.

The choice of materials for the sonic focusing system is discussed, measurements of the acoustic properties of some plastics being given. The designs of certain systems of plastic lenses in liquid media are optimised for the best resolution by a ray-tracing method.

An experimental sonic system of polystyrene lenses in water is described; it is easy to make and convenient to use. Visualisation is by a compact mirror schlieren system of 60 mm aperture. Resolution of 1 mm over a 25 x 25 mm field is demonstrated, and the performance is a considerable improvement over the previous practical systems.

Schlieren observations of the behaviour of short pulses, which confirm recent theoretical predictions, are presented. Observations in the experimental sonic lens system show that pulses are focused in the expected fashion.

It is concluded that the DUVD technique is capable of good resolution, but its principal limitation is the poor sensitivity of schlieren visualisation. General applications in medicine and to metal inspection are not feasible; possible uses lie in the rapid examination of materials where great sensitivity is not required.

CONTENTS

LIST OF TABLES

ACKNOWLEDGEMENTS

I am indebted to Dr.P.D.Hanstead for his valuable advice, constant encouragement and patience throughout the project.

My thanks are due to Prof.A.F.Brown for his help and support.

Mr.J.P.[redacted] made the observations of the pulsed field using a small probe and constructed the circular transducer. I would also like to thank him for his practical advice, particularly on transducers, and many rewarding discussions.

I am grateful to Dr.R.C.Wyatt for the benefit of his unpublished work and for allowing reproduction of the photoelastic image shown in Fig.25.

The sonic lenses were manufactured by the Central Workshop of The City University, and the schlieren mirror mounts by the Physics Department Workshop. I express my thanks to those concerned, and to other members of the technical staff of the University and of the C.E.G.B. who helped.

Financial support was provided by the Science Research Council and the Central Electricity Generating Board under a C.A.S.E. (Collaborative Awards in Science and Engineering) award. Part of the work was performed at the Scientific Services Department, C.E.G.B., Portishead.

DECLARATION

Powers of discretion are granted to the University Librarian to allow the thesis to be copied in whole or in part without further reference to the author.

[redacted]

A.J.HAYMAN

CHAPTER 1 - INTRODUCTION

Ultrasonic techniques are in widespread use for the examination of materials that are optically opaque but acoustically semi-transparent, especially in the fields of engineering and medicine. In the testing of engineering components and structures, faults such as cracks and voids are very good acoustic reflectors, and in medical diagnosis ultrasound is particularly attractive because there is no radiation danger.

Most common inspection techniques employ the pulse-echo principle (Krautkramer 1969), whose simplest application is the A-scan: a transducer (transmitter/receiver) transmits a short pulse of ultrasound in a particular direction and the received echoes are displayed along the time axis of an oscilloscope. The longitudinal resolution is determined by the wavelength, which is typically of the order of a millimetre, corresponding to frequencies of a few megahertz. From the A-scan there have been developed two-dimensional pictorial displays which are built up by mechanical scanning and electronic processing of the echoes. The B-scan is a cross-section in the plane of the ultrasonic beam (or longitudinal section) and the C-scan is a section perpendicular to the beam (transverse section).

The time involved in scanning can be a problem, particularly in medical applications, and automatic mechanical scanners capable of producing almost instantaneous pictures have been produced (McDicken et. al. 1974). Most current developments in instantaneous (or real-time) imaging, though, are concerned with electronically-switched arrays of many small-element transducers. These simulate the action of a conventional transducer, either by switching between blocks of elements along a long array so as to generate a linear scan (Whittingham 1976), or by introducing time delays between the elements so as to swing the ultrasonic beam through a range of angles (Kisslo et. al. 1975).

Other pictorial displays can be obtained using the acoustic analogies of optical devices. The principles of an ultrasonic-to-electronic image converter, which can be used in an ultrasonic camera, have been known for many years (Sokolov 1937), but its development and applications

have been limited (Brown et. al. 1975).

The acoustic equivalent of the optical hologram (Greguss 1976) offers the apparent potential for producing a three-dimensional image. The acoustical hologram can be produced, for example, as a liquid surface ripple pattern which is reconstructed simultaneously using coherent laser illumination, or it can be detected by scanning, converted to an optical hologram and reconstructed later. However, such reconstructed images are essentially two-dimensional because of the longitudinal distortion resulting from the 1000:1 ratio of ultrasonic to optical wavelengths. A detected hologram can alternatively be reconstructed by computer but the diffraction-limited longitudinal resolution is still considerably worse than the lateral resolution (viz.Born and Wolf 1970, p.440).

Thus pseudo-continuous-wave holography in imitation of light-wave holography has poor longitudinal resolution; on the other hand the pulse-echo technique (impossible optically at small ranges) has good longitudinal resolution but suffers from diffraction broadening of the narrow beam. Their combination is a system where the echoes of a short pulse are recorded as a function of time at many points over a large aperture and an image is subsequently reconstructed by computer. This technique, termed variously pulsed holography or synthetic focus imaging, has been demonstrated in crude two-dimensional form, for example by Duck et al (1977). In principle, it is a form of the ideal imaging system since maximum use is made of the time and space information in the echoes over an aperture in order to reconstruct the sources of the echoes.

Hanstead (1972a, 1973) described a new method of imaging acoustic discontinuities which he termed Direct Ultrasonic Visualisation of Defects (DUVD). An optical image of a longitudinal ultrasonic section is produced instantaneously without the need for scanning, computer reconstruction, or laser light.

The principles of DUVD are illustrated by Fig.1. The object is 'illuminated' by a pulse of ultrasound and reflections pass through an acoustic focusing system into a transparent medium where the ultrasound is made visible by a standard optical technique. By using repetitive ultrasonic pulses and suitably delayed stroboscopic light flashes in the viewing system the moving pulses are 'frozen' at the instant of best focus and a stationary image is seen.

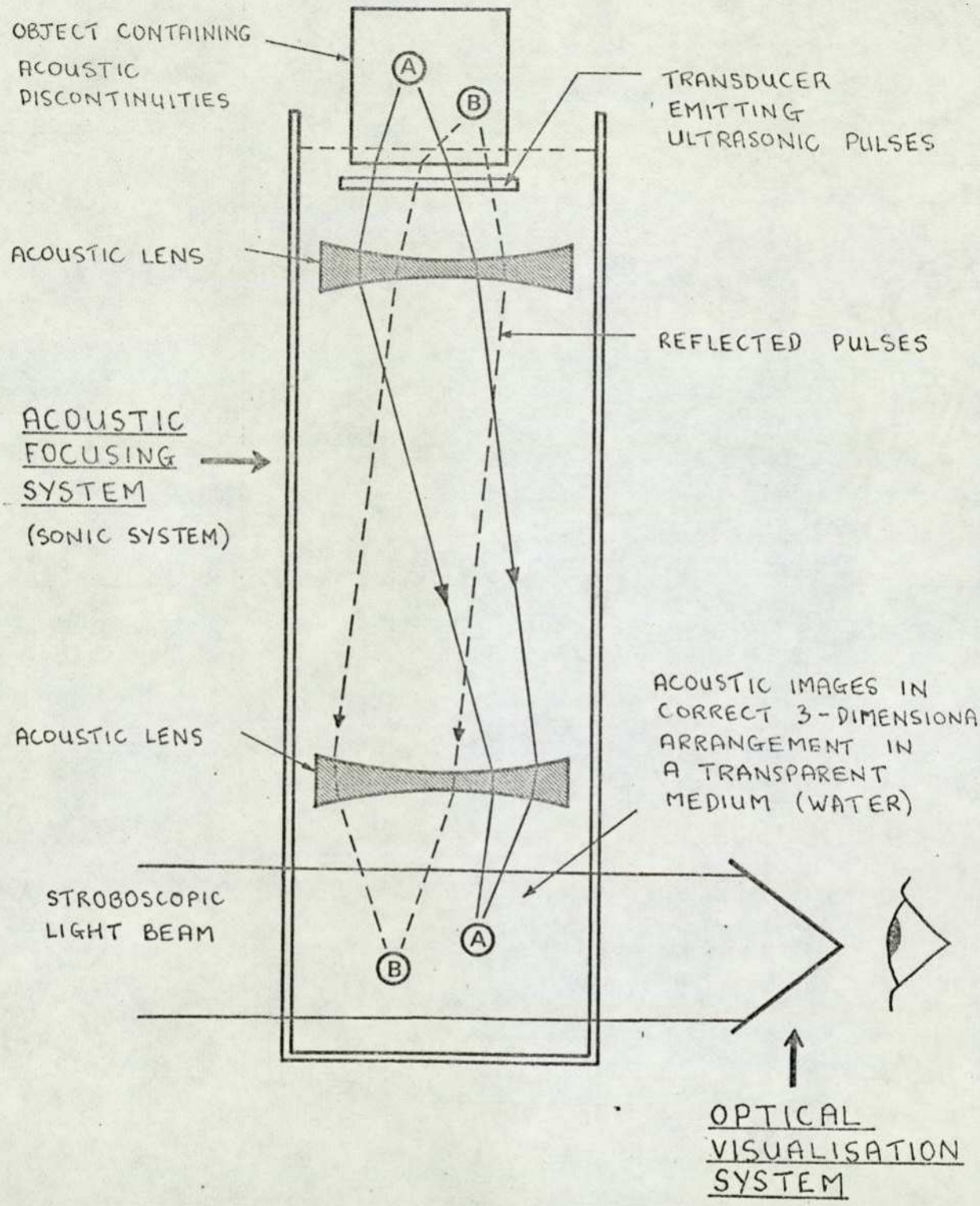

Fig.1 SCHEMATIC DIAGRAM OF A FORM OF DUVD SONIC SYSTEM EMPLOYING PLASTIC LENSES IN WATER.

The focusing system has two properties: firstly the image has the same general shape as the object and linear relationships are preserved, this being termed linearity; and secondly reflections from all parts of the object field come to their foci simultaneously. The latter, termed isochronicity, ensures that a single light flash delay time shows the whole image in correct focus.

Hanstead (1973, 1974a) showed by paraxial analysis that a coaxial assembly of two converging lenses can exhibit these desirable properties. One lens is adjacent to the object medium, the other to the image medium. Thus each lens has two focal lengths; one (the nearer) in the coupling medium and the other (the further) in the object or image medium. The two focal lengths are not necessarily equal.

Two conditions must be met : firstly, in order to achieve linearity, the nearer focal points must be coincident; secondly, for isochronicity, the further focal length in the imaging medium must be a factor of $\sqrt{2}$ longer than that in the object medium.

As a consequence of the second condition, the longitudinal magnification is a factor of $\sqrt{2}$ times the lateral magnification, the actual values being determined by the acoustic velocities in the object and image media. This elongation of the image is not a serious disadvantage and it can be rectified if viewing is by TV camera. Although a simple two--lens system has been described above, each lens could consist of only one interface or a combination of several interfaces - it is only the equivalent focal length that matters.

The ultrasound can be made visible by two standard techniques - the schlieren and the photoelastic - which exploit the small changes in optical refractive index induced in the transparent imaging medium by the ultrasonic stress wave. Both techniques can produce a bright image of a pulse against a dark background. DUVD is thus a form of ideal imaging device, which reconstructs sources of ultrasonic echoes by direct practical means, unlike the computer-calculated synthetic focus technique.

Hanstead has given practical demonstrations of DUVD with artificial defects using various focusing interfaces and lenses and both visualisation methods (Hanstead 1973, 1974b). The most successful arrangement employed an acoustic focusing system similar to that shown schematically

in Fig.1, consisting of two plastic lenses in water, and schlieren visualisation. It was apparent that various shortcomings would have to be overcome before the potential of DUVD as a practical technique could be properly assessed. The most notable improvements required were to increase the sensitivity, optimise the acoustic focusing, improve the ultrasonic pulse and increase the field of view. These practical details will be discussed in Chap.2.

The aim of the present work was further development of DUVD, principally by increasing the sensitivity. Development would be biased towards medical applications because of the interest of the author in this field and because real-time viewing is especially valuable in medicine. However, improvements achieved would also be relevant to the non-destructive testing application.

CHAPTER 2 - THE HANSTEAD DUVD SYSTEM & ITS PROSPECTIVE LINES OF DEVELOPMENT

In this chapter will be described the practical details of Hanstead's system, its performance and shortcomings, and possible improvements. It will first be necessary to explain the principles of the schlieren and photoelastic visualisation techniques.

2.1 Principles of schlieren visualisation

Fig.2 is a schematic diagram of a schlieren system. The light from the lamp is focused by a condenser system on to a small aperture which forms the effective source, is collimated by lens 1 so as to illuminate the ultrasound in a transparent medium, and is then brought to a focus on a stop by lens 2. In the absence of ultrasound the stop is arranged so as just to prevent light from reaching the eye (or a camera), but light which passes through regions of refractive index gradient such as are associated with ultrasonic stress waves can be deflected past the stop and the ultrasound appears luminous. By using stroboscopic light flashes, synchronised to repetitive ultrasonic pulses via a variable time delay, the moving pulses are 'frozen' in time and seen bright against a dark background. It is convenient in practice (See Chapter 4) to use a narrow slit source and either a parallel strip stop, or, as shown here a knife-edge stop.

2.2 Principles of photoelastic visualisation

The photoelastic method (Wyatt 1975) makes use of the anisotropic changes in refractive index induced by stress in a transparent solid. By placing the visualising medium between crossed polarising filters, regions occupied by ultrasonic stress waves appear bright on a dark background. Again, stroboscopic illumination is used to 'freeze' short pulses of ultrasound. Note that the photoelastic technique can be applied only to solids, whereas schlieren visualisation is possible in any transparent medium.

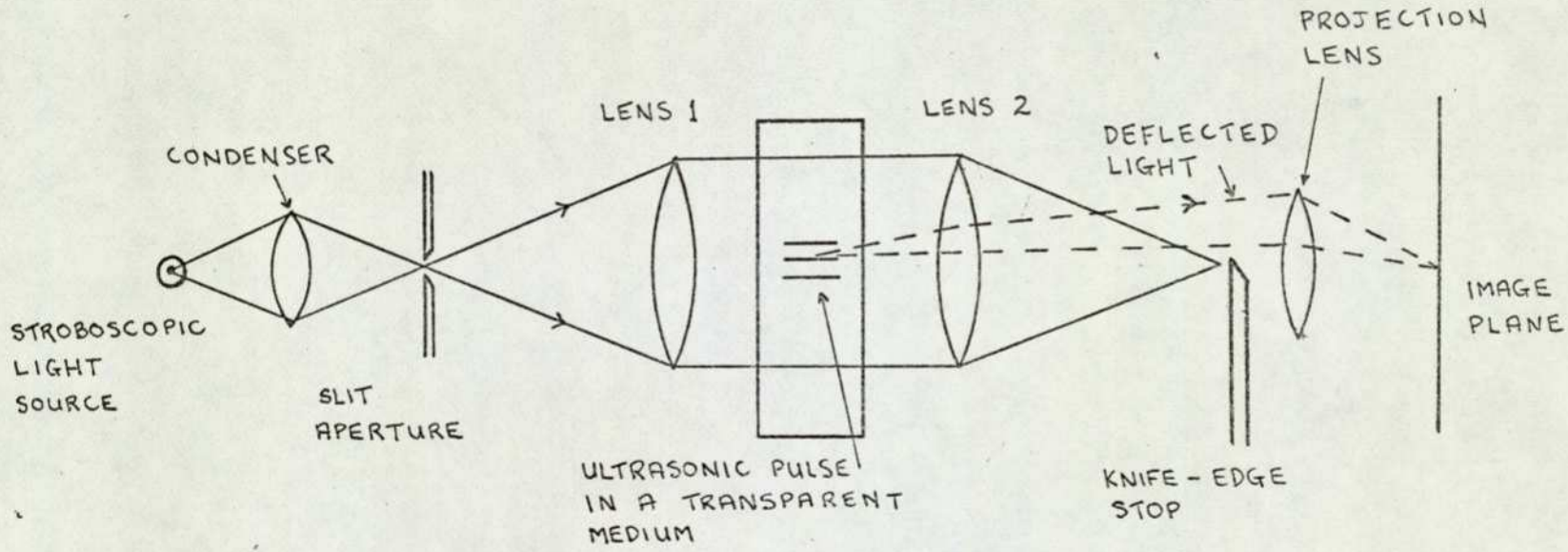

Fig.2 SCHEMATIC DIAGRAM OF A 2-LENS SCHLIEREN SYSTEM WITH STROBOSCOPIC ILLUMINATION

2.3 The Hanstead DUVD System

Hanstead gave demonstrations of DUVD using various focusing interfaces and lenses and using both visualisation methods (Hanstead 1973, 1974b). Schlieren visualisation in a liquid (water) was found to be considerably more sensitive than the photoelastic method was in any solid, and a compact schlieren apparatus was developed. The functions of lenses 1 & 2 were served by a single schlieren lens (135 mm focal length, 30 mm diameter) placed close to the water tank. A xenon-filled stroboscopic lamp (Strobotac 1538-A, General Radio Co.) gave flashes approximately 250 ns long at repetition rates upto several hundred per second, but the images were degraded by blurring since the ultrasonic pulses were of the same order of duration. A spark light source was developed which gave 40 ns flashes (Wyatt 1974) at the expense of smaller light output and limited electrode life. A TV camera was used for convenient viewing, and the whole apparatus was mounted on a metre length of optical bench.

An acoustic focusing arrangement of two perspex lenses (50 mm diameter, separation 140 mm) in water was the most successful. A study of possible combinations of solid and liquid refracting interfaces and lenses confirmed that an arrangement of plastic lenses in a liquid medium was the most promising since losses by absorbtion and reflection are minimised, plastic lenses are easily manufactured, and the more sensitive schlieren visualisation technique can be used.

The repetitive ultrasonic pulses were produced by a piezoelectric ceramic plate of resonant frequency 5 MHz, driven by voltage pulses of several hundred volts amplitude from a Kelvin-Hughes Mk.7 flaw detector. The pulses travelled directly into the object and reflections from discontinuities passed back through the transducer on their way to the sonic system. When imaging defects in steel, the plate was soldered directly to the metal surface in order to achieve good acoustic contact and to reduce multiple reflections.

Fig.3 shows some of the images of artificial holes and cracks in steel. It was apparent that greater sensitivity would be required for a practical inspection system, especially since soldering is not a reasonable way of coupling transducer to object and practical techniques introduce energy losses. The image of a pattern of steel pins in water was just visible. This could be regarded as a crude simulation of medical imaging and, since echoes from biological structures are much weaker than those from metal pins, the need for greater sensitivity is again indicated.

(a)

(d)

(b)

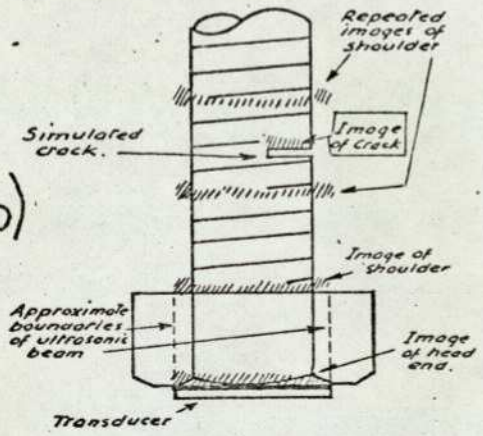

(e)

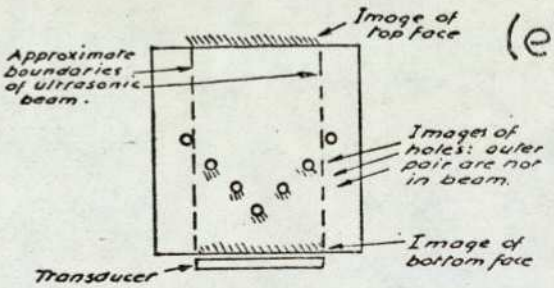

(c)

(f)

Fig.3 DUVD IMAGES OF ARTIFICIAL DEFECTS IN METALS OBTAINED BY HANSTEAD (1973).

(a)-(c) $\frac{1}{2}$ INCH BOLT WITH SIMULATED CRACK: (a) SPECIMEN (approx.actual size); (b) EXPLANATION OF IMAGE EXPECTED; (c) IMAGE OBTAINED.

(d)-(f) DRILLED 1.5 mm DIAMETER HOLES IN A STEEL BLOCK: (d) SPECIMEN (approx.actual size); (e) EXPLANATION OF IMAGE EXPECTED: (f) IMAGE OBTAINED.

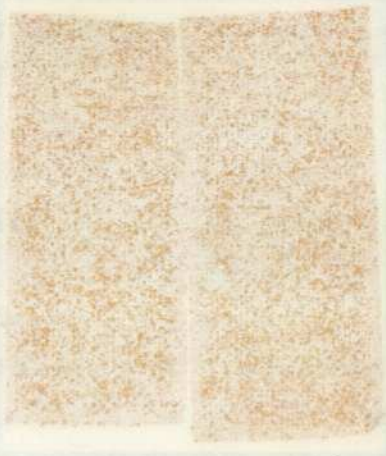

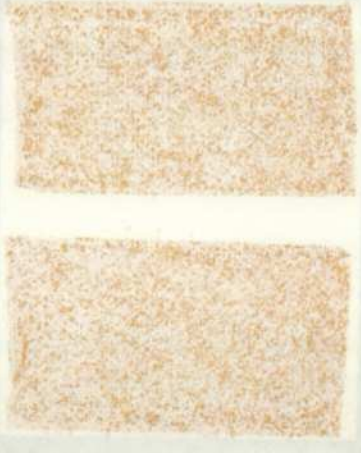

The most obvious unwanted features of the images were lateral spreading and longitudinal 'doubling'. The former was attributed to aberrations of the sonic system - not unexpected in a large aperture thick-lens system. The doubling was caused by multiple reflections in the transducer disc and possibly also in the lenses.

The remaining sections of this chapter are devoted to the possible lines of development of DUVD which were considered at the start of this project.

2.4 Methods of increasing sensitivity

(1) Use of a more sensitive visualising medium.
Water is the least sensitive liquid for schlieren visualisation. Measurements by Wyatt (1973) showed that, with certain other liquids, sensitivity might be increased by a factor of more than ten, on the basis of acoustic power needed to produce a visible image. No solid materials transparent at visible wavelengths are as sensitive as water.

(2) Improvement of the schlieren system.
The schlieren system was extremely simple and compact, but optical aberrations were apparent. There was scope for improving the optics while retaining the advantages of compactness. At this stage, there was no point in developing a sophisticated wide-aperture system which would be considerably larger and more expensive.

The above two ways of increasing sensitivity both involve consideration of the mechanism of image formation in a schlieren system.

(3) Reduction of optical scatter.
Scatter contributes to the background image intensity which limits the sensitivity of visualisation. The demonstrations of DUVD used ordinary tap water contained in a perspex tank, and the scatter could be reduced using clean water and high-grade glass. Investigations of the importance of scatter were required.

(4) Increased ultrasonic intensity.
The voltage applied to the transducer could be increased since it was not stressed to its mechanical limit. While the improvement in sensitivity can easily be calculated, practical increase in voltage would involve the construction of a special high-voltage pulse source, which has been treated as a low-priority matter.

(5) Optimum choice of materials.

The choice of visualising liquid, lens materials and coupling liquids in the focusing system is very important in order to minimise acoustic losses by attenuation and reflection. It was estimated that approximately a quarter of the acoustic energy was transmitted through Hanstead's system, the rest being lost. Plastic materials match best acoustically to liquids but data about their acoustic properties, particularly attenuation, is incomplete, so that measurements were called for. The physical and chemical compatability of lenses and liquids must also be considered.

(6) Astigmatic defocusing

Hanstead suggested that deliberate astigmatic defocusing of the sonic image in the direction of viewing would increase the light path through the regions of refractive index gradient, hence increase the deflections of the rays and perhaps treble the sensitivity. The problem is how to achieve defocusing over the whole field of view.

2.5 Optimisation of acoustic focusing

The presence of aberrations is inevitable in a system designed according to paraxial optics (or sonics) but which uses thick lenses of wide aperture. No attempt was made to control aberrations in the perspex-lens-in-water system, and lateral spreading of images was observed. Aberrations can be controlled by lens-bending, i.e. finding an optimum combination of lens curvatures, and by limiting the apertures. For the three-dimensional field of view of DUVD, these processes may be best performed by computer-aided ray-tracing.

2.6 Short-pulse transducer: design and position

In order to prevent the undesirable 'doubling' of images, the transducer disc must be prevented from 'ringing' by backing it with a suitable absorbing material and by carefully controlling the shape of the electrical excitation pulse.

If the transducer were placed between the object under examination and the lenses as in Hanstead's arrangement, then the reflections from the object would be obstructed and absorbed. One suggested solution was to place the transducer beyond the image space and employ the sonic system (in reverse) to form a real image of the transducer at the surface of the object. This double-path arrangement would double the acoustic

losses, and great care would be needed to prevent multiple reflections of the transmitted pulse from lens surfaces returning at the same time as the focused image.

An alternative suggestion was a split transducer at the surface of the object, allowing a return path for reflections. The main difficulties here are losses by obstruction of the reflections, and the highly directional nature of short pulses.

2.7 Increase of field of view

The field of view of Hanstead's system was too small for a viable examination apparatus. Its increase would require general scaling-up, resulting in greater acoustic losses by attenuation and requiring more powerful transducer drive circuitry and a larger schlieren system. Although a larger field was desirable, a practical-sized field was not necessary for the purposes of this work - development and assessment of possible performance.

CHAPTER 3. THEORY OF SCHLIEREN VISUALISATION OF ULTRASONIC PULSES

The theory of image formation in a schlieren system is first considered with the aims of understanding the fundamental limits to sensitivity and the constraints on practical parameters which must be imposed in order to achieve maximum sensitivity. Secondly the acousto-optic effect is considered and a figure-of-merit is derived for the visualisation sensitivity of a liquid in terms of known physical properties. More sensitive liquids than water are thus identified. A perfect diffraction-limited optical system and an infinitesimally short light flash are assumed.Practical shortcomings and the design of a practical system are considered in Chapter 4.

3.1 Schlieren image formation

In this section, schlieren imaging is formally described in terms of physical optics, with a view to obtaining practically useful conclusions in later sections.

A geometrical-optics description has been given in section 2.1. On this basis, if there exists a region of disturbed refractive index where the refractive index is constant in directions parallel to the optical axis but increases linearly in the vertical direction, then rays passing through the region are deflected by a uniform small angle and form a deflected image of the slit source in the plane of the stop. The brightness of the image of the region seen by the eye behind the stop (or in general formed in the image plane) is proportional to the angular deflection in air, which in turn is proportional to the vertical refractive index gradient.(For a fuller quantitative discussion see Weinberg 1963).

If the image of the slit is just cut off by the stop then the smallest deflection should be visible, and by reducing the width of the source slit infinite sensitivity against a dark background should be achieved. However, the approximations of geometric theory no longer apply under such conditions; the sensitivity is limited by diffraction. With the stop set for 'dark-field' conditions the effects of diffraction are to be seen as luminous borders around opaque objects and the circumference of the schlieren lens.

Under conditions of high sensitivity a physical optics description is required, as pioneered by Rayleigh (1920). The refractive index disturbance is not considered to deflect rays of light but to retard or advance parts of an initially plane wavefront. The retardations are assumed sufficiently small that they can be calculated along rays parallel to the axis. This has been shown a justifiable assumption for

ultrasound of moderate intensity at frequencies of a few megahertz (see later).

We shall consider an idealised system which has an infinitely thin slit source and a rectangular lens aperture of height 2A, and where all dimensions in the direction of the slit are large so that the problem reduces to two dimensions. As for the disturbance, attention will be confined to the idealised case shown in Fig.4: a pulse of ultrasound whose wavefronts are plane rectangles of length L travelling perpendicularly to the light beam. (Such conditions can be obtained approximately in the nearfield of an ultrasonic transducer). Then the disturbance is essentially one-dimensional and the phase retardation $\phi(x)$ is given by

$$\phi(x) = k.\Delta n.L \qquad (1)$$

where Δn is the refractive index modulation induced by the ultrasound, L is the interaction length, and the wave-number $k = 2\pi/\lambda$ as usual.

The problem is one of Fraunhofer diffraction, and is illustrated schematically in Fig.5. The disturbed wavefront is treated as a phase object where

$$f(x) = e^{i\phi(x)} \qquad (2)$$

and its diffraction pattern g(y) is formed in the focal plane of the schlieren lens (the stop plane). As in standard optical texts,

$$g(y) = \text{const.} \int_{-A}^{A} f(x)\, e^{ikxy/f}\, dx \qquad (3)$$

where $k = 2\pi/\lambda$, and f is the focal length of the schlieren lens.

The image formed in the image plane, optically conjugate to the phase object, is the Fraunhofer pattern of g(y), given by:

$$h(z) = \text{const.} \int_{\text{aperture}} g(y)\, e^{ikyz/f}\, dy \qquad (4)$$

This expression in fact refers to the particular case of unity magnification between object and image planes - nothing is lost by this simplification.

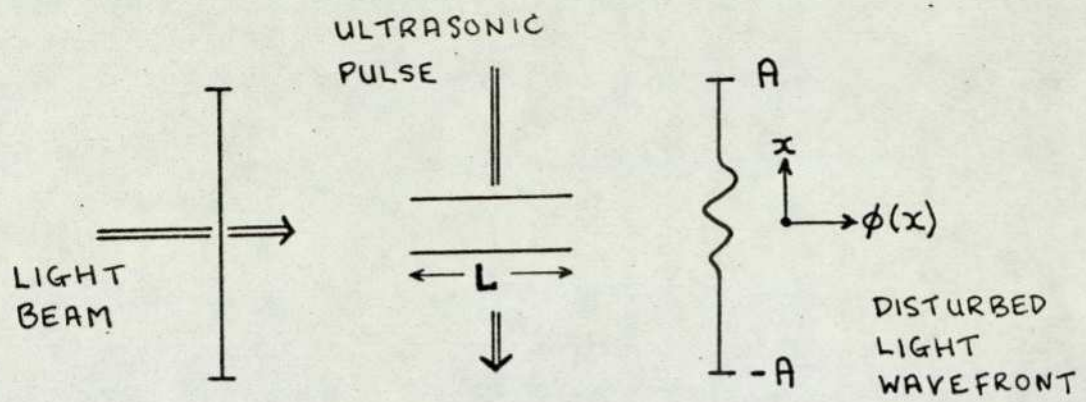

Fig.4 INTERACTION OF LIGHT WAVEFRONT WITH IDEALISED ULTRASONIC PULSE

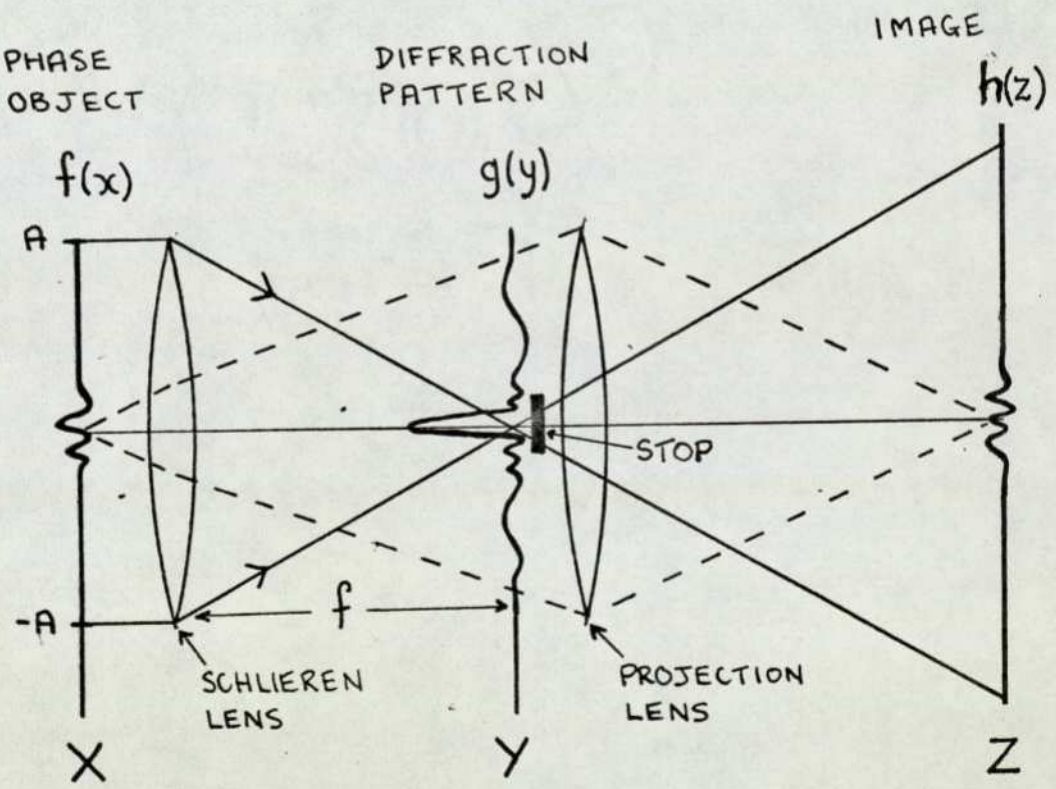

Fig.5 SCHEMATIC DIAGRAM OF SCHLIEREN IMAGE FORMATION

The entry pupil of the projection lens, which is just behind the stop, may be assumed infinitely large, to a good approximation. This is only equivalent to saying that the pupil is large enough to resolve the desired features of the phase object, which is always true in practice. Thus in the absence of a stop, perfect imaging occurs, i.e. $h(z) = f(-x)$, but since the image contains only phase variations nothing can be seen. The function of the schlieren stop is to cut off part of the diffraction pattern $g(y)$ so that $h(z)$ is modified and intensity variations appear in the image.

3.2 Disturbance of limited extent

Exact calculations along the lines indicated above, first performed by Rayleigh (1920) for the background illumination and the effect of linear gradients of retardation, were extended by Speak and Walters (1954) and Schafer (1949) to cases of linear gradients of limited extent, with wind tunnel applications in mind; Weinberg (1963) has given a useful review of all these results. Hanstead (1976), considering ultrasonic pulses idealised by linear gradients, calculated the influence of many practical system parameters by using selected simplifying assumptions.

The above calculations (apart from Hanstead's) apply to smaller degrees of diffraction pattern obstruction than occur in practical dark-field work, and the complicated nature of the solutions - even for the simplest retardations for which calculations are possible - makes them of limited practical utility, apart from the general conclusions. The discussion of schlieren imaging presented in this section lays stress on gaining insight into the fundamentals of the process, and will enable conclusions about practical parameters to be drawn and will lead to a definition of the comparative sensitivity of different liquids.

Consider a light wavefront disturbed, as by an ultrasonic pulse, over a small central region. The disturbed wavefront is equivalent to the sum of three components, as shown in Fig.6. These are:

i) The undisturbed plane wavefront (the free-field component)

ii) A plane wavefront of opposite phase, occupying the same region as the disturbance.

iii) The disturbed part of the wavefront.

(ii) and (iii) represent the effect of the disturbance and will be called the disturbance components.

The broad free-field wavefront (i) passes through a sharp diffraction-limited focus in the stop plane and spreads out again over the image plane. The limited disturbance wavefronts become relatively spread out

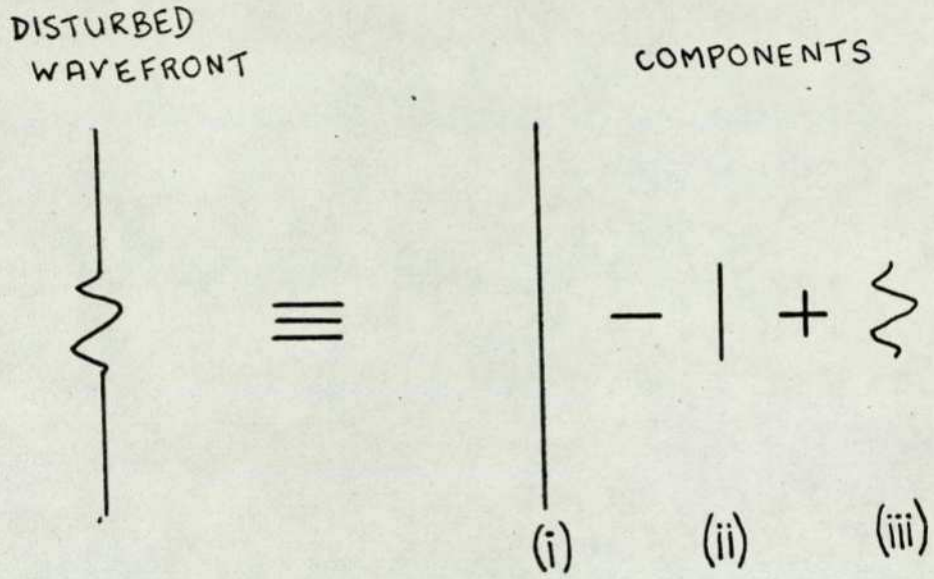

Fig.6 COMPONENTS OF A DISTURBED LIGHT WAVEFRONT

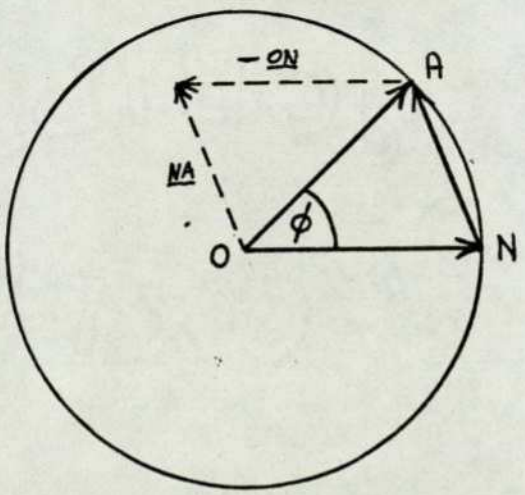

Fig.7 VECTOR REPRESENTATION OF THE DARK-FIELD IMAGE OF A PHASE OBJECT

by diffraction over the stop plane and are imaged in the image plane. In the absence of a stop, the image is a reproduction of the phase object, as already stated. Under dark-field conditions, using a strip stop, the focal spot of the free-field component is obstructed without significantly affecting the spread-out diffracted waves arising from the disturbance. Thus the free-field component in the image plane is removed and a representation of the phase object is seen bright against a dark background. The process is essentially the same as dark-ground miscroscopy (Longhurst 1967, pp 315-321).

The graphical vector representation of Fig.7 gives extra insight. A point on the phase object is represented by a vector OA whose angle ϕ with respect to the free field vector ON indicates its phase. The image is identical to the object in the absence of a stop. For simplicity, it can be assumed here that the stop completely removes the free-field component ON and hence the resultant image is represented by NA. Thus for different phase retardations ϕ in the object, not only the phase of the image but also its amplitude varies. The amplitude at first increases with ϕ, reaches a maximum value of twice the free-field amplitude at $\phi = \pi$ and then falls to zero at 2π. Note that the brightness of a point in the image depends only on the phase retardation at the corresponding object point.

We shall now discuss the above concepts in more quantitative fashion, taking the background illumination into account and bearing in mind the typical dimensions of practical systems.

The free-field diffraction pattern in the stop plane (i.e. the image of the line source) is the well-known Fraunhofer pattern for a slit of width 2A, given by the sinc function:

$$g(y) = A \frac{\sin(k A y/f)}{kAy/f} \qquad (5)$$

The width of the central bright band in which 90% of the energy is concentrated is $f\lambda/A$.

Rayleigh (1920) showed that as the diffraction pattern is cut off by a knife-edge stop the field does not darken uniformly. Most of the diffracted light goes into bright borders of the field, while away from the edge the illumination is reasonably uniform. It is shown in Appendix 1 that in order to obtain a central dark field (say less than a thousandth of the free-field illumination) it is necessary to cut off the central diffraction band plus the first few lateral bands, or the central plus first few lateral bands on either side in the case of a strip stop.

Now consider the effect of introducing a simple disturbance for which exact calculations are possible: a linear gradient of retardation extending from -a to +a, of maximum optical path retardation R at a, and maximum advance R at -a (see Fig.8), such that the phase retardation is given by

$$\phi = -kRx/a \text{ for } |x| < a \qquad (6)$$

This corresponds to a 'tilting' of the wavefront through an angle R/a or a geometrical angular deflection of light rays by R/a. The disturbance can be regarded as a crude simulation of the effect of an ultrasonic pulse consisting of a single cycle whose wavelength Λ is 2a. By splitting the wavefront into free-field and disturbance components, the diffraction pattern in the stop plane can be shown to be

$$g(y) = A.\frac{\sin(kAy/f)}{kAy/f} - a.\frac{\sin(kay/f)}{kay/f} + a.\frac{\sin ka(y/f + R/a)}{ka(y/f + R/a)} \qquad (7)$$

(i) (ii) (iii)

Where the numerals correspond to the component wavefronts. The terms are plotted in Fig.9 and consist of:

i) The sharp free-field sinc function

ii) A sinc function spread out by a factor A/a compared to (i) (and reduced in amplitude by a factor a/A)

iii) Another spread-out sinc function with its origin shifted to y=R/a.f corresponding to a geometrical angular deflection R/a.

For practical visualisation of ultrasound, typically the ultrasonic wavelength 2a is less than a millimetre while the field of view 2A is of the order of 100 mm, so $A/a \geq 100$. Thus the size of the stop needed to obstruct the free-field diffraction pattern (i.e. central and first few lateral bands) is small compared to the spread-out diffraction pattern. So, as stated earlier, the stop has little effect on the disturbance components.

To a good approximation, therefore, the free-field component is removed by a strip stop while the disturbance component is unaffected. As has been demonstrated by the graphical vector method, the image brightness then depends only on the phase retardation, so that the pulse length affects only the scale of the image. This important statement applies also in the case of a knife-edge stop, which obstructs the free-field component of the diffraction pattern plus the disturbance components below the optical axis. By a fundamental property of Fraunhofer diffraction,

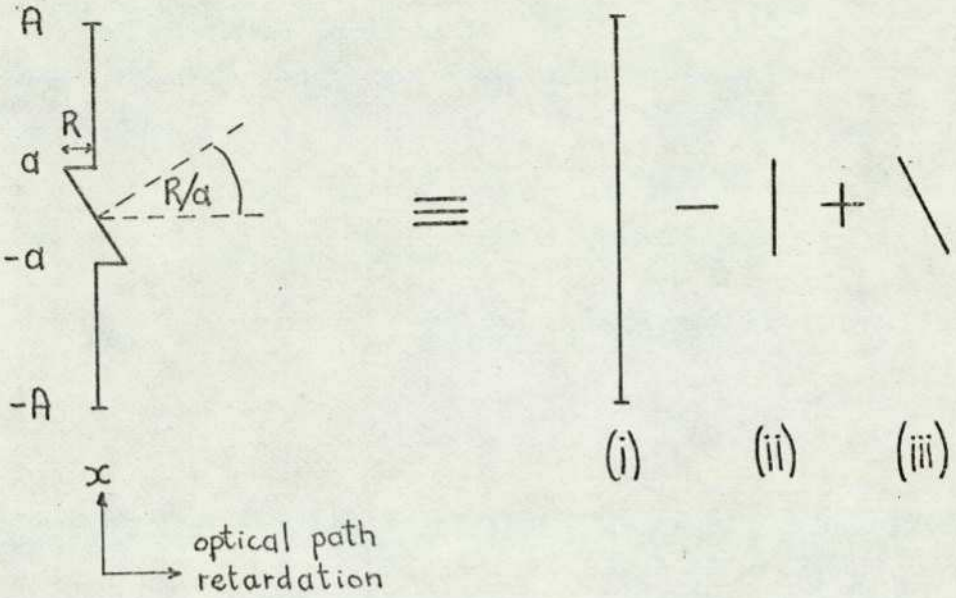

Fig.8 A LINEAR WAVEFRONT DISTURBANCE

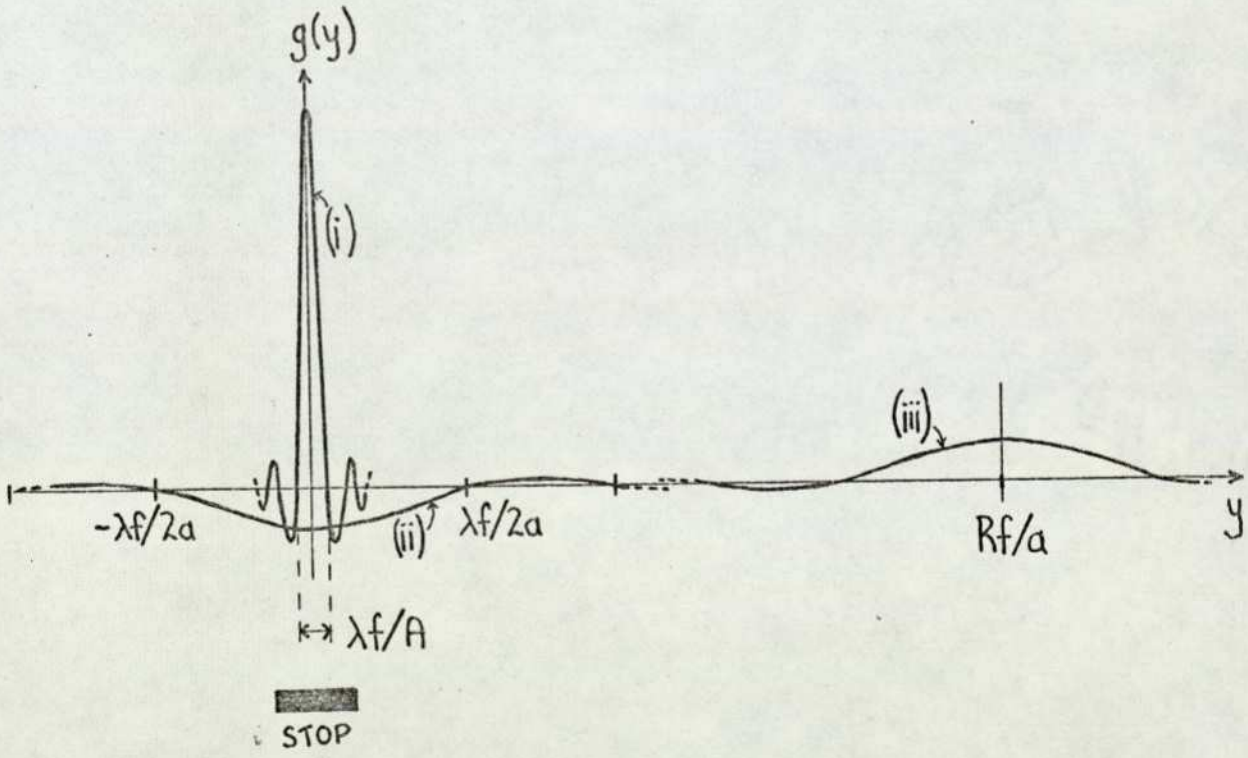

Fig.9 THE DIFFRACTION PATTERN (in the stop plane) DUE TO THE LINEAR PHASE OBJECT SHOWN IN Fig.8, FOR A/a = 10

the disturbance components of the diffraction pattern resulting from a phase object of constant amplitude but variable scale (representing different pulse-lengths) have constant form with scale inversely proportional to that of the object. This is obvious in the example discussed above, where scale is represented by length a. The effect of the knife-edge cut-off from $-\infty$ to 0 is to remove exactly the same part of the diffraction pattern irrespective of scale, and the final image has constant amplitude and form and the same scale as the object. A formal proof along these lines can be written out by using Equs. 3 & 4.

The amount of light power diffracted past the stop to form an image is the integral of the intensity diffraction pattern, which depends on the sum of disturbance patterns (ii) and (iii). For small retardations R, (ii) and (iii) almost cancel out, and as R increases the resultant intensity increases. Once the central maxima of (ii) and (iii) are separate ($Rf/a > \lambda f/a$), the diffracted light power flattens off to a maximum approximately equal to the sum of the powers in the two central maxima. It might reasonably be expected that the average image brightness would reach a maximum at the value $R = \lambda$. Since this value corresponds to an average phase retardation amplitude of π, this conclusion is in line with the earlier graphical vector description which predicted maximum image brightness at points corresponding to a phase-object retardation of π.

Let us now turn to the practical implications, firstly for the optimum size of the finite source which is used in practice. It has been shown that the image of an infinitely thin line source has a size of approximately $f\lambda/A$. This is a criterion for the minimum useful size of the geometrical image of the slit (from now on called simply the source size since in practice the focal lengths of the two schlieren lenses are usually equal, giving unity magnification between the source and its image). With the typical values of $f/A = 20$ and $\lambda = 0.5\ \mu m$, the minimum source size is 10 μm. This is impracticably small and would provide inadequate illumination. The effect of using a finite source must be considered.

The image of a finite source can be regarded as a distribution of incoherent diffraction patterns. As the source size is increased the free-field image size increases almost in geometrical fashion and can be cut off very sharply by a slightly larger stop in order to produce the dark background (see Appendix 1). On the other hand, the spread-out disturbance patterns do not begin to be seriously affected by the increased cut-off until the stop is of the same order of size as the spread. Regarding the disturbance as a crude representation of an

ultrasonic pulse consisting of a single sinusoidal cycle, an optimum source size S is suggested, of dimensions

$$S \sim \lambda f/2a$$

$$\text{or } S \sim \lambda f/\Lambda , \qquad (8)$$

where λ is the wavelength of light, Λ is the ultrasonic wavelength and f is the focal length of the schlieren lens. Substituting typical values of $\lambda = 0.5\ \mu m$, $\Lambda = 1$ mm, $f = 1000$ mm gives $S \sim 0.5$ mm which is a convenient size.

Optical aberrations, not considered yet, are taken account of by amending the above statement to: the total size of the geometrical image of the source including the effect of aberrations must not exceed $\lambda f/\Lambda$. Thus the maximum tolerable total of lateral aberrations is perhaps half this amount.

An order-of-magnitude estimate of the limit of sensitivity is possible. Under ideal conditions, the image brightness is maximum for a wavefront retardation of half a wavelength (phase retardation of π). If the dark-field background illumination is a very small fraction of the full illumination, it might therefore be expected that retardations of a small fraction of a wavelength would be visible.

The main conclusions of this section for dark-ground visualisation of ultrasonic pulses are two-fold. Firstly, under ideal conditions (diffraction-limited optics, infinitely thin slit source, field of view much larger than the ultrasonic wavelength) the brightness of the image depends only on the phase retardation induced by the ultrasound, and is expected to reach a maximum at a phase retardation amplitude of approximately π. Secondly, a criterion for the optimum size of a practical slit source and the tolerable optical aberrations is: the size of the geometrical image of the source, including aberrations, should not exceed $\lambda f/\Lambda$, where λ & Λ are the optical and acoustic wavelengths respectively and f is the focal length of the schlieren lens. The first conclusion will be used in the derivation of the visualisation sensitivity of a liquid (Section 3.4), and both will be refered to in connection with the experimental measurements of Chap.4.

3.3 Visualisation of continuous-wave ultrasound, considered as a phase-grating

It is instructive to consider also the case of stroboscopic visualisation of a long wave-train of ultrasound which occupies the entire field of view. The simplest calculation of the diffraction pattern is based on our earlier assumption that the periodic variations in refractive index retard or advance parts of the plane light wavefront, so that a corrugated wavefront emerges. Raman and Nath (1935) proved that such a grating

diffracts the light into several discrete orders whose angular separation is λ/Λ .

The conditions under which the phase-grating assumption holds good , the 'Raman-Nath conditions', as stated by Bucaro et.al.(1976) are:

a) $Q = 2\pi L\lambda/\Lambda^2 \ll 2$, (9)

where, repeating previous definitions for convenience, L is the width of the ultrasonic beam, λ is the light wavelength and Λ is the ultrasonic wavelength; and

b) $Q\, v \leq 2$, (10)

where $v = (2\pi/\lambda).\Delta n.L.$ (11)

In our notation, the phase modulation $v=\emptyset$; v is called the Raman-Nath parameter.

Essentially (a) and (b) are restrictions on the interaction length and sound intensity. For example, in water at 5 MHz ($\Lambda = 0.3$ mm) if $v = 2\pi$ then $L \leq 10$ mm.

Raman and Nath (1935) showed that,as the ultrasonic intensity is increased, progressively more light is diffracted into the higher orders until with v=2.4 radians there is none in the zero order. At higher intensities the solution becomes oscillatory. For schlieren visualisation a strip stop is set to obscure the zero order, or a knife edge obscures the zero and negative orders. Nomoto (1954) calculated the appearance of the image obtained when the zero order is removed by using a graphical vector method, similar to that outlined in section 3.2. For small retardations, the brightest parts of the image correspond to the peaks of the ultrasonic wave and the brightness increases with retardation. When the phase modulation is 2.4 radians the field appears uniformly bright, and at larger retardations extra bright peaks occur in the image. Bucaro et al (1976) verified these predictions experimentally; both they and Nomoto calculated the image obtained when various other orders and combinations of orders are obstructed, but they did not consider the knife-edge stop.

The implications for a practical system are similar to those stated in the previous section. Since the zero order must be removed without obstructing the higher orders, the size of the image of the source (including aberrations) must be less than the separation of the orders, $\lambda f/\Lambda$. A short pulse may be regarded as being made up of a spectrum of frequencies, and for maximum sensitivity the above condition must be satisfied for the largest wavelength Λ (i.e. the lowest frequency).

3.4 Visualisation sensitivity of a liquid

We want to predict which liquids are most sensitive in terms of acoustic power required to produce an image of given brightness. Consider a transducer which radiates an arbitrary pulsed pressure waveform (i.e. as a function of time) into different liquids. There are two factors which affect the brightness of the schlieren image.

a) The relationship between ultrasonic power and refractive index modulation - this acoustooptic relationship will be considered presently.

b) The ultrasonic wavelength, or pulse length in general, which is proportional to the velocity of sound in the liquid.

It was concluded in section 3.2 that under ideal conditions the brightness of the image depends only on the retardation, and the wavelength affects only the scale of the image. It is to be expected that this will be approximately true under practical conditions provided the recommendations of section 3.2. are met.

3.4.1 A theoretical visualisation figure-of-merit.

The variation in refractive index n induced by an ultrasonic wave can be expressed either in terms of the adiabatic variations in density ρ, or the adiabatic variations in pressure p :

Elasto-optic coefficient = $\rho\, \partial n/\partial \rho$; $\Delta n = (\rho \Delta n/\partial \rho)\, \Delta\rho/\Delta\rho$

Piezo-optic coefficient = $\partial n/\partial p$; $\Delta n = (\partial n/\Delta p)\, \Delta p$

The ratio of the coefficients is the adiabatic compressibility β,

$$\partial n/\partial p = \beta\, \rho\, \partial n/\partial \rho,$$

and $$\beta = 1/\rho c^2 \qquad (12)$$

where c is the acoustic velocity. Thus : $$\Delta n = \frac{\rho\, \partial n/\partial \rho}{\rho c^2}\, \Delta p \qquad (13)$$

It is convenient to use the elasto-optic coefficient here, since to a first approximation it is a function of only the optical properties of the liquid (see Raman and Venkataraman, 1939).

Now the peak intensity I in a ultrasonic pulse is given by $I = \Delta p^2 / 2\rho c$,

so : $$\Delta p^2 = 2\rho c I \qquad (14)$$

where Δp is the peak pressure modulation. Squaring (13) and substituting for Δp^2, the refractive index modulation can be expressed as :

$$\Delta n^2 = I.\ \frac{2(\rho\, \partial n/\partial \rho)^2}{\rho c^3} \qquad (15)$$

It has been shown that the image brightness is constant if the phase retardation, and therefore Δn, is constant. We can thus define a visualisation figure-of-merit M which is inversely proportional to the ultrasonic intensity required, in different liquids, to produce an image of given brightness:

$$M = 4 (\rho \partial n/\partial \rho)^2 / \rho \quad c^3 \qquad (16)$$

The factor of 4 is introduced so that M becomes identically equal to an equivalent figure (usually called M_2) which has been defined in terms of the photoelastic constant, $(\rho \partial n/\partial \rho). (2/n^3)$. M_2 is used to describe the 'efficiency of diffraction' by a long wave-train of ultrasound (see Uchida and Niizeki, 1973).

Hence, for good sensitivity, a liquid should have a high elasto-optic coefficient, and low sound velocity and density. The determination of the elasto-optic coefficient is the subject of the next two sub-sections.

3.4.2 Theoretical expressions for the elasto-optic coefficient.

In a gas, the increase in refractive index from the in-vacuo value of unity is proportional to the density (the Gladstone-Dale law) so that

$$\rho \partial n/\partial \rho = n - 1 \qquad (17)$$

For a liquid or solid it is necessary to take account of the interactions between molecules in order to calculate the dielectric constant ϵ from the molecular polarisability and obtain n from $\epsilon = n^2$. The simplest approach gives the well-known Lorentz - Lorenz equation, from which we have

$$\rho \partial n/\partial \rho = (n^2-1) (n^2+2) / 6n \qquad (18)$$

Values obtained from this equation are systematically higher by up to 10% than measured values. More complicated expressions have been proposed (some empirical) but none are in complete agreement with measured values (Uchida 1968).

3.4.3 Measurements of the elasto-optic coefficient

The earliest piezo-optic measurements were performed by the application of static pressure using an interferometric method. The results that Raman and Venkataraman (1939) obtained for six different liquids have been accepted by later workers as the most accurate. Latterly, relative values of the elasto-optic coefficient in different liquids have been found by measuring the light diffracted by an ultrasonic phase-grating into the first order. Their absolute values have been calculated using the Raman and Venkataraman value for water as a standard. Uchida (1968) has carried out the most comprehensive measurements, and they agree well with previous results. Fig.10 is a plot of the elasto-optic

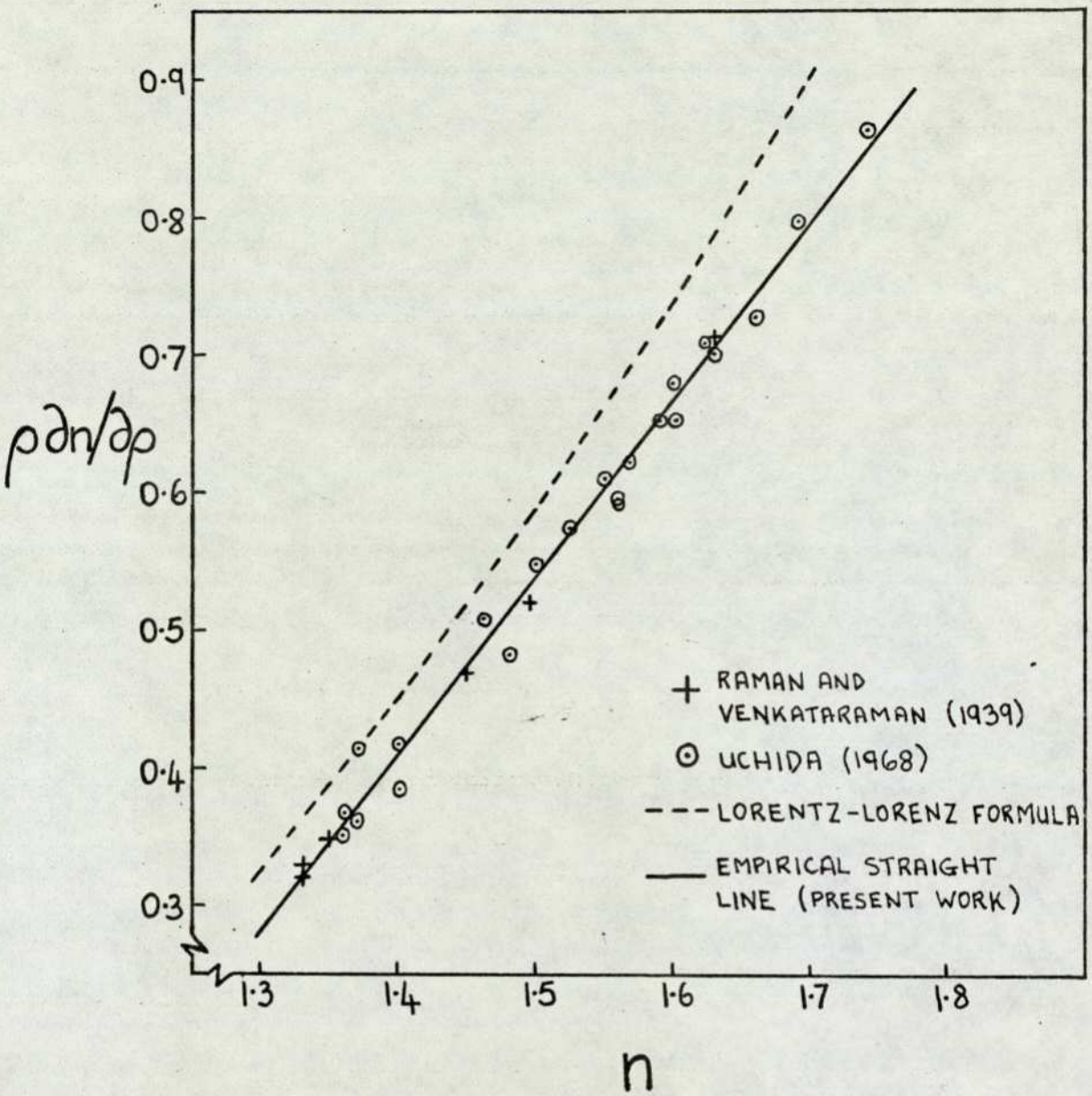

Fig.10 MEASURED ELASTO-OPTIC COEFFICIENT $\rho\partial n/\partial\rho$ OF VARIOUS LIQUIDS PLOTTED AGAINST OPTICAL REFRACTIVE INDEX n, AND COMPARED WITH THEORETICAL CURVES.

coefficients against refractive index, comparing experimental results with the Lorentz-Lorenz formula. The error in the simple theory is apparent.

Fukumoto and Watanabe (1970) measured some liquids not previously studied, but they used an inaccurate value of the elasto-optic coefficient of water. Their results, after correction using the accurate value, were plotted against refractive index and showed a wide scatter about the mean elasto-optic coefficient-refractive index trend. This calls the accuracy of the results into question, so that they have not been used here.

In order to predict the elasto-optic coefficient for liquids not yet studied experimentally, an empirical expression was derived by drawing a straight line by eye through the experimental results.

The expression is

$$\rho \, \partial n/\partial \rho = 1.29 \, n - 1.4 \qquad (19)$$

This agrees with the measured values as well as any other theoretical or empirical expression does.

3.4.4 Calculated figures-of-merit

Figures of merit were calculated for all the liquids whose elasto-optic coefficients were measured by Raman and Venkataraman and by Uchida.

For a high figure-of-merit, a liquid must have a high refractive index and high compressibility (low acoustic velocity). Additional liquids were selected on this basis and their figures-of-merit were calculated using the empirical relationship (Equ.19).

Although it is desirable that a visualisation medium has a high figure-of-merit, other factors can be just as important, such as the acoustic impedance (which determines how efficiently the acoustic energy is transferred between the medium and the other parts of the visualisation system), the acoustic attenuation, and velocity. It is convenient that all the data is available together.

Table 1 is a list of liquids and their important physical and acoustic properties, elasto-optic coefficients and figures-of-merit. Water has the lowest known figure-of-merit; the highest, held by di-iodomethane, carbon disulphide and phosphorous tribromide, are almost ten times as large as water's. The suitability of these and other liquids for use in a DUVD system will be discussed in later chapters.

TABLE 1 - ACOUSTO-OPTICAL DATA FOR LIQUIDS

		Refractive index n	Density ρ $10^3 kg.m^{-3}$	Sound velocity c $Km.s^{-1}$	Elasto-optic Coeff-icient $\rho \partial n/\partial \rho$	Figure-of-merit M $10^{-15} Kg^{-1} s^3$	Acoustic Imped-ance $Z = \rho c$ $10^6 Kg.m^{-2} s^{-1}$	Attenu-ation coeff-icient $\alpha_o = \alpha/f^2$ $dB.m^{-1} MHz^{-2}$	Boiling point ^oC
1. Water	H_2O	1.33	1.00	1.48	0.322 (a	128	1.48	0.22	100
2. Carbon tetrachloride	CCl_4	1.46	1.59	0.94	0.511 (b	790	1.49	4.7	77
3. Bromoform	$CHBr_3$	1.60	2.90	0.92(b	0.655 (b	760	2.67	2.0	151
4. Chloroform	$CHCl_3$	1.45	1.50	0.99	0.470 (a	610	1.49	3.5	61
5. Di-iodomethane	CH_2I_2	1.74	3.33	0.96(b	0.863 (b	1010	3.20	2.2 (b	182
6. Iodomethane	CH_3I	1.53	2.28	0.84	0.57 (e	980	1.92	2.9	42
7. Methanol	CH_4O	1.33	0.79	1.12	0.329 (a	390	0.89	0.37	65
8. Carbon disulphide	CS_2	1.63	1.26	1.14(b	0.713 (a	1090	1.44	50.0 (b	47
9. Trichlorethene	C_2HCl_3	1.48	1.46	1.03(b	0.486 (b	590	1.50	1.7 (b	87
10. Iodo-ethane	C_2H_5I	1.51	1.94	0.88	0.55 (e	960	1.71	0.35	72
11. Ethanol	C_2H_6O	1.36	0.79	1.16	0.351 (b	400	0.92	0.45	78
12. 1,3-dibromopropane	$C_3H_6Br_2$	1.52	1.98	1.09(d	0.56 (e	490	2.16	0.70(d	167
13. Acetone	C_3H_6O	1.36	0.79	1.19	0.371 (b	410	0.94	0.47	56
14. 1-iodopropane	C_3H_7I	1.51	1.75	0.93(d	0.55 (e	860	1.63	0.47(d	102
15. 1-propanol	C_3H_8O	1.39	0.80	1.22	0.402 (c	440	0.98	0.55	97
16. Glycerol	$C_3H_8O_3$	1.47	1.26	1.86	0.50 (e	125	2.34		290
17. Ethyl acetate	$C_4H_8O_2$	1.37	0.93	1.17	0.361 (b	350	1.09	0.45	77
18. 1-iodo butane	C_4H_9I	1.50	1.62	0.97(d	0.54 (e	790	1.57	0.50(d	130
19. 1-butanol	$C_4H_{10}O$	1.40	0.81	1.26	0.419 (b	430	1.02	0.67	118
20. 2-butanol	$C_4H_{10}O$	1.40	0.81	1.19(b	0.385 (b	430	0.96	1.2 (b	100
21. Diethyl ether	$C_4H_{10}O$	1.35	0.71	0.96	0.349 (a	610	0.69	1.2	34
22. 1,2-dibromobenzene	C_6H_4Br	1.62	1.98	1.12(d	0.69 (e	680	2.22	1.3 (d	225
23. Bromobenzene	C_6H_5Br	1.56	1.50	1.15(b	0.598 (b	630	1.73	1.3 (b	156
24. Chlorobenzene	C_6H_5Cl	1.53	1.11	1.29	0.578 (b	560	1.43	1.1	132
25. Iodo-benzene	C_6H_5I	1.62	1.83	1.13(d	0.69 (e	720	2.07	1.6 (d	188
26. Nitrobenzene	$C_6H_5NO_2$	1.56	1.20	1.48	0.612 (b	380	1.78	0.69	211
27. Benzene	C_6H_6	1.50	0.88	1.32	0.522 (a	540	1.16	7.3	80
28. Anilene	C_6H_7N	1.59	1.02	1.66	0.654 (b	360	1.69	0.43(b	184
29. Phenyl hydrazine	$C_6H_8N_2$	1.60	1.10	1.74	0.682 (b	320	1.91	1.50(b	243
30. Paraldehyde	$C_6H_{12}O_3$	1.40	0.99	1.20(f	0.41 (e	390	1.19		128
31. Hexane	C_6H_{14}	1.37	0.66	1.09(b	0.416	810	0.72	0.52(b	69
32. Toluene	C_7H_8	1.50	0.87	1.32	0.54 (e	550	1.48	0.69	111
33. 2-amino toluene	C_7H_9N	1.57	1.00	1.60(b	0.625 (b	380	1.60	0.74	200
34. 1-iodo heptane	$C_7H_{15}I$	1.49	1.38	1.07(d	0.52 (e	640	1.48	0.70(d	204
35. O-xylene	C_8H_{10}	1.51	0.88	1.35	0.582 (c	620	1.17	0.45	144
36. Quinoline	C_9H_7N	1.63	1.10	1.58(b	0.698 (b	450	1.74	1.2 (b	238
37. Cinnamaldehyde	C_9H_8O	1.62	1.05	1.56(b	0.712 (b	510	1.64	6.0 (b	253
38. 1-bromonaphthalene	$C_{10}H_7Br$	1.66	1.48	1.36(b	0.730 (b	570	2.01	1.5 (b	281
39. 1-chloronaphthalene	$C_{10}H_7Cl$	1.63	1.19	1.46(b	0.703 (b	530	1.74	1.1 (b	258
40. Tricresyl phosphate	$C_{21}H_{21}PO_4$	1.56	1.20	1.50(b	0.596 (b	350	1.80	12.0 (b	410
41. Phosphorous tribromide	PBr_3	1.69	2.85	0.93(b	0.798 (b	1110	2.65	4.3 (b	173
42. Olive oil		1.46	0.91	1.44	0.48 (e	350		12.0	
43. Turpentine		1.47	0.87	1.24	0.50 (e	600	1.07		

NOTES:

(i) Sources of data: values at 20°C compiled or calculated from standard sources (Kaye & Laby, 1972; CRC Handbook, 1974) and as indicated:
- (a) Raman & Venkataraman (1939), at 22-24°C.
- (b) Uchida (1969), at 25°C.
- (c) Riley & Klein (1967).
- (d) Fukumoto and Watanabe (1970), at 23°C.
- (e) Calculated from the empirical expression given in Equ. 19.
- (f) Measured at 28°C.

(ii) Accuracy: The probable error in c is about 1% and in $\rho \partial n/\partial \rho$ is about 2%. Thus the error in M is approximately 5% Temperature variations for data not measured at 20°C are negligible for n, ρ and $\rho \partial n/\partial \rho$, but affect c by, typically, 0.25% per °C. The values of α_o quoted have been calculated from a measurement at one different arbitrary frequency for each liquid by assuming the classical relationship, i.e. attenuation α is proportional to the square of the frequency f. This does not hold perfectly and the probable accuracy for prediction of attenuation is low.

3.5 Figures-of-merit of solid materials

There are some attractions in using a solid rather than a liquid as the medium for schlieren visualisation, such as the absence of disturbing convection currents and the possibility of achieving a more convenient acoustic focusing arrangement. The same properties are required of both solids and liquids for good sensitivity; namely, high refractive index and low sound velocity. Since solids generally have higher refractive indices and higher sound velocities than liquids, the path to a high figure-of-merit is either through a very high refractive index, which tends to shift the transmission band towards the infra-red, or through a low velocity, i.e. using soft materials such as plastics, in which the attenuation is high.

Uchida and Niizeki (1973) reviewed the acousto-optical properties of materials in connection with their possible use in light-deflection devices. The highest figures-of-merit have been found in solids whose transmission band falls in the infra-red region, and these will not be considered here. Single crystals are ruled out for the present application since the size needed is impracticably large and expensive. Table 2 gives data on some glasses and plastics which are transparent at visible wavelengths.(Note that in solids it is necessary to specify the polarisations of both light and sound beams.) Glasses have very low attenuation, but the highest figure-of-merit, that of tellurite glass, is a quarter of that of water. On the other hand, Polystyrene has a sensitivity comparable with water but a high attenuation.

In conclusion, no solid material transparent in the visible is known to be as suitable as water for visualisation of ultrasound of a few megahertz frequency, and there are good reasons for supposing this to be a fundamental limitation.

TABLE 2 ACOUSTO-OPTICAL PROPERTIES OF SOME SOLIDS FOR LONGITUDINAL SOUND WAVES

	Density $10^3 Kg.m^{-3}$	Sound Velocity C $Km.s^{-1}$	Acoustic attenuation $\alpha_o = \alpha/f^2$ $dB.m^{-1} MHz^{-2}$	Light polar.(a	Refractive Index n	Figure of merit $10^{-15} \frac{M}{Kg\ s^3}^{-1}$
Water (b	1.00	1.49	0.24	arb.	1.33	126
Fused quartz (b	2.20	5.96	0.0012	$\perp$	1.46	1.6
Tellurite glass (b	5.87	3.40	0.017	$\parallel$	2.09	24
Dense flint glass (SF-59) (b	6.17	3.26	0.12 α $dB.m^{-1}$	$\parallel$	1.95	19
Perspex (Lucite) (c	1.19	2.70	500 (d	$\perp$	1.49	40 (e
Polystyrene (c	1.06	2.35	200 (d	$\perp$	1.59	100 (e

(a) $\parallel$ & $\perp$ mean that the light is polarised parallel and perpendicular to the direction of sound propagation, respectively.
(b) Uchida and Niizeki (1973)
(c) Kaye and Laby (1972)
(d) Measured at 2.5 MHz
(e) Smith and Korpel (1965)

CHAPTER 4 MEASUREMENTS OF THE SENSITIVITY OF VISUALISATION IN LIQUIDS

This chapter presents measurements of the brightness of an ultrasonic pulse in selected liquids when visualised by an improved compact schlieren system. Observations of the influence of slit width and scattered light on sensitivity are also described, and the absolute sensitivity of visualisation is estimated.

4.1 The schlieren system

The single lens system used by Hanstead (described in Section 2.3) had a small field of view and suffered from aberrations, noticeably chromatic aberrations. It was improved by using two spherical mirrors (60 mm diameter, f10) in a conventional folded'Z' arrangement which is illustrated schematically in Fig.11. The mirrors are optically equivalent to the two schlieren lenses in Fig.2. The first mirror collimates the light from the slit source in order to illuminate the ultrasound with a parallel beam, and the second mirror brings the light to a focus on the stop.With this new arrangement, the field of view was approximately doubled to 60 mm while the system remained compact, being mounted on a pair of metre-length optical benches arranged side-by-side as shown in Fig.12.

The use of large f-number spherical mirrors in a Z arrangement is a simple and inexpensive way of achieving high optical quality. The design of practical schlieren systems has been considered in detail by Holder and North (1963), Weinberg (1963), Speak and Walters (1954), and Marsh (1973), the last being concerned with a sophisticated system for viewing ultrasound. Nevertheless, a summary of the merits of a Z arrangement is appropriate here. Mirrors, unlike lenses, do not suffer from chromatic aberrations and, because they have only one surface each, the problems of surface finish and cleanliness and internal glass quality which can cause disturbing effects in a lens system are much reduced.

A spherical mirror used to focus parallel light suffers from spherical aberration, which can be made very small by using a large f-number, as will be seen. The off-axis aberrations which can occur are coma and astigmatism, but coma is cancelled out in the symmetrical Z arrangement. Astigmatism is the aberration which causes an oblique parallel bundle of light to come to a focus not at a point but as two mutally perpendicular line images in separate planes. If a slit source is employed, astigmatism does not matter since only one line focus is used - that parallel to the slit.

Expressions for aberrations have been given by some of the above authors, but not in the most convenient form. In Appendix 2 it is shown that

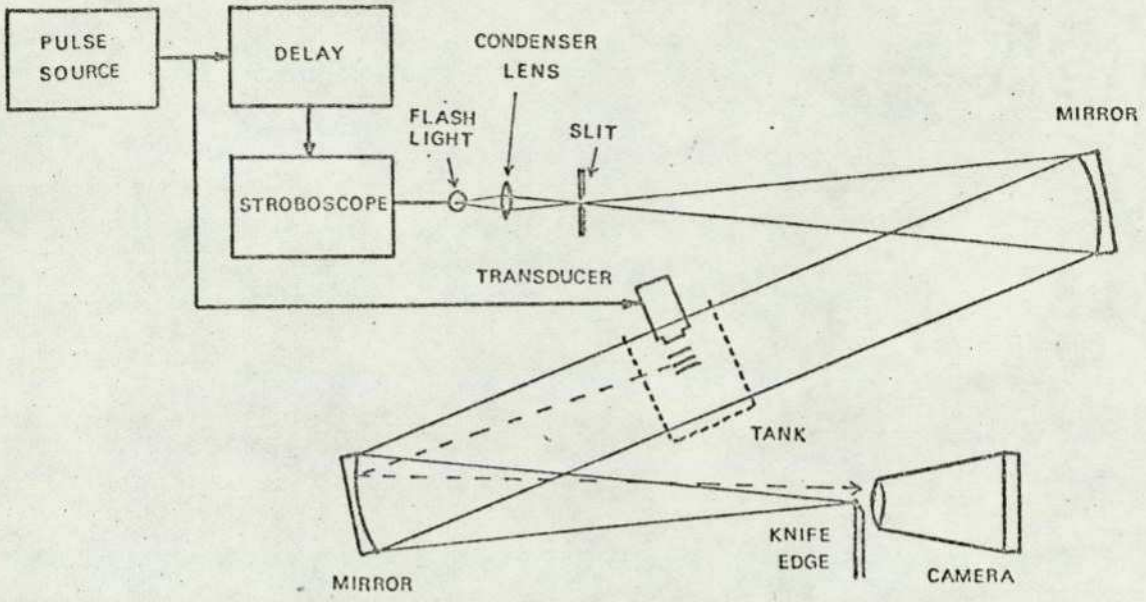

Fig.11 SCHEMATIC DIAGRAM OF THE 2-MIRROR 'Z' SCHLIEREN SYSTEM.

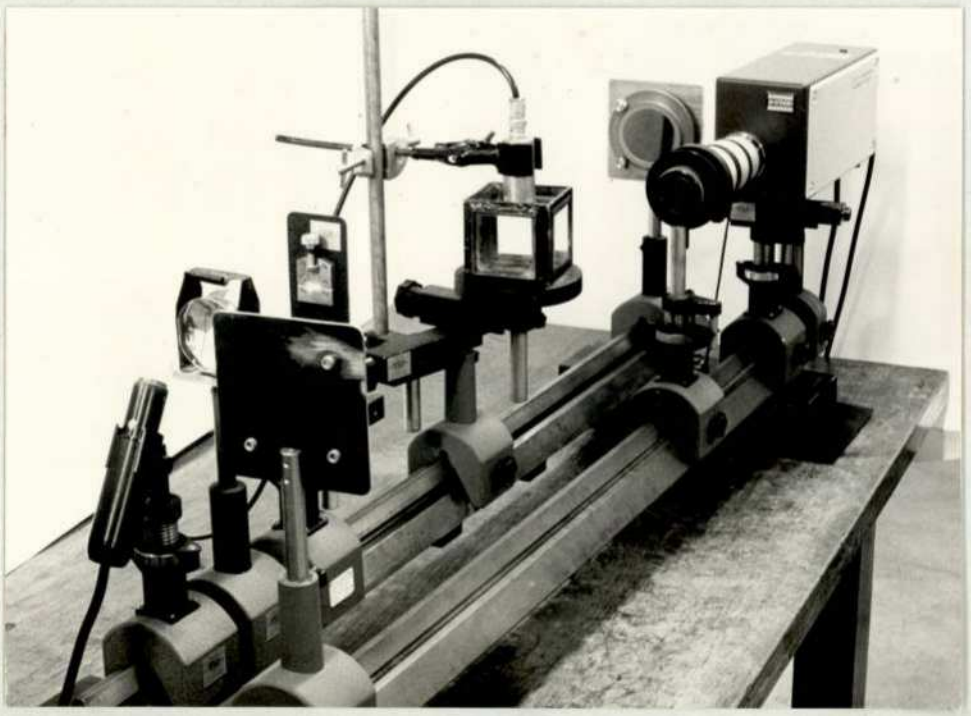

Fig.12 PHOTOGRAPH OF THE SCHLIEREN SYSTEM IN USE WITH A TV CAMERA.

the transverse aberrations (total spread of a point image in the focal plane) of the Z system are given by:

Transverse spherical aberration $= d/16N^2$ (19)

Transverse astigmatism $= 2\, d\emptyset^2$ (20)

where d is the mirror diameter, N is the f-number (f/d) and $\emptyset$ is the angle of obliquity of the parallel light beam.

For the practical system (d = 60 mm, N=10, $\emptyset$ = .075 rad.), spherical aberration = 0.04 mm.

It is to be expected that manufacturing errors of a few times the diffraction broadening $\lambda f/d$ will introduce an extra error of the order of 0.02 mm. These aberrations must be compared with the theoretical criterion for the maximum size of the image of the source, from Equ.8. For 2 MHz ultrasound in water (Λ= 0.75 mm) the criterion is

$$\lambda f/\Lambda = 0.4 \text{ mm}$$

Thus the optical quality is well within the limit and there is scope for visualisation at longer wavelengths.

The calculated astigmatic spread is 0.68 mm, which is immaterial using a slit source, but could be corrected by a cylindrical lens if it was desired to use, for example, a pinhole source and circular stop.

4.2 Experimental arrangements

The schlieren system was set up in a dark room, using the Strobotac 1538-A pulsed light source together with a slit aperture and a knife-edge stop. A short pulse of ultrasound was launched vertically downwards into a liquid contained in a small glass cell, and the edges of the cell, which appeared bright due to refraction and scatter, were screened off to facilitate observation of the dark background.

The ultrasonic transducer consisted of a 5 mm radius, 0.5 mm thick (4 MHz resonant frequency) disc of ceramic lead zirconate titanate (PZT) backed by a cylinder of Wood's metal, a low-melting-point alloy. Wood's metal backing was chosen both because it is a good acoustic match to PZT, necessary for the production of a short pulse, and because it would be resistant to chemical attack by the liquids to be tested. The production, propagation, and measurement of short pulses will be considered in Chap.5.

The transducer was driven by an electrical excitation pulse from the Kelvin-Hughes Mk.7 generator, and the measured acoustic pressure pulse is shown in Fig.13. The frequency spectrum of the pulse appears by inspection to be centred on about 2.5 MHz. The excitation voltage was controlled by an attenuator, calibrated against peak voltage with the transducer connected, and it was ensured that the excitation and acoustic waveshapes remained constant over the range of attenuations

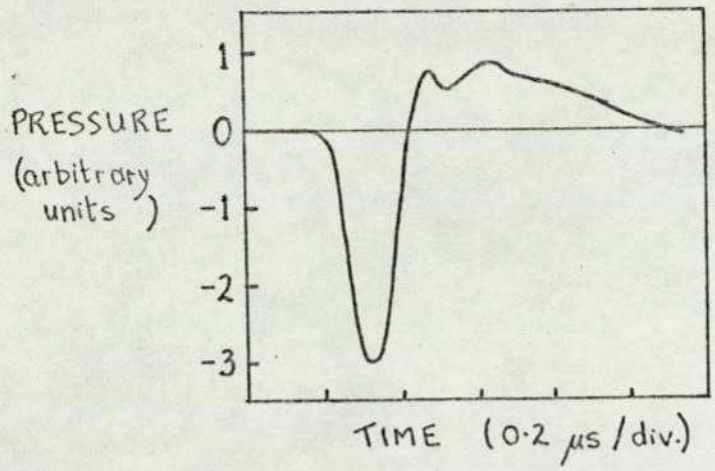

Fig.13 PRESSURE WAVEFORM OF THE ULTRASONIC PULSE USED TO OBTAIN THE RESULTS PRESENTED IN FIGS.14-16.

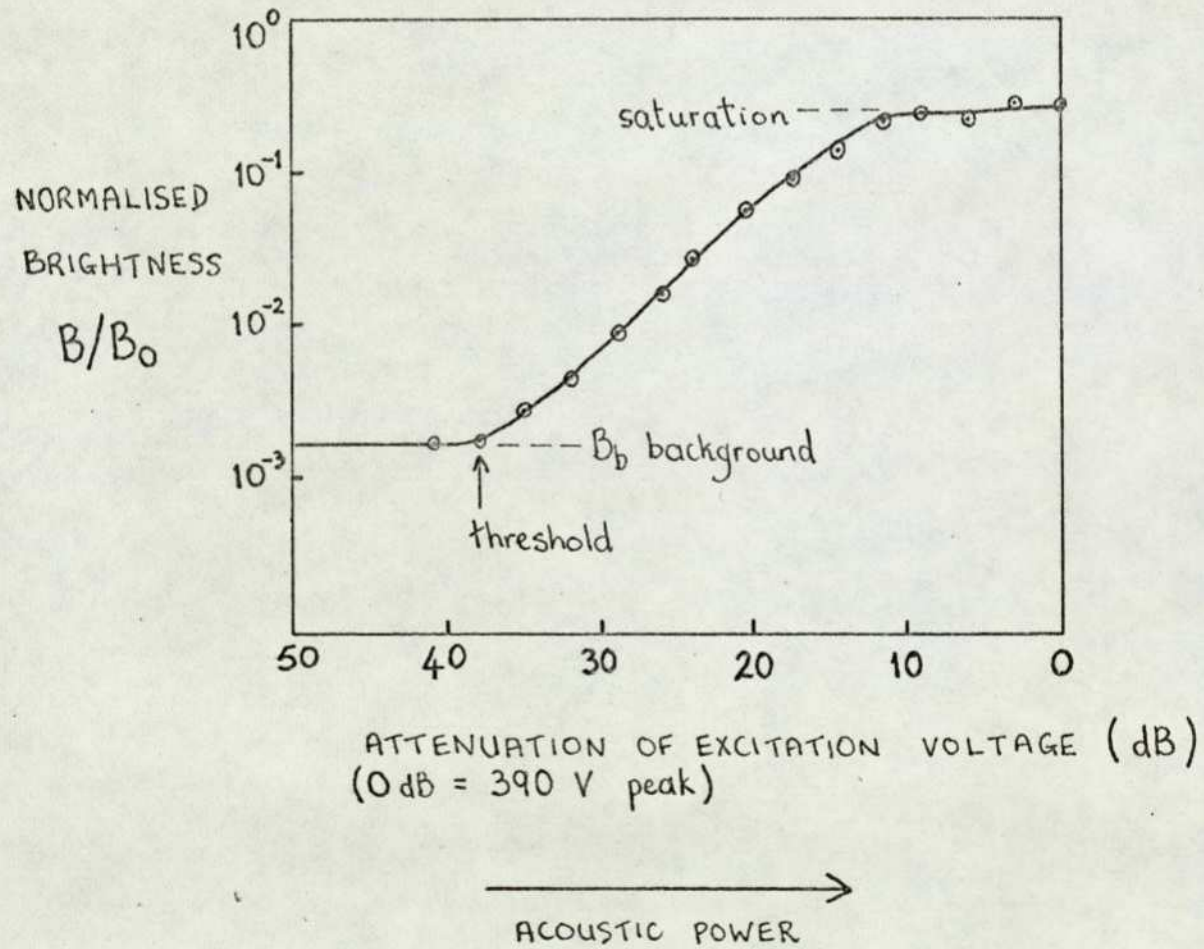

Fig.14 THE MEASURED BRIGHTNESS OF THE SCHLIEREN IMAGE OF AN ULTRASONIC PULSE IN WATER AS A FUNCTION OF THE ACOUSTIC POWER.

applied in the experiments.

Brightnesses were measured with an SE1 spot photometer, which involved adjusting the brightness of a small illuminated spot (extending over $\frac{1}{2}^{o}$) to match that of the region studied. For an accurate observation of the short ultrasonic pulse, it was necessary to magnify its image by means of a 3x telescope placed behind the knife-edge. Because the light flash had about the same duration as the ultrasonic pulse, detailed variations in image brightness were blurred out and the average brightness was effectively measured.

4.3 The ultrasonic power-image brightness response

Fig.14 shows the brightness B of the image of the ultrasonic pulse in water, measured as a function of attenuation of the electrical pulse (expressed in dB so that the scale also gives the relative acoustic powers). A thin (.05 mm) slit source was used.

At low acoustic power, the pulse is invisible against the constant background brightness B_b; once the threshold of visibility is reached there is an approximately linear relationship between brightness and power; then the curve flattens off to a saturation brightness. The brightnesses are plotted relative to the illumination brightness B_o, i.e. the brightness seen with the knife-edge adjusted so as not to obstruct the light. Such relative brightnesses will be called 'normalised brightnesses'. The dynamic range or ratio of saturation to threshold power is about 28 dB and the normalised background brightness about 10^{-3}. The values of absolute acoustic power and optical retardation will be calculated in a later section (4.7).

A response curve similar to Fig.14 was first observed by Hanstead (1972b, 1976) and predicted by his computer-aided simplified theory.

4.4 Background brightness

The threshold of sensitivity of visualisation is limited by the background brightness. This was investigated by measuring the background B_b under visualisation conditions and then removing the water-filled cell and measuring the background B_b' of the schlieren system alone. Measurements were taken over a range of different slit widths and the results, expressed as the logarithm of the normalised brightness, are given in Table 3.

TABLE 3 BACKGROUND BRIGHTNESSES

Slit width (mm)	'No cell' background log (B_b'/B_0)	'With cell' background log (B_b/B_0)
0.05	- 3.60 $\pm$ 0.1	- 3.10 $\pm$ 0.1
0.10	- 3.65	- 3.05
0.20	- 3.75	- 3.10
0.40	- 3.75	- 3.20

Since the 'with cell' background is about four times the 'no cell' value and remains sensibly constant with increasing slit width, scatter is the major cause of background in practice. In fact small particles of dust, etc. in the de-ionised water used for these experiments contributed noticeably to the background. Lower levels of background were observed when different liquids were used (see next section). It is reasonable to suppose that the 'no cell' background is close to the irreducible minimum background attainable in practice. There appears to be scope for improving sensitivity by a factor of two or three by careful attention to the cleanliness of the water and cell and the quality of glass. Unfortunately a specially-ordered high-quality cell was not available in time for these measurements.

4.5. Effect of slit width on sensitivity

It was noted in the last section that the normalised background was independent of the slit width. From theoretical considerations (Equ. 8) the slit width is not expected to have a significant effect on the sensitivity of visualisation of 2 MHz ultrasound in water provided the size of its image is less than about 0.4 mm.

Fig. 15 shows brightness-power curves plotted for a series of increasing slit widths. The only discernible effect is the upward shift of the curves resulting from the greater illumination. The maximum effective slit width was about 0.5 mm because of the finite size of the stroboscopic lamp element - measurements at greater slit widths were little different from those at 0.4 mm. The conclusion is that the sensitivity is independent of slit width up to 0.4 mm and this width was used for all the work described in subsequent parts of this thesis.

4.6 Figures-of-merit of selected liquids

Liquids were selected for experimental study from the list in Table 1 (p.28). The first criterion used was a high theoretical figure-of-merit. Then from each group of chemically similar compounds, such as iodo-methane and iodo-ethane, the liquid of best sensitivity was chosen.

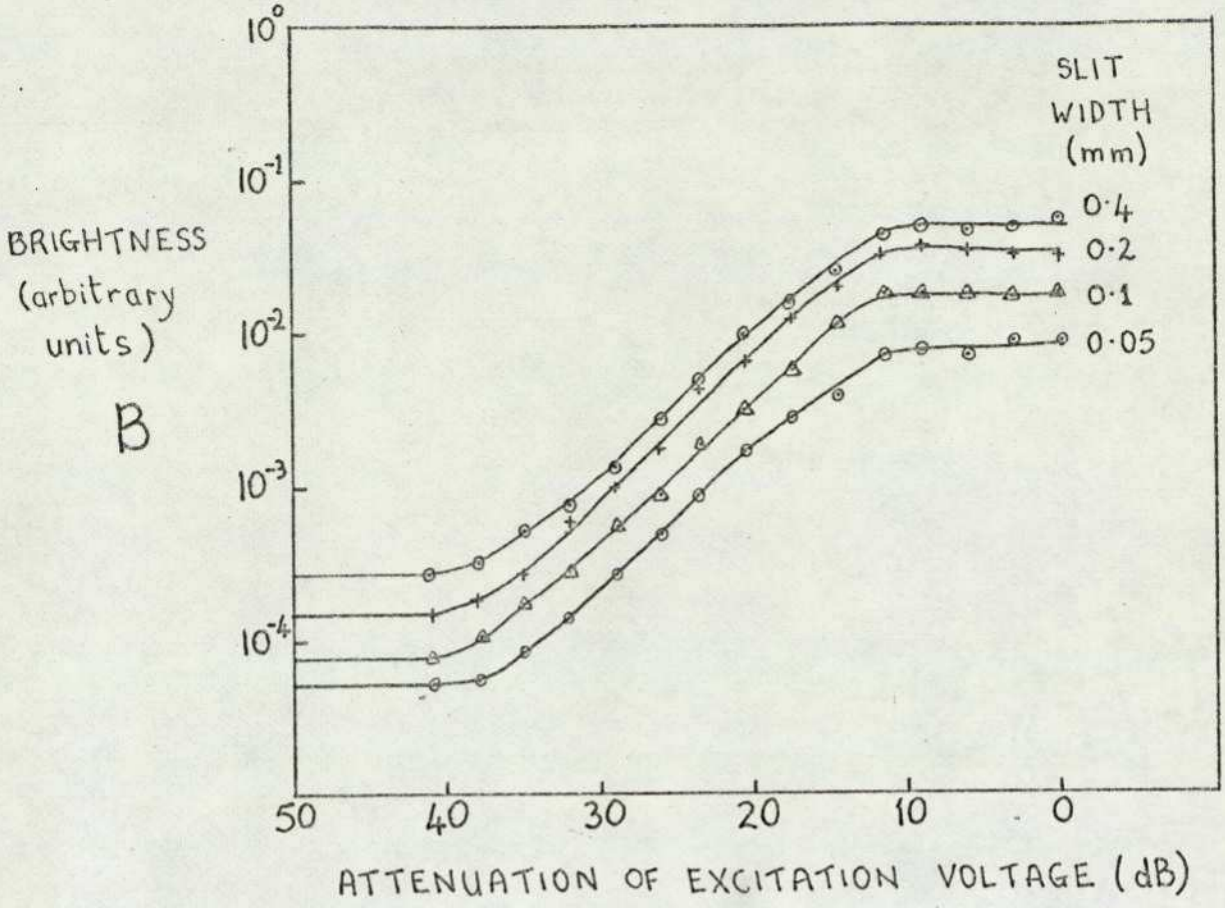

Fig.15 IMAGE BRIGHTNESS - ACOUSTIC POWER CURVES OBTAINED USING DIFFERENT SLIT WIDTHS.

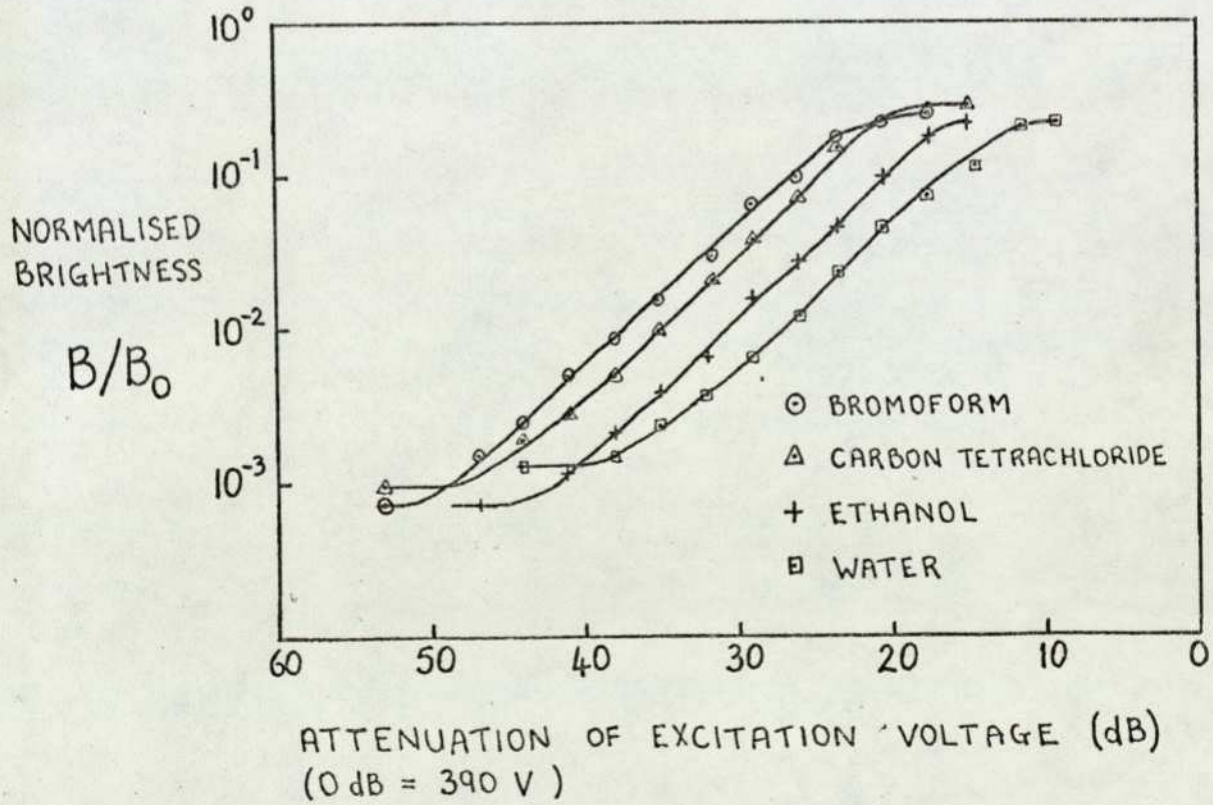

Fig.16 MEASURED RESPONSE CURVES OF VARIOUS LIQUIDS.

Carbon disulphide was ruled out because of its exceptionally high attenuation coefficient. Liquids of extreme toxicity, for example phosphorous tribromide, trichloroethene and iodo-benzene, were not studied. Ethanol and toluene were included as examples of liquids of low toxicity and low chemical reactivity. The resulting list is in Table 4.

The image brightness-electrical attenuation relationship was observed for each liquid, and just a few examples (for the sake of clarity) are shown in Fig.16. The curves had the same form as that for water, although there were different levels of background brightness (due mainly to variations in cleanliness of the liquids) and saturation brightness. The slopes of the linear region of the curve (in terms of log. brightness versus log.power) all lay in the range 0.87 to 1.04 with a mean of 0.93.

The figure-of-merit of each liquid relative to water was found by measuring the horizontal separation of each curve from that of water (at normalised brightness 10^{-2} in the middle of the linear region) and then taking account of the acoustic power transmission coefficient from the transducer into the liquid (see Chap.5).
The results are shown in Table 4, together with the theoretical figures calculated directly from the values of M in Table 1,(p.28). Within the rather wide limits of experimental error and theoretical uncertainty, the measured and predicted figures are in accord, thus giving confidence that the theoretical figures for liquids not included in this list represent the true visualisation sensitivity.

TABLE 4. FIGURES-OF-MERIT OF SELECTED LIQUIDS (relative to water)

Liquid (ref.Nos.from Table 1, P. 28)	Measured figure-of--merit dB ($\pm$ 1)	Predicted figure--of-merit dB ($\pm$ 0.5)
1. Water	0	0
2. Carbon tetrachloride	8	7.9
3. Bromoform	7.5	7.7
4. Chloroform	7.5	6.8
5. Di-iodomethane	8.0	9.0
6. Iodomethane	8.0	8.8
11. Ethanol	5.5	4.9
23. Bromobenzene	5.5	6.9
27. Benzene	6.0	6.3
31. Hexane	8.0	8.0
32. Toluene	5.5	6.3

There are apparently gains of 8-9 dB in DUVD sensitivity to be had by using a liquid other than water. Whether such a gain is possible in practice will be discussed in later chapters.

The principal cause of error in the above results is the imprecision of the brightness measurement. The photometer spot had a yellowish hue compared to the Strobotac lamp output and the exact reading depended on the method of matching its brightness to that of the pulse. In order to reduce error, a systematic matching method was used, and two sets of readings were taken, one in order of increasing acoustic power, the other in reverse order.

The smearing effect of the finite light flash (~250 ns) reduces the apparent brightness of the pulse, but this effect depends only on the time durations of the light flash and ultrasonic pulse, which are common to the different liquids tested. Therefore smearing has no effect on the relative sensitivities of the different liquids. The absolute sensitivity is affected, however. For the pulse used in the experiments above, the maximum brightness would be approximately halved, thus reducing the sensitivity by about one-half. As Hanstead (1972b)showed, the net result is equivalent to an increase in background brightness.

4.7 Calculation of absolute visualisation sensitivity

The sensitivity of ultrasonic detection techniques is usually expressed in terms of threshold intensity. This is not the best criterion for schlieren sensitivity since the optical retardation R is given by (Equ.15)

$$R = L.\Delta n = L.\ \rho \frac{\partial n}{\partial \rho} \sqrt{\frac{2I}{\rho c^3}} \quad , \qquad (21)$$

which depends on both the intensity I and the interaction length L. A better criterion is the power A. For a rectangular pulse wavefront of given shape, having length L in the direction of viewing and width w, the optical retardation is

$$R = \rho \frac{\partial n}{\partial \rho} \sqrt{\frac{2AL}{\rho c^3 w}} \quad . \qquad (22)$$

Threshold sensitivity can thus be conveniently defined as the power in a square beam (L = w).

Incidentally, Equ.22 shows the dependence of the sensitivity on the ratio L/w as pointed out by Hanstead (1973). He suggested that a focused DUVD image could be astigmatically defocused so as to increase the interaction lengths in the direction of viewing, and thus increase the sensitivity.

The peak pressure radiated into a liquid can be calculated from the physical constants of the transducer and the excitation voltage waveform. In Chap. 5 it is shown the peak pressure P radiated into water in the experiments described in this chapter is related to the peak voltage

V by

$$P \simeq 1.3 \times 10^{3} \; V \quad N.m^{-2} \; , \tag{23}$$

and the intensity is

$$I = P^{2}/2Z_{1} \simeq 0.56 \; V^{2} \quad W.m^{-2} \; . \tag{24}$$

Since the interaction length (the diameter of the transducer) was 10 mm the equivalent square-beam power is

$$A = L^{2} \; I \simeq 0.56 \times 10^{-4} \; V^{2} \quad W \; . \tag{25}$$

From the response curve the attenuation at threshold visibility in water was about -39 dB, and at saturation about -11 dB (0 dB = 390 V). The calculated acoustic powers and optical retardations are displayed in Table 5.

TABLE 5 CALCULATED VISUALISATION SENSITIVITY IN WATER

	Optical retardation ($\lambda = 0.5\,\mu m$)	Peak acoustic power
Threshold	0.016 λ	1 mW
Saturation	0.36 λ	700 mW

There have been other estimates of theshold sensitivity. Hanstead's figure, obtained by the same method, was 0.7 mW. Previous estimates, stated in terms of intensity, were 0.3 $mW.cm^{-2}$ (Oschepkov et.al. 1955) and 1 $mW.\ cm^{-2}$ (Smyth et.al. 1963), but these probably refer to a practical beam area of around 1 cm^{2}. Thus all the estimates are of the same order of magnitude.

The ultimate sensitivity which could be attained using a shorter light flash and cleaner water, as discussed in previous sections, is of the order of a quarter of the 1 mW figure.

The calculated optical retardation at saturation is consistent with the theory of Section 3.2, which predicted peak brightness at a retardation of $\lambda/2$, and this provides confirmation that the estimates of power are reasonable. The calculated retardations in liquids other than water are similar since the figures-of-merit are in accord with theory.

4.8 Summary

The dark-field schlieren image of a short ultrasonic pulse in a liquid is invisible below a threshold set by the background brightness; its average brightness then increases approximately linearly with acoustic power up to a saturation brightness corresponding to an optical retardation of about one-half wavelength. The dynamic range of the linear

region is about 30 dB. The experimental threshold sensitivity in water was 1 mW, and the ultimate sensitivity is perhaps a quarter of this. The theoretical prediction that other liquids have up to 9 dB more visualisation sensitivity than water was confirmed experimentally.

CHAPTER 5 - THE GENERATION, PROPAGATION AND MEASUREMENT OF SHORT PULSES

The resolution of a DUVD imaging system depends on the acoustic pulse length. Conventional pulse-echo techniques, by electronic processing of the echoes, can obtain range resolution of about one-half wavelength when the pulse may consist of two or more damped sinusoidal oscillations. However, in DUVD the whole pulse (above a threshold amplitude) is visualised and therefore a very short pulse is needed. The practical means of producing such short pulses, their behaviour as they travel away from the transducer, and the measurement of the pulse waveform are considered in this chapter.

5.1 Generation

Ultrasonic pulses are usually produced by applying an electrical excitation pulse between the faces of a piezoelectric plate transducer, whose front face is in contact with the 'load' to be insonified, and whose back face is bonded to an absorbent backing material, acoustically matched to the transducer. The form of the acoustic output can be predicted from the shape of the excitation pulse and the relative acoustic impedance of the transducer, load and backing by a method due to Redwood (1963).

The major shortcoming of DUVD is poor sensitivity, so that the maximum acoustic pressure must be radiated into the object. The most powerful excitation source available, the Smiths Mk.7, could provide unidirectional pulses of up to 1000 V amplitude. Attempts to improve the acoustic waveform by 'tailoring' the excitation pulse shape resulted in reductions in acoustic output, so for the work described here the excitation pulse was fed directly to the transducer.

The most suitable piezoelectric material for high amplitude generation is ceramic lead zirconate titanate (PZT). The form known as PXE-5 (Mullard Ltd.) or PZT-5A (Vernitron Ltd.) was used successfully, although in fact PXE-4 (PZT-4) is superior for resistance to depolarisation and for tensile strength.

It is difficult to achieve a perfectly matched backing in practice. For the transducer used in the measurements of schlieren sensitivity (Chap.4), Wood's metal backing was used. This low melting point alloy (70°C) has

an acoustic impedance of about 23×10^6 $Kg.m^{-2}.s^{-1}$, compared with 33×10^6 $Kg.m^{-2}.s^{-1}$ for PZT. The construction technique was simply to float a tinned PZT disc on a column of the molten metal and leave to cool. The metal formed the back-face electrical connection and a solder connection was made to the front-face electrode. This form of backing is ruled out for DUVD because it does not have a high attenuation and the desired pulse is followed by multiple reflections from within the backing. This did not matter for the measurements of pulse brightness.

It was found by experiment that, for practical purposes, the backing was sufficiently good that the acoustic waveform could be theoretically predicted from the excitation waveform using the simple assumption that the backing was perfect. The theoretical acoustic waveform then consists of just two pulses of the same shape as the excitation pulse; one from the front face of the transducer, followed by another of equal but opposite amplitude from the back face, after a time delay due to the acoustic transit time across the transducer. The construction by this method of the acoustic pulse used in the sensitivity measurements is shown in Fig.17, together with the measured acoustic pulse (see Section 5.5), and close correspondence is apparent.

This example illustrates that, in order to make most efficient use of the excitation pulse, its rise time should be less than the acoustic transit time across the transducer. Then the front-face pulse reaches its maximum amplitude before arrival of the negative back-face pulse. The absolute amplitude of the pressure radiated by the front face is given by

$$P = hCV \frac{1}{2} \left(\frac{2}{Z_t/Z_l + 1} \right), \qquad (26)$$

where h is a piezoelectric constant, C is the electrical capacitance per unit area of the transducer, V is the excitation voltage, and Z_t and Z_l are the acoustic impedances of the transducer and load, respectively. The bracketed term is the stress (or pressure) transmission coefficient from the transducer to the load.

For the transducer described above (4 MHz resonant frequency), $hC = 3.2 \times 10^4$ and the stress transmission coefficient into water is 0.084 so that

$$P = 1.3 \times 10^3 \, V \quad N.m^{-2} \qquad (27)$$

which is the result used in Chapter 4.

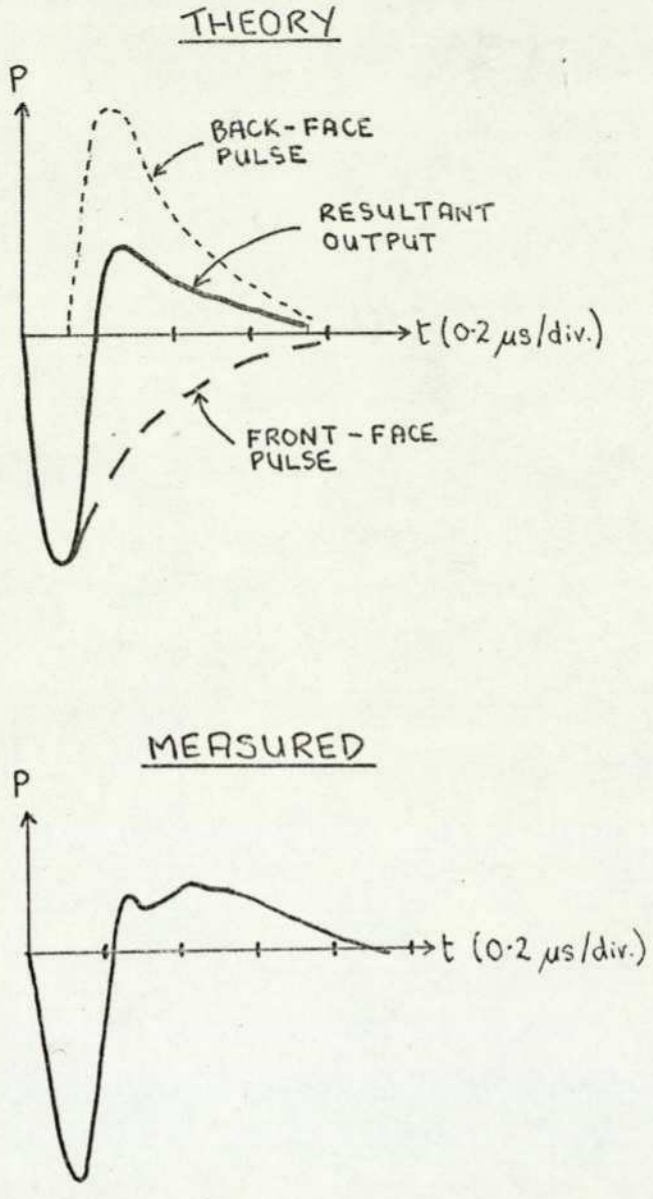

Fig.17 THE THEORETICAL CONSTRUCTION OF AN ACOUSTIC PULSE FROM THE EXCITATION VOLTAGE WAVEFORM; THE MEASURED PULSE IS ALSO SHOWN.

The other transducers, employed for observations of the pulsed field, and for demonstrations of DUVD systems not yet described, had conventional backings of epoxy loaded with tungsten powder. The acoustic matching to the transducer is not as good as with Wood's metal, but the attenuation is very high. The tungsten-epoxy mixture can be centrifuged as it sets in order to increase the packing of the tungsten and increase the impedance in contact with the transducer. This technique was employed for the circular transducer used for observations of the pulsed field (see Section 5.3), but the rectangular transducers used for demonstrations of DUVD systems (Chap.8) were too large to permit this approach and hence the acoustic pulses generated were not as short as desired.

5.2 Theory of transient radiation into a fluid

Ultrasonic pulses have so far been referred to as if they were plane waves of unchanging waveform; this can be a valid approximation under certain conditions. However, a good understanding of the pulsed field is necessary for the proper design of an imaging system and an appreciation of its limitations.

Theoretically, the field of a plane transducer is calculated by assuming it to behave as a rigid piston set in an infinite baffle. The familiar description of the steady-state field of an oscillating piston, in terms of near and far fields, is given in the standard texts: the far-field solution is well-known, and detailed near-field computations have been published, for example by Zemanek (1971) for the circular piston. For many practical purposes, this theory can be used to determine the pressure-amplitude distribution set up by a pulsed transducer, provided that it oscillates for a few cycles, although the actual near-field maxima and minima will be less pronounced than predicted by theory.

However, when the transducer produces a short pulse, the steady-state theory is no longer adequate and a transient solution is needed. The surface integral expressing the transient field as the sum of contributions from pulsed Huyghens' sources has been known for a century (Rayleigh 1945). Relatively recently, attention has been devoted to obtaining numerical solutions, and a simple expression for the field resulting from an impulse velocity motion of the transducer has been derived by several authors (for example, Stepanishen 1971, Robinson et.al. 1974). The solution applies to arbitrary piston shapes and to

any point in the field; the pressure resulting from an arbitrary velocity motion can be found by convolution of the velocity with the impulse response.

Although this form of impulse response is useful for exact calculations, insight into the structure of the field, particularly for the interpretation of schlieren observations, is obtained by introducing the concept of edge waves. The last-named authors do not refer to edge waves, but their results are readily explained in these terms, as shown by Tupholme (1969), and in a separate publication (Weight and Hayman 1978). .

As stated by Tupholme, the field contains two components: the direct wave and the edge wave. The motion of the piston as a whole gives rise to the direct plane wave, which propagates in the right cylindrical region having the piston as its base, whilst the relative motion of the piston and baffle creates the diffracted edge wave which propagates in all forward directions from the edge of the piston.

The pressure in the direct wave is proportional to the piston velocity at the time of departure. The portion of the edge wave radiated (by a small edge element) outside the cylinder having the piston as its base has the same polarity as the direct wave, whereas the inward-going portion has inverted polarity.

The edge-wave description, of course, also applies to steady-state radiation. In fact, Kozina and Makarov (1961), who were among the first authors to apply the concept to the pulsed field, derived their result by transforming the corresponding continuous-wave theory from the frequency to the time domain. It is interesting that one of the earliest theories of the diffraction of light, put forward by Thomas Young in 1802, was based upon the concept of boundary waves scattered from the edge of a diffracting object. It was not until the 1920's that it was proved equivalent to the Fresnel-Kirchoff theories (Born and Wolf 1970,Chap.8.9.) Diffraction effects result from the interference of the incident wave and an edge wave (phase shifted by π) in the geometrically illuminated region, and from the edge wave alone in the shadow region.

A qualitative description of the pulsed field of the two most common shapes of transducer - circular and rectangular - will now be given.

For the graphical illustrations a transducer velocity motion consisting of a single sinusoidal cycle is assumed.

The field of a circular piston has been discussed in detail by Robinson et.al (1974), both with reference to the impulse response and to various arbitrary piston motions. Pressure waveforms resulting from a single-cycle sinusoidal velocity have been computed by Beaver (1974) and Duck (1977).

On axis, the inward-going edge waves (negative polarity) arrive simultaneously, so that the direct wave is followed by an inverted replica. Fig.18(a)-(d) shows pressure waveforms at a series of axial points of increasing distance from the transducer. The time separation between the direct and edge waves becomes smaller with increasing range and they eventually overlap. At the range corresponding to the last axial maximum in the field for continuous waves of the same wavelength Λ (range $\simeq d^2/4\Lambda$ where d is the transducer diameter), the direct and edge waves reinforce where they overlap. As the range is increased further, the plane and edge waves start to cancel. The far-field may be defined as the region where the pressure waveform resembles the acceleration of the piston and the amplitude becomes inversely proportional to the range (just as for continuous waves).

Off axis but inside the cylindrical region in front of the transducer (i.e. inside the 'geometrical beam') there are two major edge-wave contributions from the nearer and further parts of the edge - contributions from the rest of the edge being 'smeared out' in time. Being inward-going waves, these give two distorted inverted replicas of, and following, the direct wave (Fig.18(e)).

Outside the geometrical beam there is no direct wave, just two major edge-wave contributions from the nearer and further parts of the edge. As shown in Fig.18(f), the first, consisting of outward-going waves, gives a distorted replica pulse, and the second (inward-going) an inverted distorted replica. The amplitude of these pulses decreases as the distance off-axis increases.

The field of a rectangular piston is more complicated, particularly in the nearfield. The edge-wavefronts are cylinders. In the geometrical beam region there are, in general, four major edge-wave contributions, from the nearest part of each edge. At field points where some of these

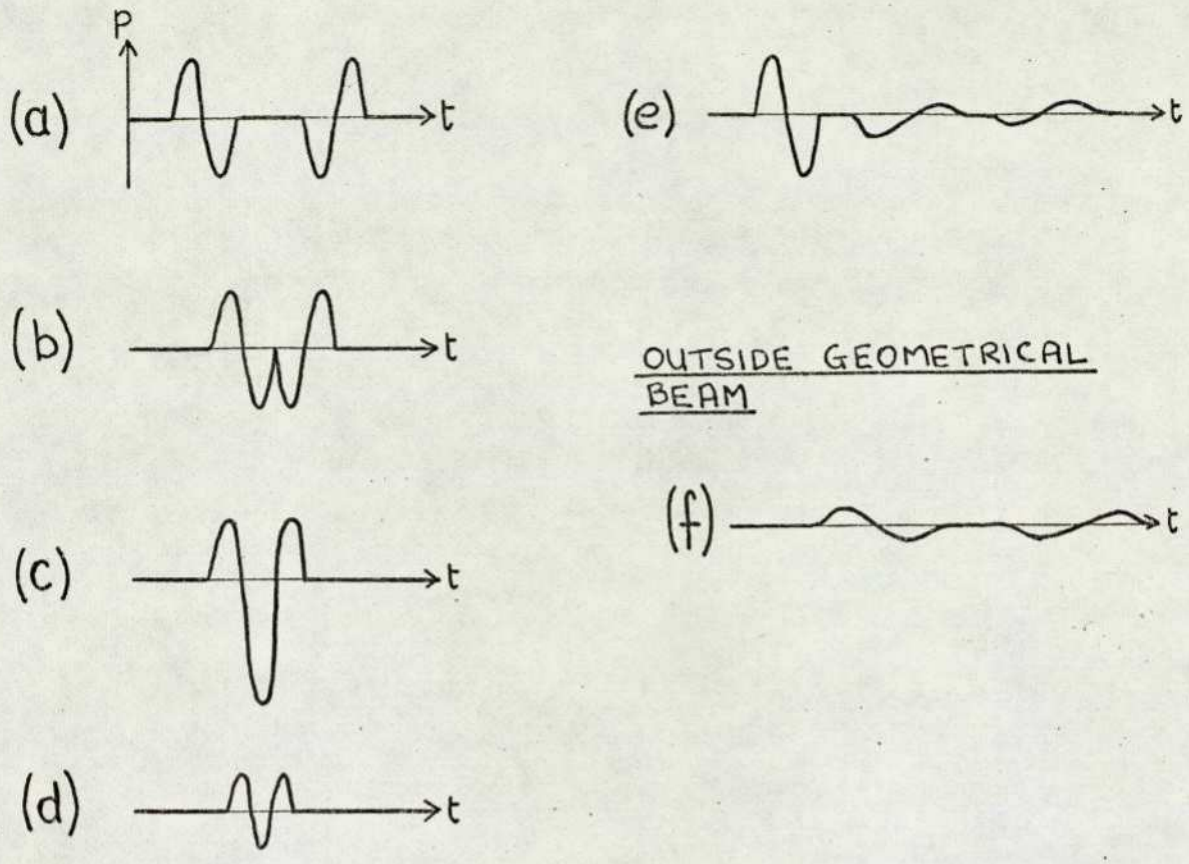

Fig.18 THEORETICAL PRESSURE WAVEFORMS IN THE FIELD OF A CIRCULAR PISTON GIVEN A PULSED SINGLE-CYCLE VELOCITY MOTION.

(a)-(d) AT INCREASING RANGE ON AXIS

(c) AT THE POSITION OF THE LAST AXIAL MAXIMUM IN THE CONTINUOUS-WAVE FIELD

(d) IN THE FAR FIELD.

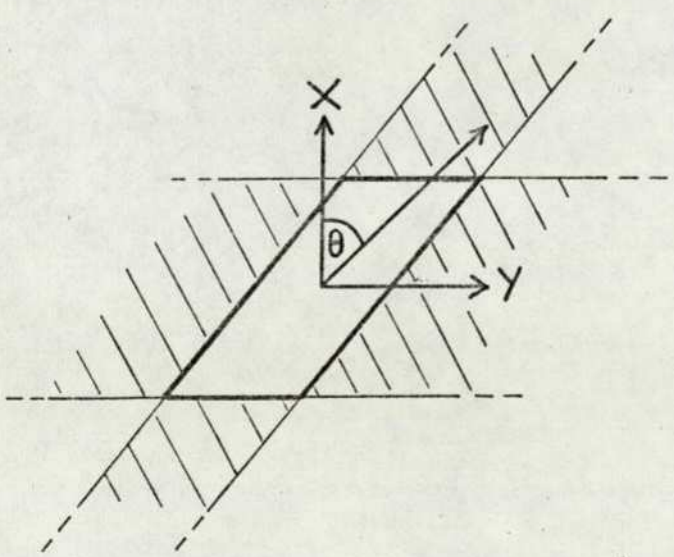

Fig.19 RECTANGULAR PISTON GEOMETRY.

contributions arrive simultaneously, they will add up; but even on the axis of a square transducer (where all four arrive at once) the edge-wave amplitude will be less than the direct-wave amplitude. Outside the geometrical beam, the most significant edge-wave contributions occur in those regions where the cylindrical wavefronts propagate, i.e. the projection of the areas shown shaded in Fig.19.

The far-field of the rectangular piston has been considered by Stephanishen (1971) and Otani (1972). The axial far-field pressure is proportional to the acceleration of the piston. The far-field in a central plane off-axis (the X-Y plane in Fig.19) is particularly simple. The (outward-going) edge-wave contributions from all parts of the nearer edge arrive simultaneously at the field point, as do those (inward-going) from the further edge. Thus the pressure consists of a scaled replica of the piston velocity followed by another of negative polarity. The amplitude of these waves falls off with angle θ. The transition to far-field-like behaviour in a central plane occurs at the range $\sim d^2/4\Lambda$ where d is the dimension of the piston in that plane. Thus the nearfield in the plane parallel to the short dimension of the rectangle (as illustrated) is effectively shorter than that in the plane parallel to the long dimension.

To summarise, the most important component of the nearfield of a piston driven by a very short velocity pulse is a plane wave travelling as a geometrical beam. This is followed by edge waves, which have smaller amplitudes (except on the axis of a circular piston). The nearfield of a rectangular piston may be said to be more uniform than that of a circular transducer. The edge-waves become increasingly important at large ranges, and determine the far-field structure. The far-field may be defined as the region where the axial pressure is proportional to the acceleration of the transducer and the amplitude is inversely proportional to range. The transition to far-field-like behaviour, for a pulse consisting of a truncated sinusoid, occurs at the same range as it does for continous waves of the same frequency.

5.3 Observations of pulse propagation in water

The theory of transient radiation by a piston is well understood, but experimental observations are lacking. Conventional measurements of the field of a pulsed transducer are concerned with the distribution of peak amplitude, no account being taken of the pulse structure.

Published observations of pulse shapes include those of Christie (1962), who measured the amplitudes of successive half-cycles of pulses a few cycles long and determined the regions of transient and steady-state behaviour for each half-cycle; his probe was 4.5 wavelengths in diameter at the lowest frequency used. Carome et.al (1964), observing the propagation of short impulses with a large receiver, noted the effect of edge waves as a smeared impulse following the plane wave. Freedman (1971) resolved the two edge-wave components in the central plane of the off-axis far field of a 28 kHz square transducer.

The schlieren system (described in Chap.4) was used to observe short pulses radiated into water by circular and rectangular transducers. Pressure waveforms at points in the field of the circular transducer were measured with a specially-constructed small (150 μm) probe which had approximately omnidirectional response in a frequency band extending above 5 MHz. Fuller practical details and further experimental observations are given in a separate publication (Weight and Hayman 1977).

The circular transducer consisted of an 8 mm radius disc of PZT, 0.2 mm thick (resonant frequency 10 MHz), backed with tungsten-loaded epoxy and driven by unidirectional electrical pulses.

Fig. 20 is a series of schlieren photographs showing a pulse travelling out from the circular transducer. The plane and edge waves are clearly seen as, respectively, a horizontal wavefront and two circular arcs emanating from the edges of the transducer. Fig.21 shows the effect of placing a small reflector - a flat-ended brass cylinder of diameter 0.8 mm - on the axis of the transducer. There are two time-resolved reflections: one from the direct wave, the other from the edge wave. As the reflector is small, the reflected waves have spherical form. In Fig.22 the reflector is slightly off-axis and it is just possible to observe two separate edge-wave reflections, one slightly behind the other and just behind the direct-wave reflection.

When the small receiving probe was used to measure pressure waveforms in the field, time-resolved direct and edge waves were observed, and the direct wave maintained constant amplitude at all field positions where it did not overlap the edge waves. The excitation pulse was

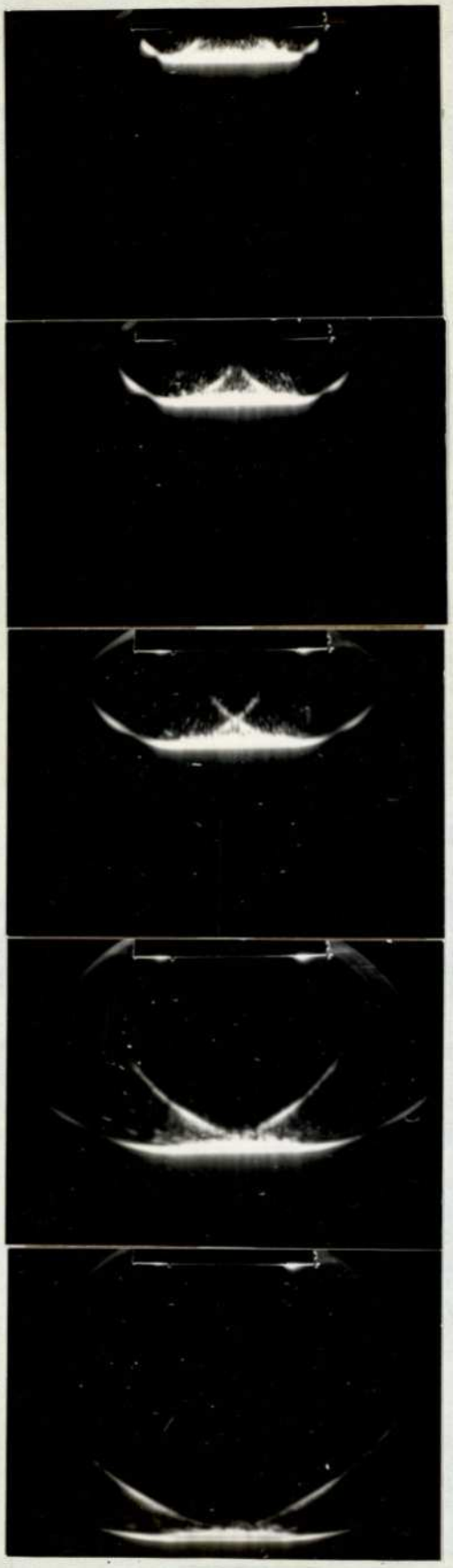

Fig.20 SEQUENCE OF SCHLIEREN PHOTOGRAPHS SHOWING A SHORT PULSE TRAVELLING (downwards) FROM AN 8 mm RADIUS CIRCULAR TRANSDUCER IN WATER. SCALE APPROXIMATELY ACTUAL SIZE.

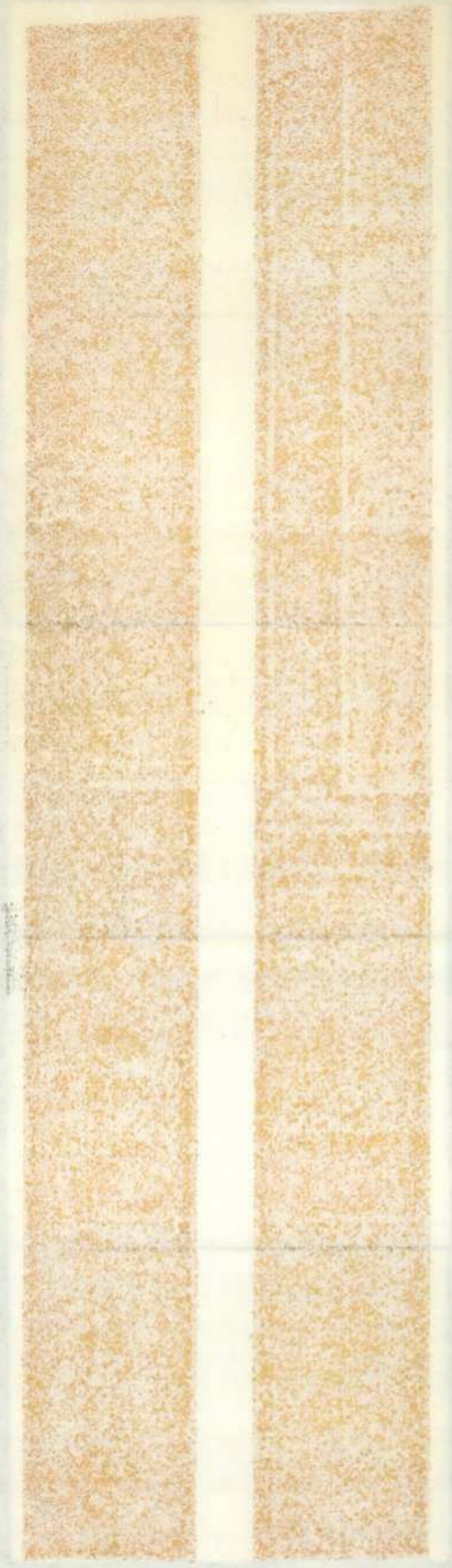

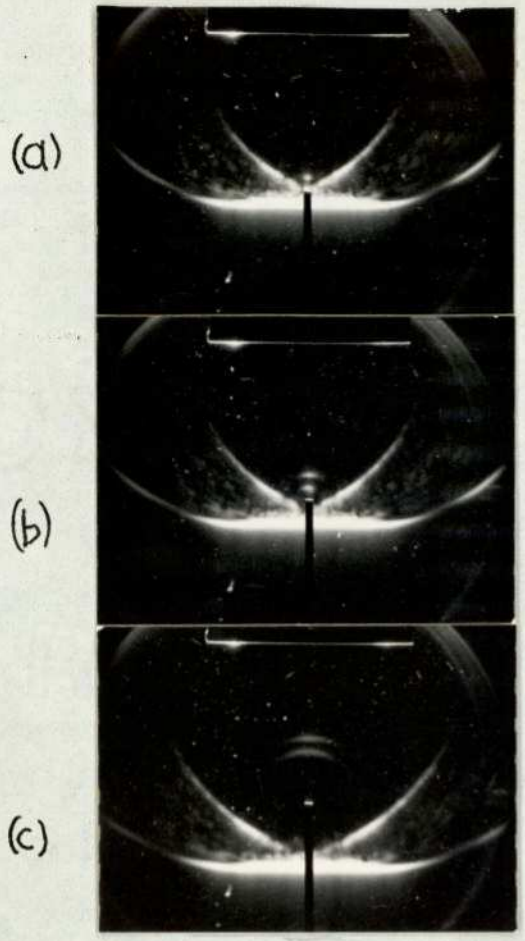

Fig.21 SCHLIEREN SEQUENCE SHOWING A PULSE FROM A CIRCULAR TRANSDUCER REFLECTED BY A 0.8 mm DIAMETER FLAT-ENDED CYLINDER ON AXIS. The cylinder appears black against the pulse in (a) where only the direct wave reflection is seen, then in (b)& (c) the edge wave reflection is also seen.

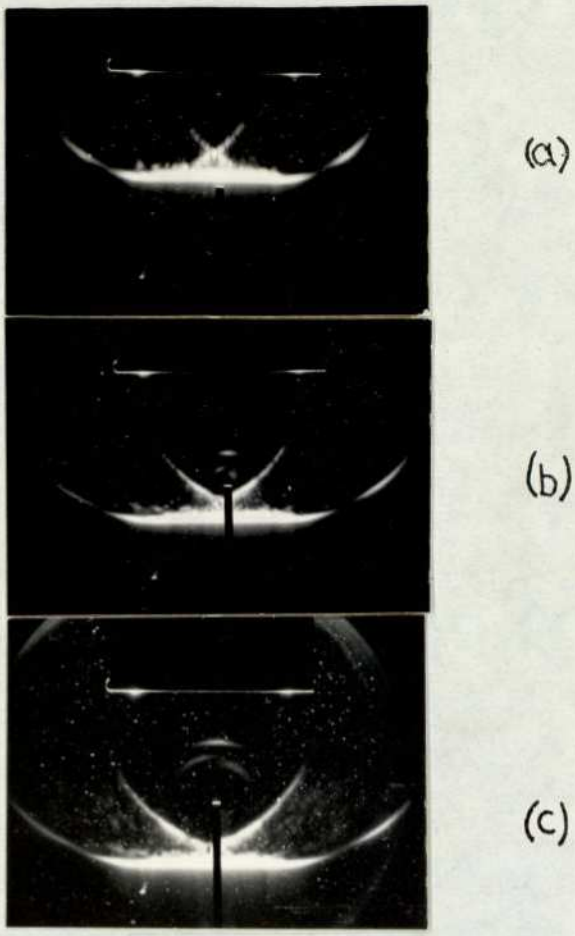

Fig.22 REFLECTION OF PULSE BY A CYLINDER OFF-AXIS: Two edge wave reflections are visible.

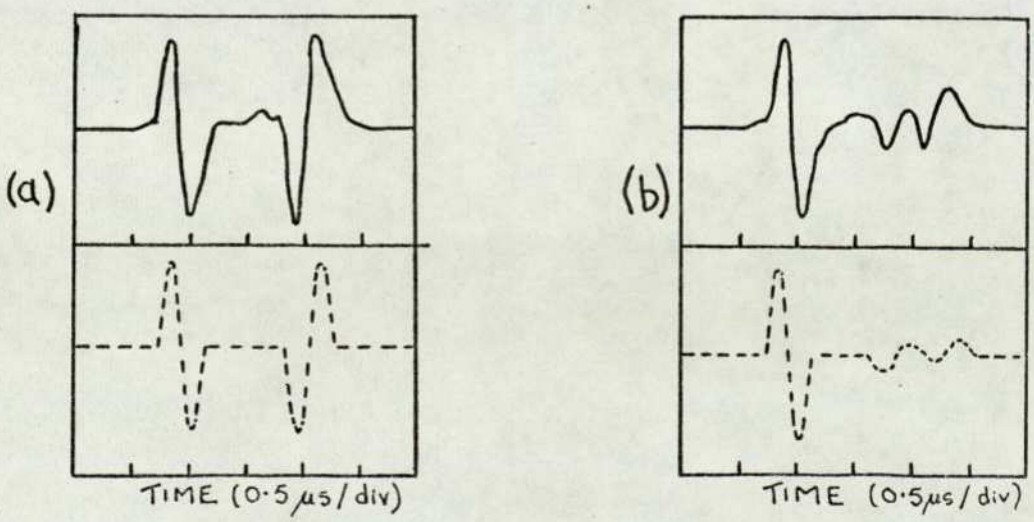

Fig.23 MEASURED PRESSURE WAVEFORMS DUE TO A PULSED 8 mm RADIUS CIRCULAR TRANSDUCER AT 20 mm RANGE (upper), COMPARED WITH THEORETICAL RESULTS CALCULATED ASSUMING A 3 MHz SINGLE-CYCLE PISTON VELOCITY (lower): (a) ON AXIS (b) 1 mm OFF AXIS.

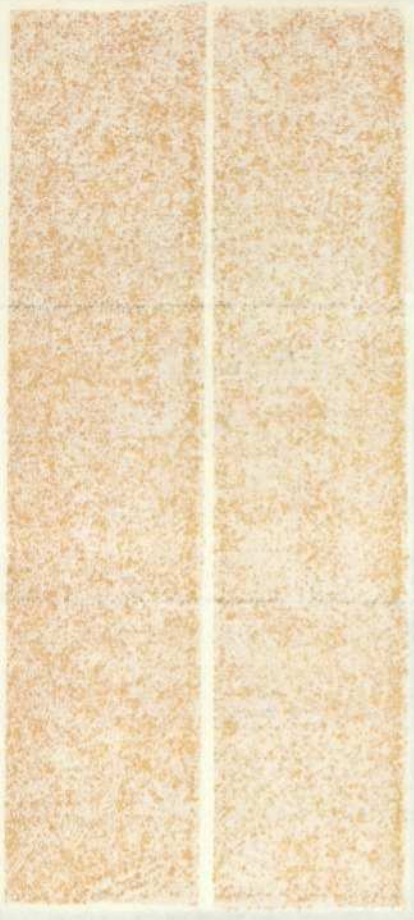

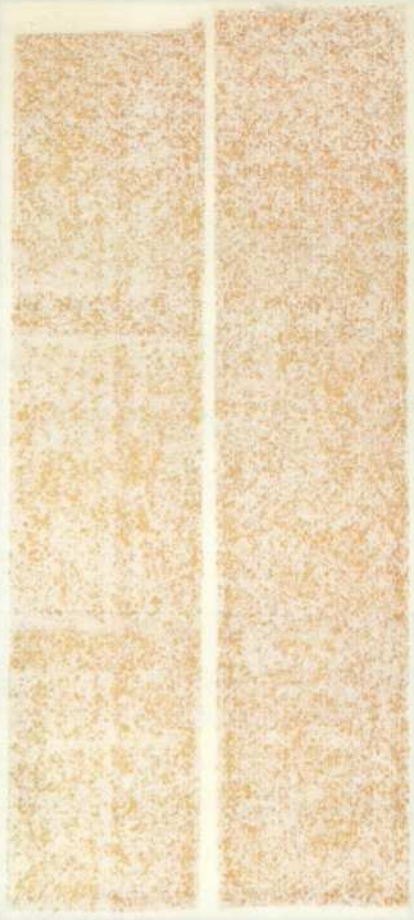

adjusted so that the direct wave became approximately a single cycle of a 3 MHz sinusoid. Fig.23 shows measured waveforms at a range of 20 mm both on-axis and 1 mm off-axis, together with the theoretical results for a 3 MHz single-cycle transducer velocity. The measurement of one edge-wave pulse on-axis and two off-axis corresponds to the above schlieren observation of one edge-wave reflection by a small axial target and two reflections when the target is off-axis.

At a range of about 1.4 transducer radii on-axis the edge-wave appeared to be about four times larger than theory predicted. The 'focal region' was very small and occurred at the same relative range with several different transducers. The effect is visible in the schlieren photographs. In Fig.20(c) the edge waves are close to the measured axial 'focus' while in (d) and (e) that portion of the edge wave which has propagated through the 'focus' appears brighter than the rest of the wavefront. More detailed observations of this effect were possible with the rectangular transducer, as described below.

The rectangular transducer was a 45 x 9 mm plate of PZT, 0.5 mm thick (4 MHz resonant frequency), backed by tungsten-loaded epoxy. It was one of the transducers used in tests of a DUVD system to be described.

Schlieren photographs showing a pulse travelling away from the transducer are displayed in Fig.24. The transducer is oriented with its long axis parallel to the light beam, i.e. in the direction of viewing. The direct and edge-wave structure is evident, and the edge waves appear brighter than in the circular transducer photographs because the cylindrical wavefronts are parallel to the light beam, giving a long interaction length. The transducer is narrow enough to show far-field-like structure: in Fig.24(d) the direct and edge waves have coalesced on axis, while off axis the field consists of two edge waves.

Two additional plane wavefronts are visible in these pictures, inclined at about 30° to the transducer face. They are most clearly seen in Fig.24(a), and they merge with parts of the edge wave as they travel out. A re-examination of the circular transducer pictures (Fig.20) will show that similar waves could be responsible for the brightening and thickening of parts of the edge waves there. Careful observations showed that each plane wavefront is caused by a wave which leaves the edge of the transducer at the same time as the edge wave, and travels across the transducer at about 3000 $m.s^{-1}$, radiating into the water

Fig.24 SCHLIEREN SEQUENCE OF A PULSE TRAVELLING AWAY FROM A RECTANGULAR TRANSDUCER OF DIMENSIONS 45x9 mm ALIGNED WITH ITS LONG AXIS IN THE DIRECTION OF VIEWING. SCALE APPROXIMATELY ACTUAL SIZE.

Fig.25 PHOTOELASTIC IMAGE OF THE PULSE STRUCTURE PRODUCED BY A COMPRESSION--WAVE TRANSDUCER (not seen) BONDED TO THE TOP SURFACE OF A GLASS BLOCK.
(Acknowledgements to Dr.R.C.Wyatt).

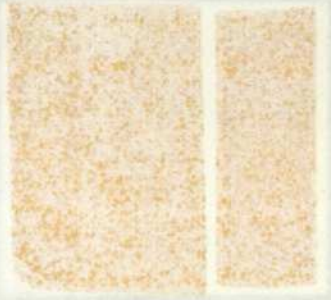

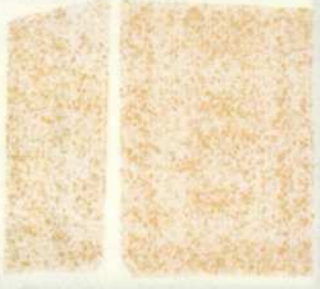

(velocity 1500 $m.s^{-1}$) as it travels. As a consequence of the mechanical properties of a solid, when the thickness of a piezo-electric transducer changes its diameter must also change, and this is known to cause the 'plate mode' of vibration which is so troublesome in pulse-echo work. It appears that the effect of such a 'plate wave' has here been observed directly.

The observations described above are therefore in good agreement with the theory for piston radiators, and they demonstrate the usefulness of the direct and edge-wave description of the field. Departures from theory are caused by the non-ideal behaviour of a practical transducer, owing to the presence of plate waves. The effect of these plate waves appears to be significant only close to the transducer, within about one transducer diameter.

5.4 Pulse propagation in a solid

A fluid can support only compressional (longitudinal) acoustic waves, whereas a solid can support both compression and shear (transverse) waves. The structure of an acoustic pulse in a solid is therefore more complicated and it will be influenced by the solid concerned, the type of transducer and the method of coupling it to the solid.

Photoelastic visualisation in transparent solids has shown that pulses are made up of direct and edge-wave components. Fig.25 is a photoelastic image due to Wyatt (1977), showing the waves emitted by a compression wave transducer bonded to a glass block. Not only are compression direct and edge waves seen, but also shear edge waves, which can be distinguished by their lower velocity (about 0.6 of the compression wave velocity).

The edge-wave concept is used in a theory of shear-wave transducers being developed by Coffey and Wickham (1977). However, no complete transient solution has yet been published for any type of transducer.

A knowledge of the pulsed field is important for ultrasonic imaging of defects in a solid. Also, unwanted waves, such as the shear waves in Fig.25, could give rise to spurious images.

5.5 Measurement of the waveform of a short pulse

The previous sections have shown that the structure of a pulse changes as it travels away from the transducer. If it is desired to measure a waveform which, together with the transducer geometry, will unambiguously define the field, then there are two possibilities: the axial far field pressure (proportional to the acceleration of the transducer face) or the direct-wave pressure in the near field (proportional to the velocity). The first is usually inconvenient to measure in practice, but the second can be readily observed for a short pulse. It is worth emphasising that Redwood's analysis of the piezoelectric generation of pulses, referred to in Section 5.1, gives the waveform of a plane wave emerging from the transducer, i.e. it gives the direct-wave pressure.

A receiver placed close to the transducer can be used to measure the direct wave before the arrival of the edge waves, provided the receiver diameter is a few times smaller than the transducer and the pulse length is short compared to the acoustic transit time across the transducer face. These conditions were first stated by Carome et.al. (1964).

The experimental results of Carome et.al. also showed, however, that provided the receiver was close to the transducer the effect of the edge waves was small. This is because the plane direct wave is incident at all points on the receiver at once, whereas the edge waves sweep across the face of the receiver and are 'smeared out'. Thus for many practical purposes it suffices to use a receiver of about the same size as the transmitting transducer, and placed as close as possible to it. The minimum separation is set by the fact that the acoustic transit time between transmitter and receiver must be longer than the initial period of electrical breakthrough from the excitation pulse and long enough to delay multiple acoustic reflections.

A simple wide-band receiver is a piezoelectric disc of very low resonant frequency, shunted by a small electrical resistance and connected directly to an oscilloscope (Redwood 1963, Wyatt 1972). The waveforms shown in this report were measured with such a PZT disc of 25 mm diameter and 7 mm thickness, shunted by 50 Ω. The frequency band extended above 5 MHz and pulse lengths of up to 1.75 μs could be recorded.

CHAPTER 6 THE SONIC SYSTEM - MATERIALS

This chapter is concerned with the design of a DUVD sonic system from the point of view of minimising acoustic energy losses. The problems involved are mainly those of materials; measurements of the acoustic properties of lens materials are described, together with tests of their chemical resistance to liquids of good visualisation sensitivity.

6.1 General arrangement of the sonic system

Many possible configurations of sonic system were discussed by Hanstead (1973). We have seen that a liquid visualising medium is desirable on the grounds of sensitivity; liquid coupling to the object under examination is indicated as a consequence of the large area of coupling required and the obvious difficulties of manoeuvreing a bulky system into good acoustic contact with an object; and the long sonic path between the two acoustic lenses (or refracting interfaces) is also conveniently occupied by a liquid.

The best arrangement therefore appears to be two thin lenses in liquid media, which was the form of Hanstead's most successful system (Fig.1,P.3). This arrangement is the most flexible, and thin lenses are easy to manufacture.

The volume of object to be imaged must be decided upon. Although DUVD produces a three-dimensional acoustic image, the information in the direction of viewing is lost in schlieren viewing because the viewpoint is a large distance from the image, i.e. the optical image is essentially two-dimensional. Hence the method is used to its best advantage by insonifying just a 'slice' of the object so that the image is of a longitudinal cross-section (similar to a conventional B-scan). A suitable well-defined beam can be produced in the nearfield of a pulsed transducer, as discussed in Section 5.3.

The alternative methods of insonification have been outlined in Chap.2. The first is a transducer in the conventional pulse-echo position near the surface of the object. It is difficult to conceive of a way of thus insonifying a slice of object with a well-defined beam without obstructing the most important reflections. Therefore it was decided to confine attention to the alternative 'transducer image' method, which is shown schematically in Fig.26. The transducer is beyond the image space, and for insonification the ultrasonic pulse travels through the sonic system from the image space to the object space and forms a real image of the transducer near the surface of the object. This

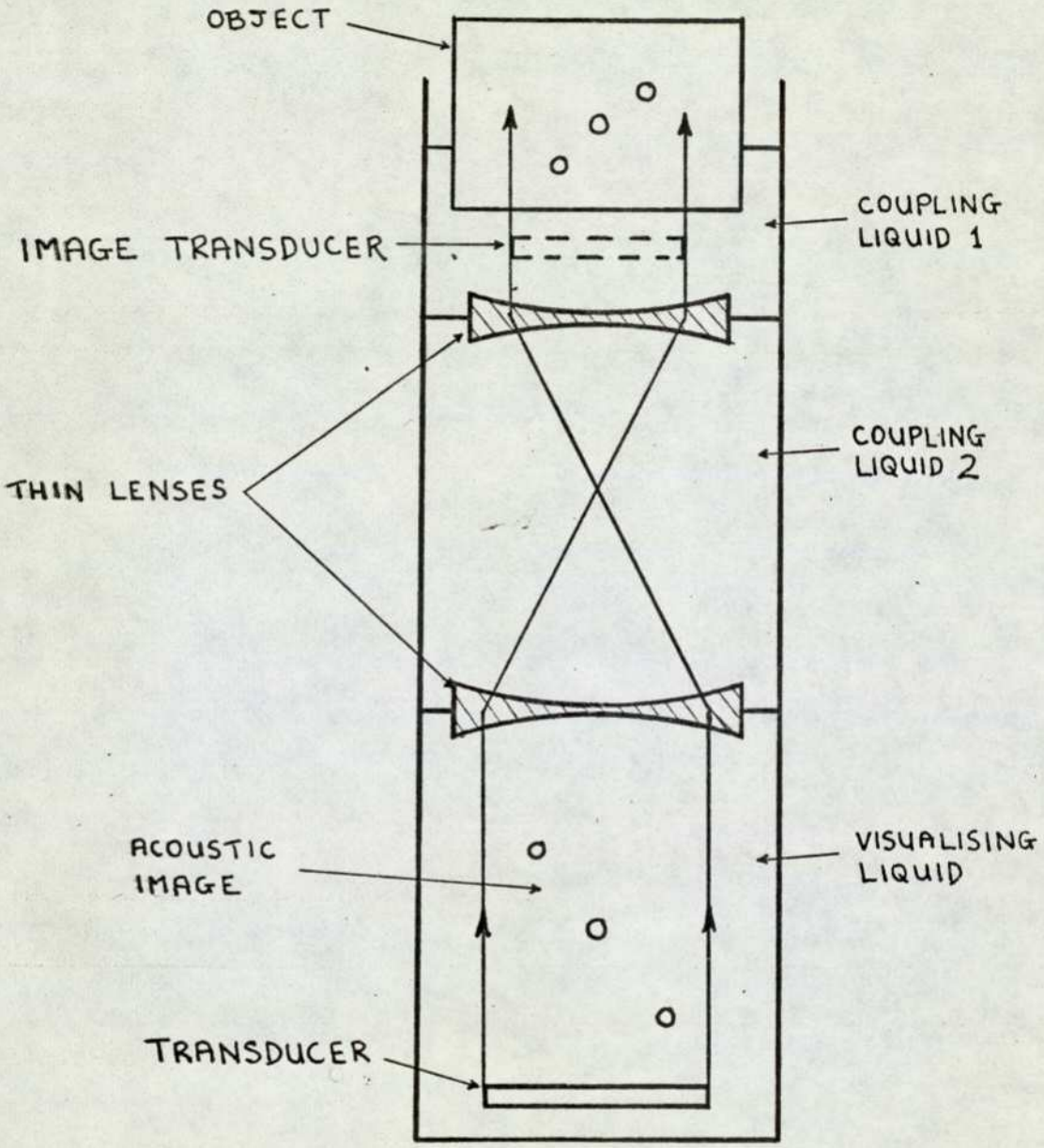

Fig.26 THE GENERAL ARRANGEMENT OF A SONIC SYSTEM EMPLOYING PLASTIC LENSES AND THE 'TRANSDUCER IMAGE' METHOD OF INSONIFICATION.

method involves the ultrasound in a double-pass through the sonic system - first insonification and then focusing of the reflections - and it is therefore particularly important to minimise acoustic losses in the sytem.

6.2 Acoustic lenses

The important requirements for an acoustic lens material are as follows:

(1) The material should be a good acoustic match to the adjacent media. The acoustic energy reflection coefficient R and transmission coefficient T, for a longitudinal plane wave incident normally upon a plane interface between media of acoustic impedances Z_1 and Z_2, are given by the fundamental equations:

$$R = \left(\frac{Z_2 - Z_1}{Z_2 + Z_1}\right)^2 \qquad (28)$$

$$T = 1-R = \frac{4 Z_2 Z_1}{(Z_2 + Z_1)^2}, \qquad (29)$$

where Z is the product of the density ρ and acoustic velocity c:

$$Z = \rho c \, . \qquad (30)$$

The coefficients, expressed in dB, are plotted in Fig.27 as a function of Z_2/Z_1. An impedance ratio of 2.0 between lens and liquid might be considered acceptable for a DUVD system, since the loss at one interface is then 0.5 dB, and the total loss on both insonification and imaging of echoes (8 interfaces in all) is 4 dB. The transmission coefficient at oblique angles of incidence is considered in section 6.5.

(2) The lens material should have a high acoustic refractive index, i.e. the ratio of acoustic velocities in lens and adjacent media should be large. The higher the ratio is, the thinner the lens, thus reducing attenuation losses, and the smaller the sonic aberrations.

(3) The material should have a low acoustic attenuation coefficient.

(4) The material should be resistant to chemical and physical attack from adjacent liquids.

Water is the best liquid for the coupling liquids 1 and 2 (Fig.26), on the grounds of convenience and low attenuation, but it is desirable to use a visualising liquid of high figure-of-merit. The acoustic impedance of the liquids in Table 1 (P.28) is typified by that of water, 1.5×10^6 kg.m^{-2}.s^{-1}.

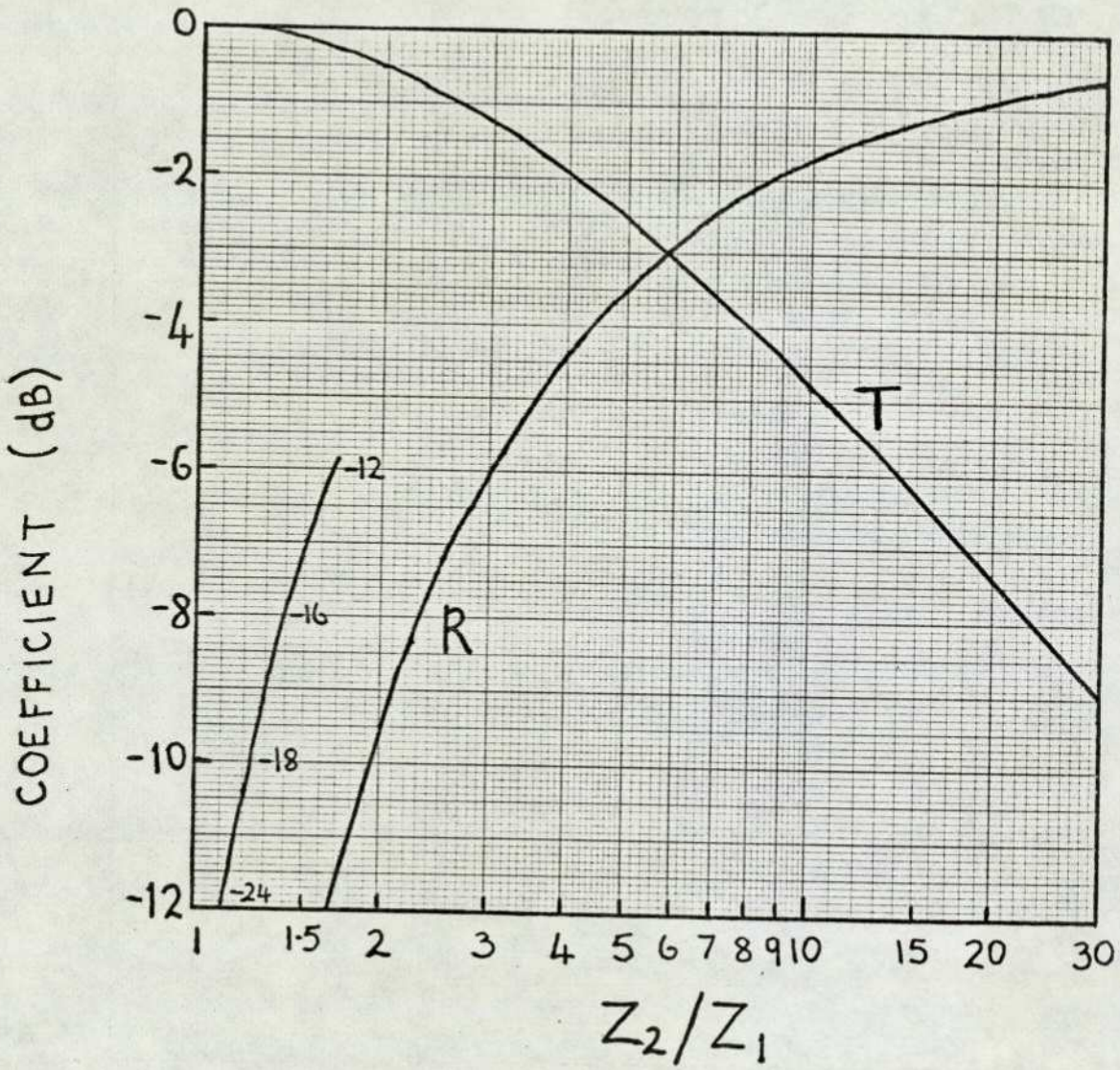

Fig.27 ENERGY TRANSMISSION AND REFLECTION COEFFICIENTS FOR A WAVE INCIDENT NORMALLY UPON AN INTERFACE BETWEEN MEDIA OF ACOUSTIC IMPEDANCES Z_1 AND Z_2.

The requirement of good acoustic matching rules out glasses and metals as lens materials, for their impedances are in the range 15-100 $x10^6 kg.m^{-2}.s^{-1}$. Good matching and low attenuation can be achieved, in theory, with lenses consisting of a liquid or soft rubber enclosed by a very thin membrane. However, the practical difficulty of obtaining a membrane which is stiff enough to hold its shape whilst remaining thin enough to be acoustically transparent has not been solved. Metal foils introduce significant losses (Ernst 1945) while plastic sheets can be used only in stretched planar form and are liable to bulge (Szilard and Kidger 1976).

Plastics and rubbers with acoustic impedances less than twice that of water are available, and rigid plastic lenses are easy to manufacture. It was decided to use plastic lenses for the present development of DUVD. The disadvantage of a plastic is its high attenuation. Perspex and polystyrene have been most commonly used, and according to Wells (1969, P.60) polystyrene is superior because of its lower attenuation, even though its acoustic velocity ratio relative to water is lower. This is in accord with literature attenuation values, but there has been no systematic study of attenuation in plastics over the frequency range of interest here, say 1-5 MHz. The available data (Mason and McSkimin 1952, Folds 1972 and 1973, Hartmann and Jarzynski 1974) is mainly at different frequencies, and comparable measurements disagree significantly.

The attenuation in some common plastics was therefore measured. Since Perspex and polystyrene are dissolved by many of the possible visualising liquids, materials of superior chemical resistance were sought. From the available data, nylon appeared to have the lowest attenuation amongst plastics of good resistance, and polyethylene was included because of its excellent resistance.

6.3 Measurements of the ultrasonic properties of plastics

Using the instrumentation of the ultrasonics group at The City University, it was a straightforward matter to measure attenuations over a frequency band from 1-5 MHz. The velocities of the materials were also measured because, although literature values are consistent to about 5%, velocities are known to vary between different samples of the same material.

6.3.1 Materials

The plastics tested were:

Perspex (polymethyl methacrylate), also known as Plexiglass and Lucite,

manufactured by ICI.

Polystyrene, manufactured by Monsanto Ltd.

Nylon 6, trade name Monocast 901, manufactured by Polypenco.

Polyethylene, manufacturer unknown.

Specimens of nylon 66 and nylon 11 (manufactured by ICI) were not sufficiently homogeneous to test, as will be explained.

The plastics were machined into discs of about 70 mm radius and various thicknesses, the most suitable thickness being used for each particular measurement.

6.3.2 Apparatus

Pulse-echo techniques were used for both velocity and attenuation measurements. Since attenuation increases with frequency, an ultrasonic pulse was required which contained most of its energy in the higher frequency components of the 1-5 MHz band. A well-backed transducer of 10 mm diameter and 5 MHz resonant frequency was used, which provided a pulse whose spectrum peaked at about 4.5 MHz when driven by a suitable electrical excitation pulse.

The electronic instrumentation has been described in detail by the designer (Weight 1975). The principal components are a wide-band gated amplifier (0.5 - 20 MHz), provided with a calibrated attenuator, and an analogue spectrum analyser. The adjustable electronic time gate allows the signal of interest to be isolated from unwanted multiple echoes, etc. and fed into the spectrum analyser. The output from the analyser can be recorded on an X-Y plotter, as can the time-domain signal, via a sampling oscilloscope.

The delay facility between the beams of a double-beam oscilloscope (Tektronix 556 with 1A1 and 1A2 plug-in units) was employed for time-of-flight measurements. This was calibrated with a very accurate 10 MHz sine wave, and proved to be linear over the range of delays used in the experiments.

6.3.3 Longitudinal velocity measurements

A simple pulse-echo technique was used. The sample and transducer were immersed in water and the sample was aligned perpendicular to the ultrasonic beam. Echoes from the front and back faces of the sample were observed. Accurate alignment was carried out by first adjusting for maximum echo amplitude, and then finally adjusting for maximum high frequency components in the spectrum.

The echoes were displayed on both beams of the double-beam oscilloscope and the calibrated delay was adjusted so as to superimpose the traces exactly. The delay was then adjusted to shift one trace so that the back-face echo coincided with the front-face echo on the other trace. Because of the frequency-dependant attenuation, and the phase reversal occuring upon reflection at the front face, the back-face echo had a smoothed waveform and opposite polarity compared with the front face echo. For most accurate results, the back-face echo trace was therefore amplified and inverted and the initial steep rises of the echoes were superimposed. Thus the time delay due to the pulse travelling twice through the sample of known thickness was obtained, to an accuracy of better than 1% in every case.

The thickness of the sample was measured with a micrometer, and the density was calculated from the dimensions and mass.

The results are given in Table 6. The precision of the longitudinal velocity measurements (~1%) is more than adequate for lens design, but it should be noted that the results do not correspond to a well-defined frequency or temperature. If they are regarded as measurements at 5 MHz and 20°C then the probable error is about 2%. Literature values of shear velocity are also given - they will be referred to later.

TABLE 6 MEASURED LONGITUDINAL ACOUSTIC VELOCITIES AND ACOUSTIC IMPEDANCES OF PLASTICS

	Sample thickness mm	Longitudinal velocity c $km.s^{-1}$	Density $10^3 kg.m^{-3}$	Acoustic impedance $Z = \rho c$ $10^6 kg.m^{-2}.s^{-1}$	Shear velocity (a $km.s^{-1}$
Perspex	12.9	2.73	1.19	3.25	1.35
Polystyrene	12.9	2.32	1.05	2.44	1.12
Nylon 6	11.8	2.76	1.15	3.17	1.12(b
Polyethylene	7.05	2.10	0.92	1.93	0.98

(a) Mean of values quoted by Hartmann and Jarzynski (1974)

(b) Value for nylon 6,6.

6.3.4 Longitudinal attenuation measurements

A water-immersion pulse-echo technique was again used, and the experimental arrangement is illustrated in Fig.28. The ultrasonic beam was initially aligned perpendicular to the plane glass reflector and the spectrum of the echo-pulse was recorded; this was the 'reference'

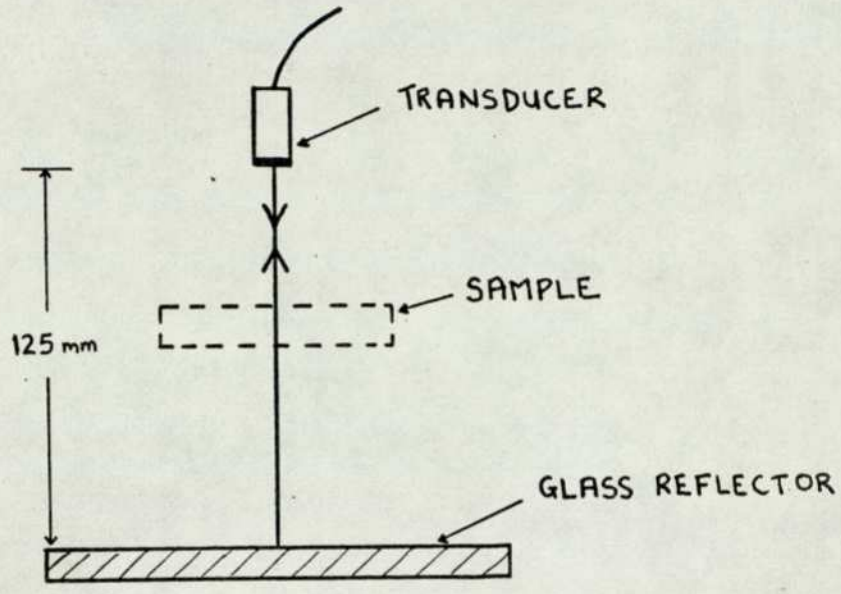

Fig.28 THE EXPERIMENTAL ARRANGEMENT FOR MEASUREMENTS OF ACOUSTIC ATTENUATION.

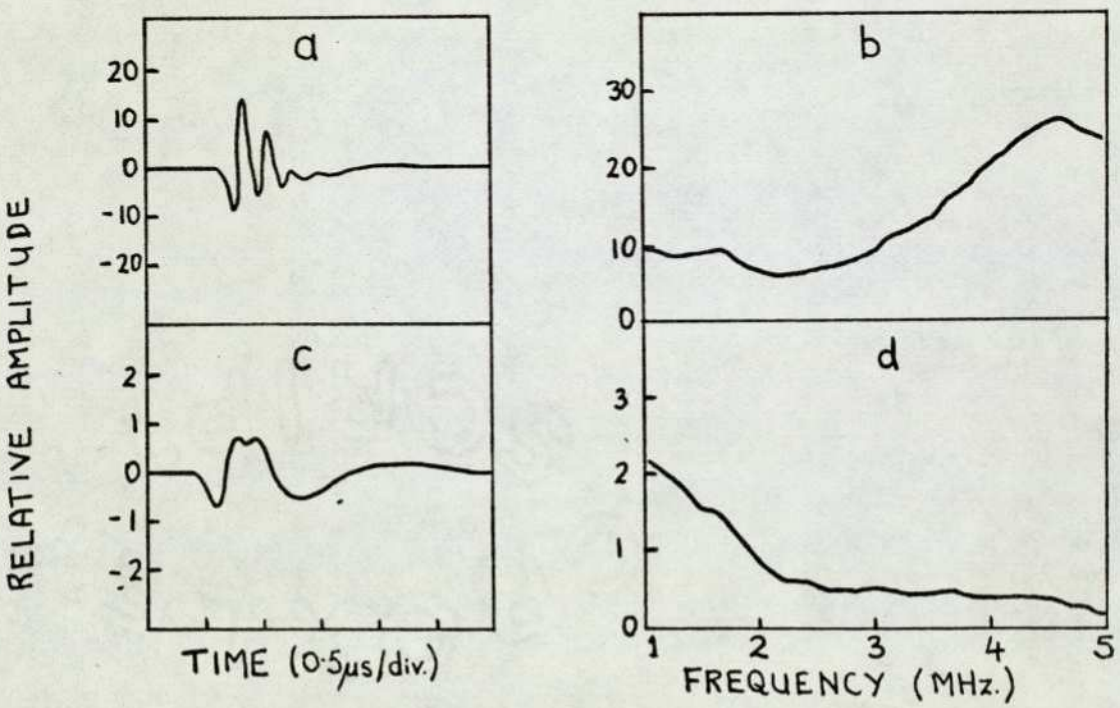

Fig.29 ECHO WAVEFORMS AND CORRESPONDING FREQUENCY SPECTRA: (a),(b) REFERENCE ECHO FROM GLASS REFLECTOR; (c),(d) ECHO WITH A SAMPLE OF NYLON 6 of 12 mm THICKNESS INTERPOSED.

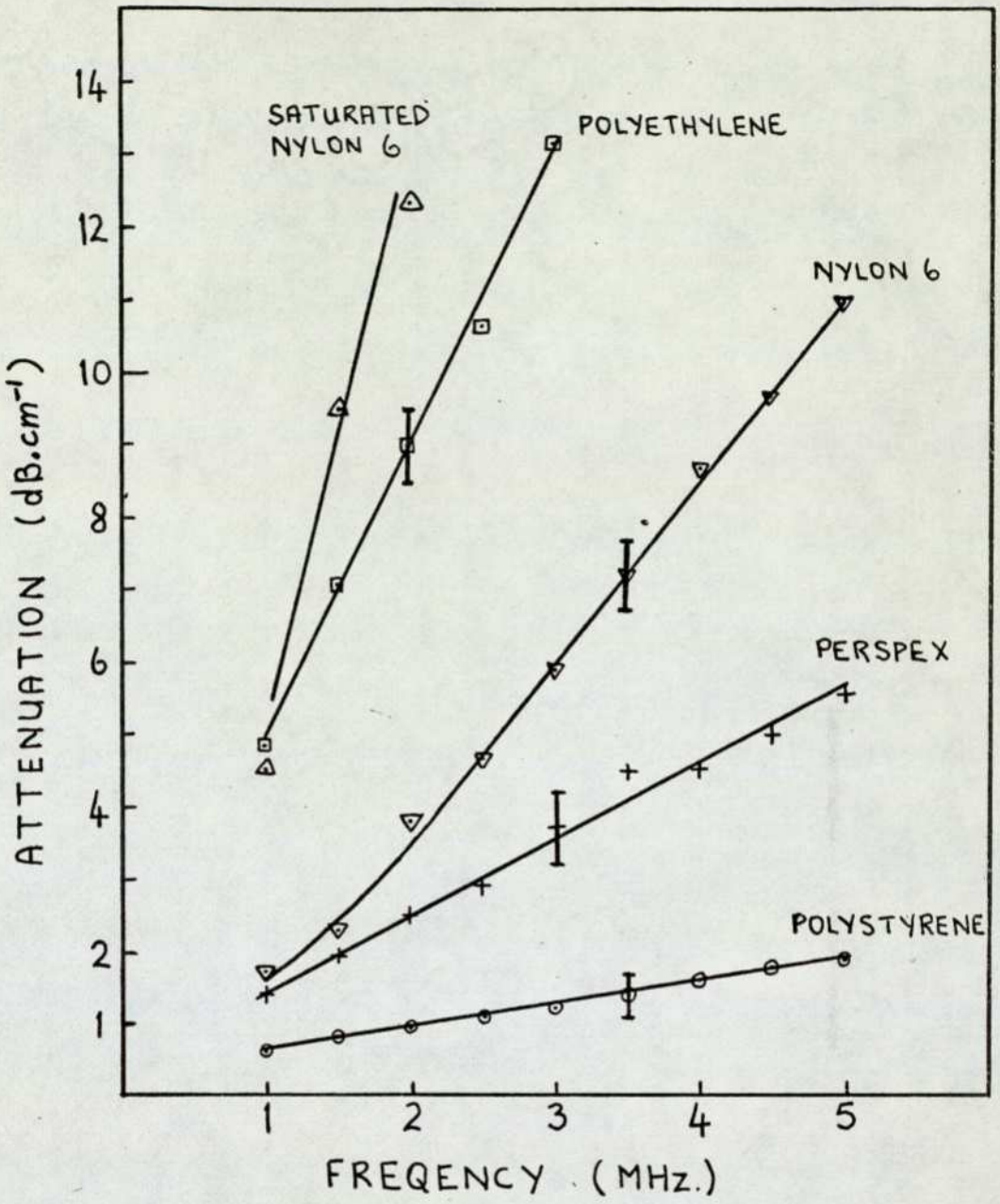

Fig.30 MEASURED LONGITUDINAL ACOUSTIC ATTENUATIONS AS A FUNCTION OF FREQUENCY IN VARIOUS PLASTICS.

spectrum. The sample was then interposed about midway between the transducer and reflector and perpendicular to the beam (although the alignment was not critical in practice), and the modified spectrum was recorded. The total energy loss due to the double-pass through the sample could thus be calculated at any frequency in the recorded spectrum. Examples of pulse waveforms and frequency spectra are shown in Fig.29.

In order to avoid the effects of non-linearities in the amplifiers and display, the loss at 0.5 MHz frequency intervals was determined more accurately by comparing the attenuation necessary to bring the displayed spectrum up to the same amplitude both without and with the sample present.

The total loss is the sum of attenuation and reflection components. The reflection loss at the sample-water interfaces was calculated from the fundamental formula (Equ.29) using the measured impedance values from Table 6. As a check, the reflection coefficient was determined experimentally. The amplitude of the echo from a material of high, known impedance (aluminium) was compared with that from the sample at the same range, again by means of the calibrated attenuator. The results were in perfect agreement with theory within the limits of the equipment ($\pm$ 0.5 dB for the reflection coefficient, corresponding to better than $\pm$ 0.1 dB for the transmission coefficient).

A possible source of error was investigated: the reduction in sonic path resulting from interposing the sample. The glass reflector was moved 10 mm closer to the transducer, reducing the sonic path by 20 mm, and the spectrum of the echo was compared with the standard. There was no measurable difference. As the largest reduction in sonic path incurred was equivalent to 12 mm of water, it was concluded that any error was negligible.

The results, plotted in Fig.30, indicate a linear relationship between attenuation and frequency. The attenuation in polystyrene is lower by a factor of three than in the next-best material, Perspex. The 'saturated nylon' result will be referred to in Section 6.5.

Samples of nylon 66 and nylon 11 were also tested. In each case, as the sample was moved laterally across the ultrasonic beam the shape and spectrum of the pulse changed significantly, and it was impossible to measure the attenuation because of this acoustic inhomogeneity. Careful examination by eye revealed a ring structure in the materials (obtained in cast rod form), and the manufacturers confirmed that the problem

was caused by thermal gradients occurring during casting.

6.4 Effect of attenuation in lenses on system performance

The significance of the measured attenuations for the design of a sonic system can be estimated. The 'optical' design of a sonic system (see Chap.7) imaging objects in water (or a material of similar sound velocity such as biological tissue) requires that, for a transverse field of view of 60 mm, the maximum thickness of a plastic lens is more than 30 mm and the 'average' thickness is about 10 mm. Since the ultrasound passes through two lenses twice, these figures are multiplied by four to obtain the total lens thickness traversed. Rough estimates of the attenuation loss in systems designed for medical work at 2 MHz are therefore: using polystyrene lenses 4 dB, perspex 10 dB, nylon 6 16 dB, and polyethylene 35 dB. Thus polyethylene must be ruled out, and probably nylon 6 as well.

It should be borne in mind that the above estimates are crude averages. An ultrasonic ray passing through the centre of the lenses suffers comparatively little loss whereas a ray passing through the outermost parts is attenuated by roughly three times as much. This has two consequences. Firstly, for an object near the edge of the field of view, both the insonifying rays and many of the reflected rays pass through the outer regions of the lens. Therefore the sensitivity can fall off considerably towards the edge of the field of view, which is thereby effectively reduced. Secondly the effective diameter of the lenses is reduced, thus degrading the diffraction-limited resolution. These factors make it even more important than is at first apparent to keep the attenuation to a minimum.

The estimated losses refer to a 2 MHz water or tissue-imaging system. In the non-destructive testing (NDT) of metals etc., a higher frequency must be used in order to achieve similar resolution, because of the greater sound velocities in these materials; 5 MHz is typically employed. Calculations from the design formulae given by Hanstead (1974) and ray-plots not reproduced in this report showed that a DUVD system imaging steel, with the same field of view as the medical system, requires thinner lenses. To a first approximation, this reduction in lens thickness counterbalances the increase in attenuation due to the higher frequency, so that the lens attenuation losses in medical and NDT systems are similar.

The conclusion is that, on the grounds of attenuation losses,

polystyrene is the best lens material for a DUVD sonic system. Perspex is a poor second choice.

6.5 Acoustic energy transmission at oblique incidence

When a plane longitudinal acoustic wave is incident normally upon an extended plane interface with another medium, only longitudinal reflected and transmitted waves are produced, as already described (Equs. 28,29, and Fig.27). In fact, in a sonic system longitudinal waves are generally incident non-normally upon boundaries between liquids and solid lenses. The situation is complicated by the production of both longitudinal and shear (transverse) waves in the solid at these oblique angles.

The theoretical formulae for the reflection and transmission coefficients involved (Mayer 1965) are not simple. Therefore they were programmed into a computer and calculated for various combinations of lens materials and liquids, using the data of Table 1 (P.28) and Table 6 (P.63).

Fig.31 shows the most important coefficient, the longitudinal energy transmission coefficient, plotted against angle of incidence in the liquid for various liquid/lens boundaries. The coefficient is the same for transmission from the lens to the liquid, the angle still referring to the angle in the liquid. All the curves fall gradually with increasing angle of obliquity, then suddenly drop to zero at the critical angle for longitudinal wave transmission.

The coefficients for water/polystyrene and ethanol/polystyrene differ by 0.75 dB at normal incidence due to the better impedance match of the former combination, but they exhibit the same general fall-off. The curves for di-iodomethane/nylon and di-iodomethane/Perspex illustrate that, even in cases of nearly perfect impedance matching, the transmission falls with increasing angle. Here, however, the rates of fall differ because the shear velocity is higher in Perspex than nylon and more energy is converted into shear waves in Perspex.

In the DUVD sonic systems designed by ray-plotting (Chap.7) the range of angles of incidence does not exceed about 2/3 of the critical angle. This is because aberrations become intolerable at greater angles. A crude average for the angles of incidence encountered by rays insonifying and reflected from an object at the edge of the designed field-of-view is 1/3 of the critical angle per lens/liquid interface; for an axial object, the average is about 1/6 of the critical angle. By reference to plots such as these in Fig.31, it may be estimated

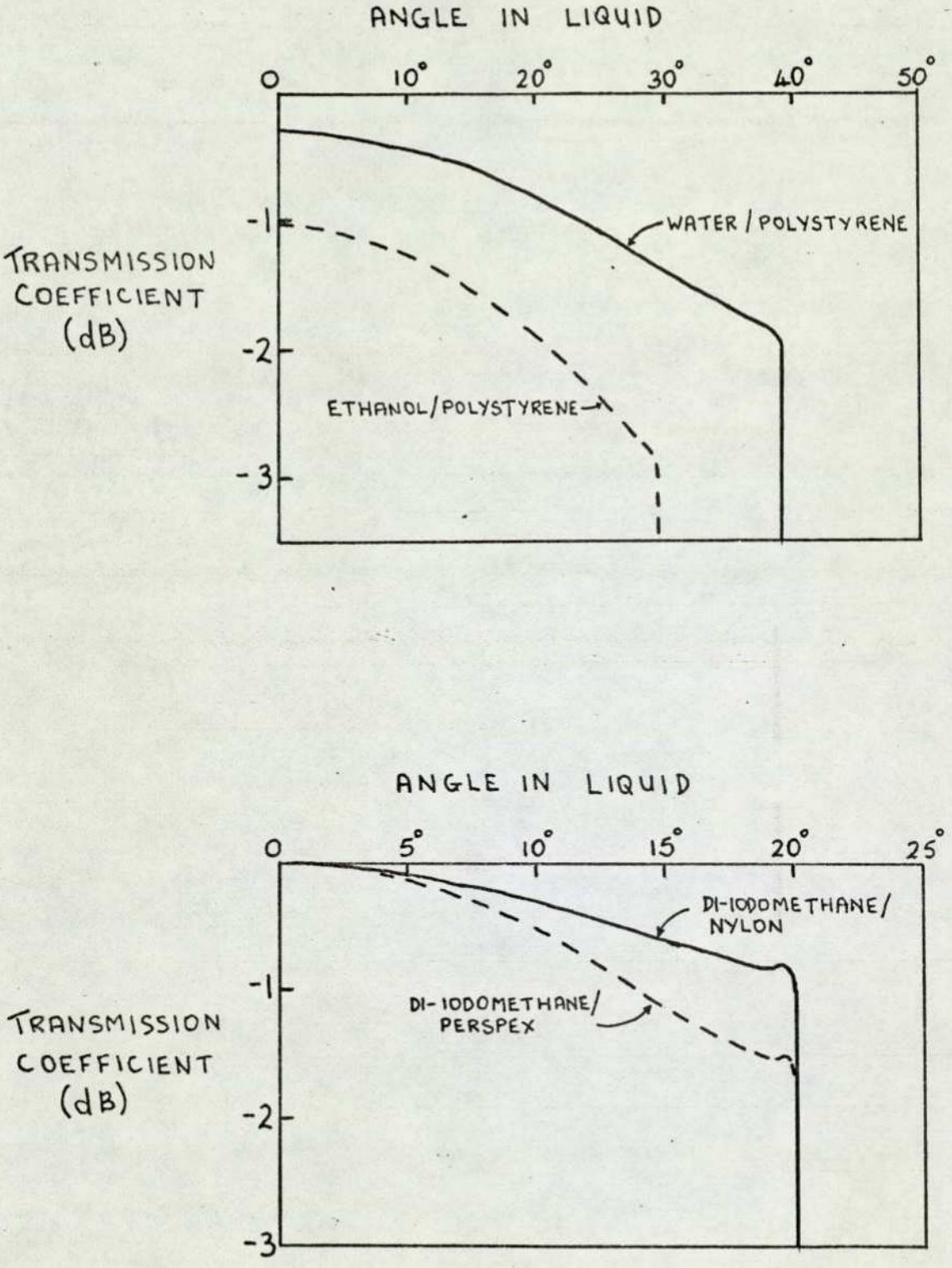

Fig.31 LONGITUDINAL-WAVE ENERGY TRANSMISSION COEFFICIENTS AT VARIOUS PLASTIC/LIQUID INTERFACES, AS A FUNCTION OF ANGLE IN THE LIQUID.

that the extra losses incurred as a result of oblique incidence are negligible for axial objects and amount to about 0.25 dB per interface (2 dB in all) for objects at the edge of the field-of-view. The effect is less important than attenuation in the lens material.

Therefore the normal incidence coefficient (Equ.29) adequately respresents the transmission characteristics of a plastic lens/ liquid boundary. It should, however, be noted that the effects of oblique incidence cause a drop in sensitivity of about 2 dB at the edge of the DUVD field.

6.6 Chemical and physical resistance of lens materials

Many liquids of good visualisation figure-of-merit are also good solvents, and polystyrene and Perspex, the best sonic lens materials, are extremely susceptible to solvent attack. Although a certain amount of information is available from manufacturers' data and handbooks (for example Brandrup and Immergut, 1975) the only sure way in many cases to discover if a particular plastic and solvent are compatible is by experiment.

Immersion tests were carried out on samples of polystyrene and Perspex in the selected liquids whose figures-of-merit had been determined experimentally (Chap.4). The results of a superficial inspection after two weeks are presented in Table 7.

TABLE 7 ACTION OF SELECTED LIQUIDS ON POLYSTYRENE AND PERSPEX

Liquid (ref. Nos. as in Table 1)	Action (✓ denotes unaffected x denotes dissolved)	
	Polystyrene	Perspex
1. Water	✓	✓
2. Carbon tetrachloride	x	slightly attacked
3. Bromoform	x	x
4. Chloroform	x	x
5. Di-iodomethane	x	✓ (colours)
6. Iodo-methane	x	x
11. Ethanol	✓	✓
23. Bromobenzene	x	x
27. Benzene	x	x
31. Hexane	✓	✓
32. Toluene	x	x

Polystyrene is dissolved by most of the liquids and is less resistant than Perspex. Nylon and polyethylene are not dissolved by any of the liquids in Table 7.

Although nylon has good chemical resistance, it has high water absorption - about 6% at saturation in nylon 6, according to the manufacturer's data. The effect of water absorption on the ultrasonic properties of nylon 6 was therefore investigated.

Samples were immersed in water, both at room temperature and at 80°C for accelerated testing, and weighed periodically. The rate of absorption was most rapid at first, then flattened off as the saturation value was reached. (This took about 2 months at room temperature). It was confirmed that the saturation absorption was about 6%, although this value was attained only in samples less than 6 mm thick.

The ultrasonic velocity and attenuation were measured in a saturated sample 12 mm thick which had absorbed 2.5% of water. The velocity was 2.67 km. s^{-1}, about 10% less than the value in the 'dry' material, and the attenuation had more than doubled, as shown by the 'saturated nylon' results plotted in Fig.30.

A lens made of nylon 6 cannot therefore be left in prolonged contact with water. Data on the water absorption in different nylons varies, but it appears that it is lower in nylon 11 and 12 by a factor of at least three. One of these may be suitable for water contact. The sample of nylon 11 obtained was not sufficiently homogeneous for measurement, as already mentioned.

If it is desired to use a lens material and visualising liquid which are incompatible, then the lens must be protected with a thin, acoustically transparent, film. Possible protective films are a heat-shrunk polyethylene sheet and a deposited metallic film. However, such techniques remain to be investigated in practice.

6.7 Choice of visualising liquid

The theoretical visualisation figures-of-merit of many liquids have been given in Table 1 (P.28) and have been confirmed experimentally for selected liquids. (Table 4, P.38). The most promising liquids have about 9 dB advantage over water. In order to determine their effective sensitivity in a complete visualisation system, the acoustic impedance matching must be taken into account.

The effective sensitivities of the liquids in Table 4 when used in the transducer image sonic system (Fig.26) were calculated, and the results are given in Table 8. Also shown are the measured figure-of--merit M, the energy transmission coefficient T_t from a PZT transducer into the liquid, and the transmission T_l from the liquid into a typical plastic lens of impedance 2.5×10^6 $kg.m^{-2}.s^{-1}$, all these values being relative to those for water. The sensitivity was calculated from the formula:

effective sensitivity = $M + T_t + 2\,T_l$,

where the values are expressed logarithmically in decibels.

TABLE 8 EFFECTIVE SENSITIVITIES OF SELECTED VISUALISING LIQUIDS IN A DUVD SYSTEM (relative to water).

	Acoustic impedance Z $10^6 Kg.m^{-2}.s^{-1}$	Measured figure-of--merit M dB	Transducer transmission Coefft. T_t dB	Lens transmission coefft. T_l dB	Effective sensitivity (b) $M+T_t+2\,T_l$ dB
1. Water (a	1.48	0	0	0	0
2. Carbon tetrachloride	1.49	8.0	0	0	8.0
3. Bromoform	2.67	7.5	2.5	0.3	10.6
4. Chloroform	1.49	7.5	0	0	7.5
5. Di-iodomethane	3.20	8.2	3.3	0.2	11.9
6. Iodomethane	1.92	7.9	1.1	0.2	9.4
11. Ethanol	0.92	5.6	-2.1	-0.7	2.1
23. Bromobenzene	1.73	5.3	0.7	0.2	6.4
27. Benzene	1.16	6.1	-1.1	-0.3	4.4
31. Hexane	0.72	8.1	-3.1	-1.3	2.4
32. Toluene	1.48	5.5	0	0	5.5

(a) The absolute values of the transmission coefficients for water are: $T_t = -7.9$ dB, $T_l = -0.3$ dB.

(b) Higher figure indicates better sensitivity.

The acoustic impedance matching has as great an influence on the effective sensitivity as does the figure-of-merit. The effective sensitivity of a high-impedance liquid, di-iodomethane, is almost 10 dB greater than that of a low-impedance liquid, hexane. The low-impedance liquids appear to be ruled out since the small gains in sensitivity hardly justify their use in preference to water. The most promising visualising liquids are those of high figure-of-merit and high acoustic impedance. Since a requirement for a high figure-of-merit is a low

acoustic velocity, and $Z = \rho c$, these liquids have very high densities.

The most promising liquids are also good solvents (see Table 7). The only liquids in Table 8 which do not attack polystyrene (the best lens material) are hexane and ethanol, which have poor effective sensitivity. The second choice lens material, Perspex, is resistant to the liquid of apparently greatest sensitivity, di-iodomethane. However, this liquid has one crucial shortcoming - it turns deep red on exposure to light, and attenuates the intensity of a light beam by a factor of about 30 per cm. Unless some means can be found of preventing the colour change, di-iodomethane is ruled out as a practical visualising medium. If a resistant nylon lens were used, its high attenuation would nullify most of the advantage gained from using a sensitive liquid.

Therefore, of the visualising liquids studied in detail, none is both compatible with the best plastic lens materials and offers sufficient gain in system sensitivity to justify its use in preference to water. The most promising liquid is bromoform, which could potentially increase sensitivity by about 10 dB. In order to exploit this gain a way of protecting the lens material would have to be found. Alternatively a wider search for suitable liquids might produce one compatible with the lens materials.

6.8 Summary

The design of a sonic system of optimum sensitivity is primarily a problem of materials. A basic sonic configuration of two thin plastic lenses in liquid media is indicated. Water is the best liquid for coupling the object to the system and for occupying the volume between the lenses: it is also the most convenient liquid to use as the visualising medium.

The problems arise in the choise of lens material(s) and visualising liquid. Plastics have high acoustic attenuation, and it is therefore important to choose the one of lowest attenuation. Polystyrene is the best readily-available material. Water is not a sensitive visualising medium, and several organic liquids could increase the overall sensitivity of the visualisation system by about 10 dB. However they are good solvents which dissolve polystyrene (and Perspex, the second choice). The use of the more resistant nylon is not a solution because of its high attenuation.

Thus, if optimum sensitivity is to be achieved with the sonic configuration considered here, either a method of protecting plastics from solvents must be developed or a wider search for a compatible, yet sensitive, liquid performed. These developments were not pursued because of limitations of time.

CHAPTER 7 'OPTICAL'DESIGN OF SONIC SYSTEMS

The shortcomings of the DUVD systems demonstrated by Hanstead were not only in sensitivity, which has been the main concern of the report so far, but also in resolution. However, the poor resolution was not a fundamental limitation, for no attempt was made to control aberrations. In this chapter the 'optical' design of some simple sonic systems is described, with the main aims of determining the useful field of view and optimising the resolution over that field.

7.1 Introduction

It has been concluded in Chap.6 that the most promising sonic configuration is that shown in Fig.26 (P.58), consisting of two thin plastic lenses in liquid media, with insonification of the object by the transducer image method. Since the resolution required - of the order of the ultrasonic wavelength - is considerably less demanding than is required in an optical system, there appeared to be scope for obtaining adequate resolution by optimising the design of a system employing simple spherical-surface lenses, without introducing such refinements as aspherical surfaces, multi-element lenses or correcting lenses.

The fundamental differences between an optical system and a DUVD system suggest that direct application of optical techniques of balancing the various analytically-described aberrations over the field in order to achieve an optimum is difficult. Nevertheless, some understanding of aberration theory is useful, as will be seen. Ray-tracing methods (extensively employed in modern optical design) are, on the other hand, ideally suited to sonic applications; for the resolution needed is such that the performance of a system can be conveniently assessed by inspection of ray-plots showing complete ray paths from the object to the image.

Hanstead (1973) demonstrated the power of a computer-assisted ray-tracing method in the design of a DUVD configuration not subsequently put into practical form. Facilities, developed by Hanstead,for ray-tracing using a desk-top programmable calculator (Tektronix Tek 31) with linked plotter (Digital Plotter 4661)were available at CEGB Portishead. It was therefore decided to use an empirical ray-tracing method to optimise the design of some sonic systems. Only systems suitable for imaging media with average

velocity similar to water (e.g. biological tissue) were studied in detail, but the general conclusions can probably be applied to other types of system.

7.2 Paraxial design equations

The paraxial design equations for a two-lens DUVD system, derived by Hanstead (1973, 1974a), are given in Table 9, and the symbols are defined in Fig.32 above it. The following important properties of the system are worth re-iterating: the nearer focal points of the lenses are coincident, the focal length in the image medium is a factor of $\sqrt{2}$ times that in the object medium, and the longitudinal magnification is $\sqrt{2}$ times the transverse magnification. All dimensions are conveniently expressed in terms of the focal length f_1 of the first lens in the object medium, and this natural length unit will be referred to simply as a 'unit'.

Although the focal lengths of each lens are specified, the radii of curvatures of the lens surfaces can take on a wide range of values. This freedom to 'bend' the lens into a variety of shapes can be made use of in order to reduce aberrations. The equation expressing the possible radii of curvature of a lens of specified focal length is quoted in Appendix 3 (Equ.a27).

7.3 Field of View

In the paraxial design formulae, the only limits to the field are longitudinal, such that no object can be nearer than the object lens, nor further than the distance where its image coincides with the image lens. The useful field of view in a practical system is, of course, more limited, both longitudinally and transversely.

The most fundamental limitation is due to the finite apertures of the lenses, and means that the useful angular cone of rays from an object, i.e. the cone which passes through the lenses and forms an image, becomes smaller with increasing distance from the middle of the field. This purely geometrical factor was investigated by some simple manual ray-tracing under paraxial assumptions. For a DUVD system comprising two f1 lenses in one sonic medium, the dimensions of the region where the useful cone of rays was greater than half the maximum value were about 0.5 units transversely

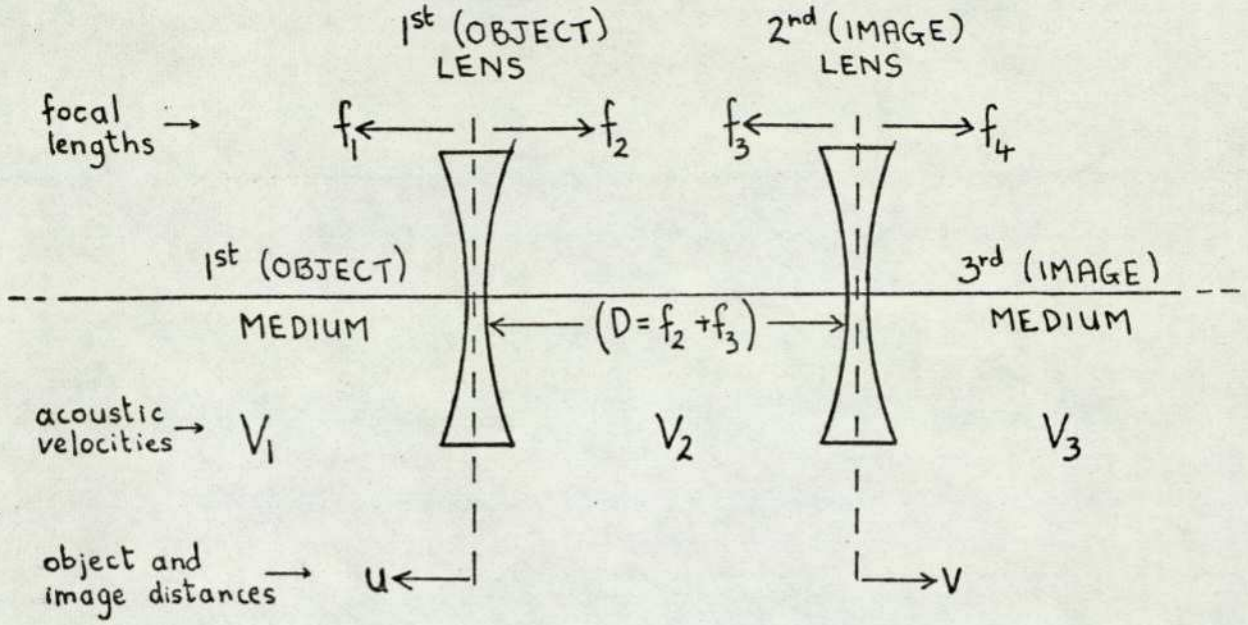

Fig.32 - SYMBOLS FOR THE PARAXIAL DESIGN OF A 2-LENS DUVD SYSTEM

TABLE 9 DESIGN EQUATIONS FOR 2-LENS DUVD SYSTEM (paraxial analysis)

Symbol	Definition	Value in terms of independent variables
V_1	Sonic velocity in 1st medium	Independent variables
V_2	Sonic velocity in 2nd medium	
V_3	Sonic velocity in 3rd medium	
f_1	1st focal length of 1st lens	
f_2	2nd focal length of 1st lens	$V_1/V_2 \cdot f_1$
f_3	1st focal length of 2nd lens	$\sqrt{2}\ V_3/V_2 \cdot f_1$
f_4	2nd focal length of 2nd lens	$\sqrt{2} \cdot f_1$
D	Distance between lenses	$(V_1/V_2 + \sqrt{2}\ V_3/V_2) \cdot f_1$
u_{max}	Maximum object distance	$(1+V_1/\sqrt{2}\ V_3) \cdot f_1$
v_{max}	Maximum image distance	$(\sqrt{2} + 2\ V_3/V_1) \cdot f_1$
M_L	Longitudinal magnification	$-2\ V_3/V_1$
M_T	Transverse magnification	$-\sqrt{2}\ V_3/V_1$

(half the lens diameter) and 1 unit longitudinally.

A reduction in the useful cone of rays not only reduces the sensitivity, it degrades the fundamental limit of resolution imposed by diffraction. It has already been shown (Chap.6) that the effects of attenuation in the lens material and reduced transmission at oblique angles of incidence reduce the effective cone of rays for non-axial objects. Also the preliminary computer-calculated ray plots for a system of Perspex lenses in water showed that aberrations worsened rapidly outside the limits stated above.

Taking all these factors into account, it was decided that the design field over which aberrations were to be minimised would have dimensions of 0.8 x 0.4 units, as shown in Fig.33. The centre of the field is the focal point of the object lens, and the image field is therefore centred on the focal point of the image lens. The symmetry of the object and image fields leads to a useful economy in the design process.

7.4 Optimisation Procedure

The aim of the optimisation process was to obtain maximum resolution over the defined field. Owing to the use of the transducer image method of insonification, it was also necessary to ensure, by ray-tracing, that the field was adequately insonified. The procedure will be illustrated by referring to the first system considered, which comprised two Perspex lenses in water.

Once the sonic media and lens material of a sonic system have been chosen the paraxial design equations allow just two independent variables, the lens-bendings of the two lenses. Now the paraxial design may not be an optimum for non-paraxial rays from objects distributed over the field of view, and there are several parameters which might be varied in an effort to achieve an optimum design. In order to reduce their number to manageable proportions, a design framework was needed.

The basis of the framework was the symmetry of the sonic system and of the object and image fields. The paraxial formulae for the focal lengths were retained, so that the ratio of further focal lengths f_4/f_1 was $\sqrt{2}$. The ratio of the radii of curvature of the lens surfaces 'facing' each other in the second sonic medium was also set at $\sqrt{2}$,

$$\text{i.e.} \quad R_3/R_2 = \sqrt{2} \quad , \tag{32}$$

where the symbols are defined in Appendix 3.

The paraxial equation (Equ.a27) giving the possible bendings of a lens in terms of its focal lengths was used. Thus, through Equ.(32) the bendings of the two lenses became automatically linked. Finally, the lens separation D was not fixed at its paraxial value, but allowed to vary.

Only two adjustable parameters therefore remained to be explored by ray-tracing: the lens-bending of the first lens, and the separation of the lenses.

Aberrations can be minimised for any given axial object position using a standard optical result. As a starting-point for the optimisation procedure, the bending of the lenses was optimised for an object at the centre of the field of view. The derivation of the expressions for the radii is given in Appendix 3.

The apertures of the object and image lenses were initially set at 1 and 1.41 units, respectively. These correspond to apertures of f1, expressed relative to the focal lengths in the object and image media, respectively.

An array of 6 object positions was considered: one at the centre of the field and 5 at positions around the boundary, as indicated by crosses in Fig.33. A cone (or strictly speaking a fan) of rays separated by 15° intervals was traced through the system from each object. Plots for the system of Perspex lenses in water are shown in Fig.34. Purely for aesthetic reasons an array of 9 object positions (and corresponding images) is shown; the plots for the 3 objects below the axis are mirror images of those for the objects above the axis. The sharp focus at the centre of the field is clearly seen. A system, such as this, with both object and image media of water, has a lateral magnification of $\sqrt{2}$ and longitudinal magnification of 2.

For comparison, Fig.35 shows the performance of a system whose lens-bending was determined on the arbitrary basis of each lens having two equally concave surfaces ($R_1/R_2 = -1$).

The ray-tracing program incoporated a special feature which simulated the actual mechanism of DUVD image formation. The point on each ray representing a given constant transit time from a transducer (placed adjacent to the object) to the object to the image field could be

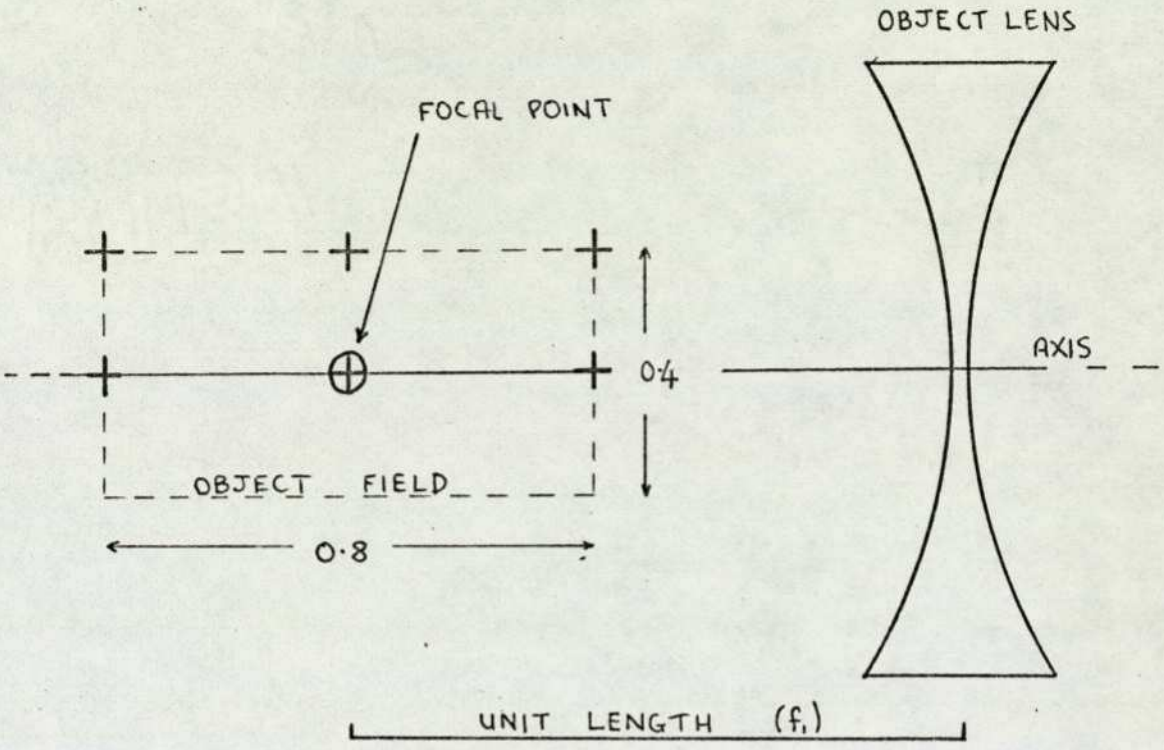

Fig.33 THE DESIGN FIELD OF VIEW OF THE SONIC SYSTEM.

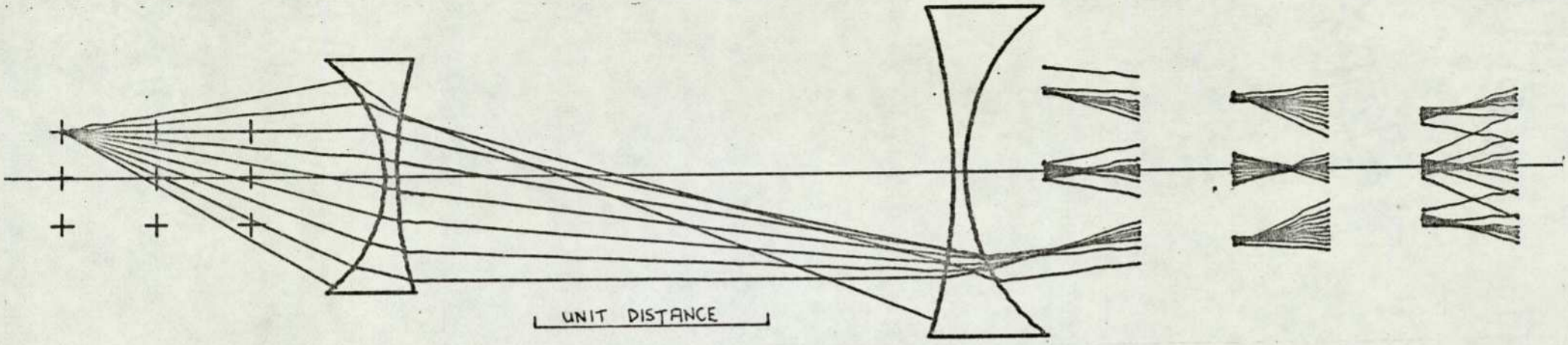

Fig.34 A SONIC SYSTEM OF PERSPEX LENSES IN WATER WITH LENS-BENDING OPTIMISED FOR AN OBJECT AT THE CENTRE OF THE FIELD: RAY PLOTS FOR A MATRIX OF OBJECT POSITIONS.

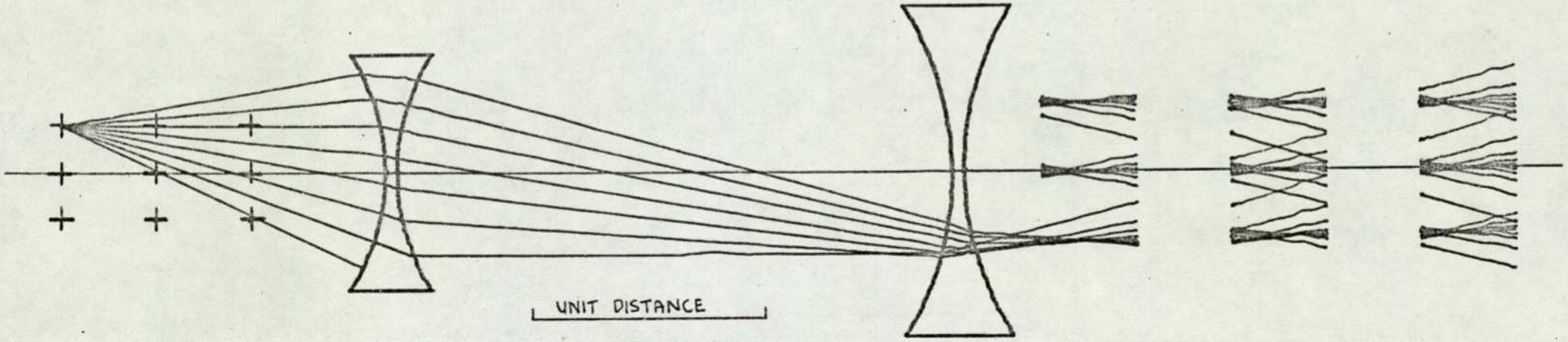

Fig.35 RAY PLOTS FOR A SYSTEM OF PERSPEX LENSES IN WATER WITH 'EQUAL RADII' LENS BENDING (i.e. SYMMETRICAL LENSES).

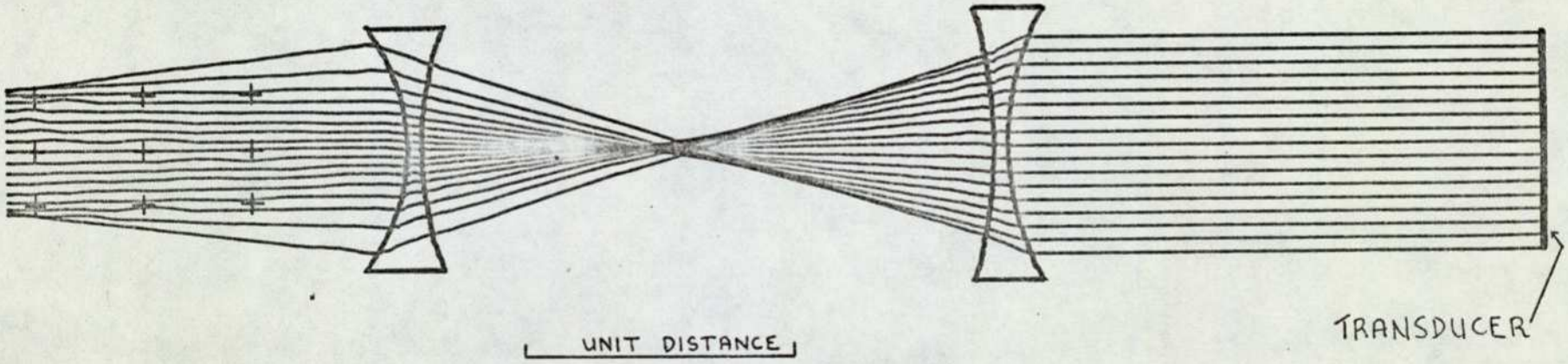

Fig.36 FINAL OPTIMISED DESIGN OF PERSPEX LENSES IN WATER (SYSTEM S1):
RAY-PLOT SHOWING UNIFORM INSONIFICATION OF OBJECT FIELD.
RAYS TRAVEL RIGHT-TO-LEFT FROM THE TRANSDUCER.

indicated, such points being termed 'isochrons'. Thus the transit time could be adjusted to produce the best image just as the light flash delay is adjusted in practice.

The performance of each modified form of sonic system was assessed quantitatively by means of a resolution score obtained as follows: the isochron time was adjusted to an optimum and the number of isochron points inside an arbitrary transverse resolution limit (0.035 units) was determined. The 'scores' for each of the 6 images were added to give the total resolution score.

The lens-bending and the separation were then varied systematically, and the resolution scores were indicated on a map whose X and Y axes represented the bending and separation respectively. This enabled convergence to the optimum, indicated by the maximum score. In this way, the optimum design for focusing of rays reflected from objects distributed over the whole field was obtained.

However, this design was far from the optimum for focusing the insonifying rays from the transducer. The plane pulse emitted by the transducer was represented by rays parallel to the axis, and it was found that the whole of the design field was not insonified, due to convergence of the outer rays. It was therefore necessary to modify the design slightly to achieve uniform insonification of the field as shown in Fig.36.

The final step was to reduce the lens apertures to exclude rays which did not contribute usefully to the image, i.e. fell outside the arbitrary limits of resolution, at the same time being careful not to exclude any useful rays.

7.5 The Systems Designed

The full specifications of the optimised systems are given in Appendix 4. The designs all have lens-bending roughly midway between the optimum for rays from the centre of the field (as illustrated in Fig.34) and an 'equal radii' bending (Fig.35). The separation of the lenses is less, in every system, than the value given by the paraxial design equation (the sum of the paraxial nearer focal lengths). This is readily understood, for the cause of the aberrations is the over-deviation of rays by the outer parts of the lenses, which effectively reduces the focal lengths of the lenses.

Fig.37 is an expanded ray-plot showing the performance of the final design of the system of Perspex lenses in water, over an array of 15 object positions. The isochrons are indicated by ticks.

Fig.38 is a similar plot of an optimised system of polystyrene lenses in water. The resolution is not quite so good as is obtained with Perspex lenses, because Perspex has a higher 'sonic refractive index' in water than polystyrene, i.e. a higher acoustic velocity ratio to water. However, the difference in resolution is not sufficient to affect the conclusion of Chap.6 that polystyrene is the superior material because of its lower attenuation.

Configurations employing more sensitive visualising liquids as image media were also investigated. Fig.39 shows the performance of a system with bromoform as the image medium, the other media being water, and the lenses polystyrene. The magnification, and hence the image size, is smaller than in the previous plots because the acoustic velocity of bromoform is low compared to water.

The systems imaging a water-velocity object medium can be regarded as models of systems for imaging biological tissue, and in particular for medical applications. The model is not exact, however, since the average acoustic velocity in human tissue at 37°C is 1.540 km.s^{-1} (Wells 1969, p.155) compared to the velocity in water at 20°C of 1.480 km.s^{-1}, as used for the above designs. The tissue velocity can be matched by a coupling bath of warm water or saline between tissue and object lens in order to obtain an object medium of approximately uniform velocity. The sonic system could, of course, be modified for imaging tissue, but for interest's sake the performance of a 'water velocity' system in imaging a tissue-velocity medium was investigated by ray-tracing. The resolution obtained was negligibly different from that in water, and it was concluded that a single sonic system can be applied to object media with acoustic velocities differing by at least 4%.

7.6 Assessment of Resolution Achieved

The performance of the sonic systems should be compared with the fundamental limits of resolution imposed by the wave nature of ultrasound and the particular form of ultrasonic pulse to be employed. Optical diffraction criteria do not apply rigorously, since a short pulse has no well-defined wavelength, and the image is not formed on a

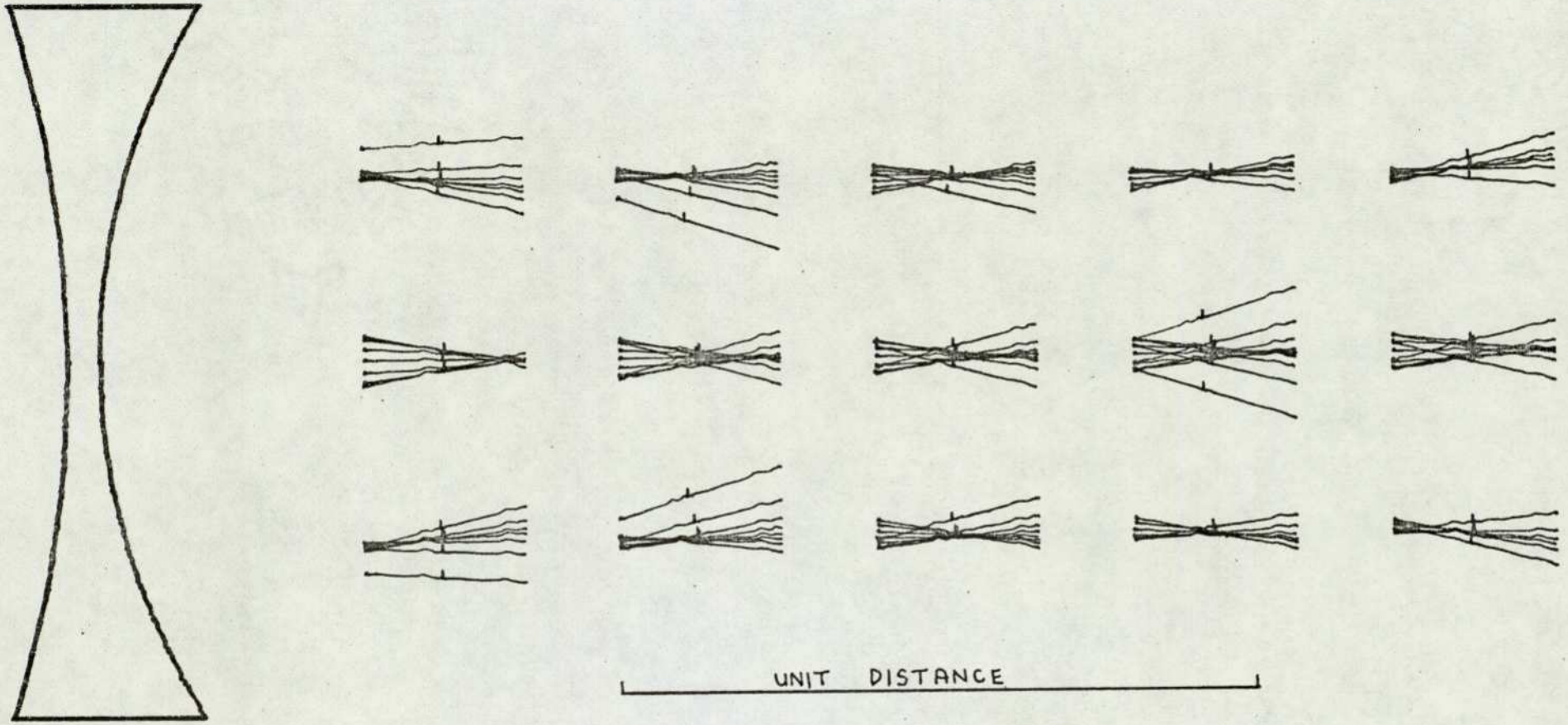

Fig.37 IMAGE FIELD OF OPTIMISED SYSTEM OF PERSPEX LENSES IN WATER (S1). ISOCHRONS ARE INDICATED BY TICKS.

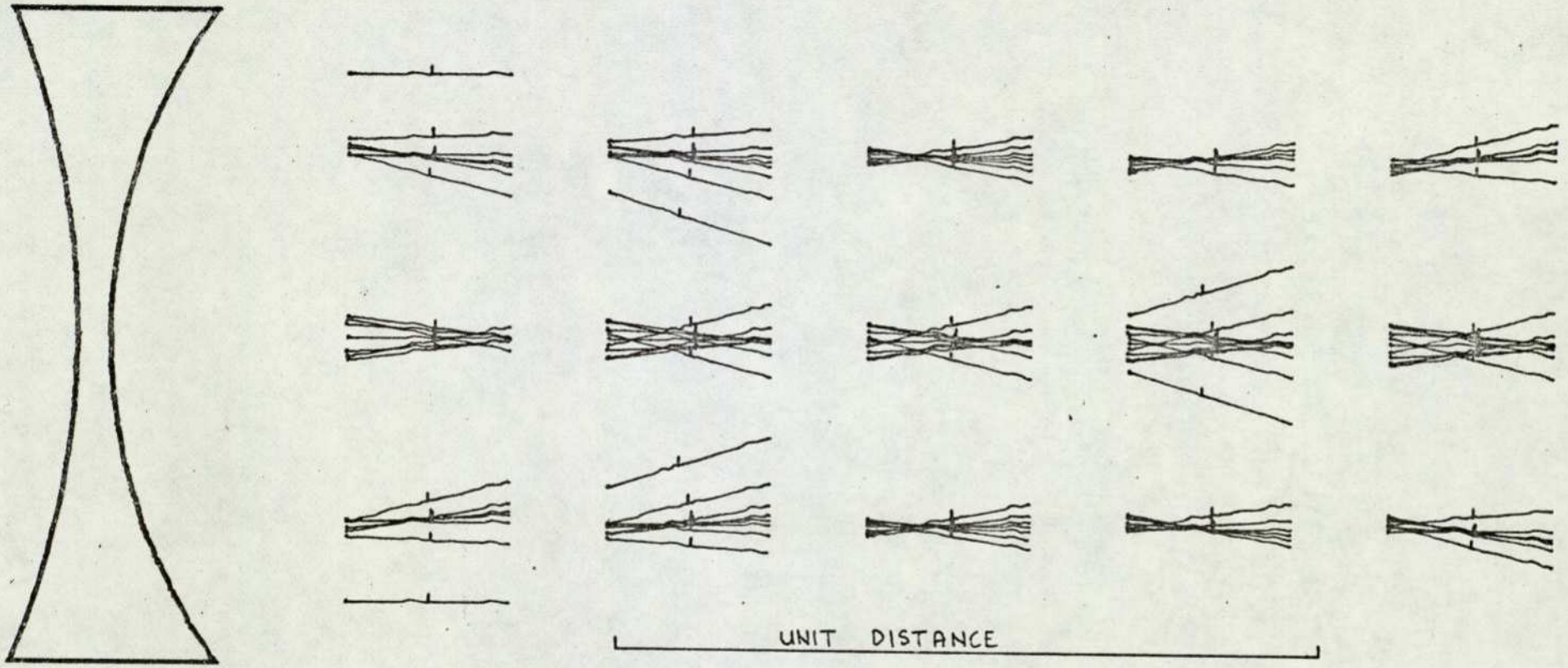

Fig.38 IMAGE FIELD OF OPTIMISED SYSTEM OF POLYSTYRENE LENSES IN WATER (S2).

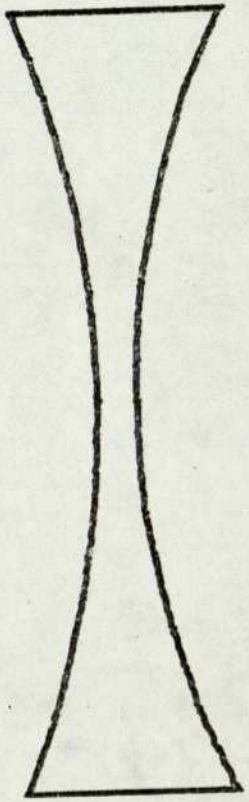

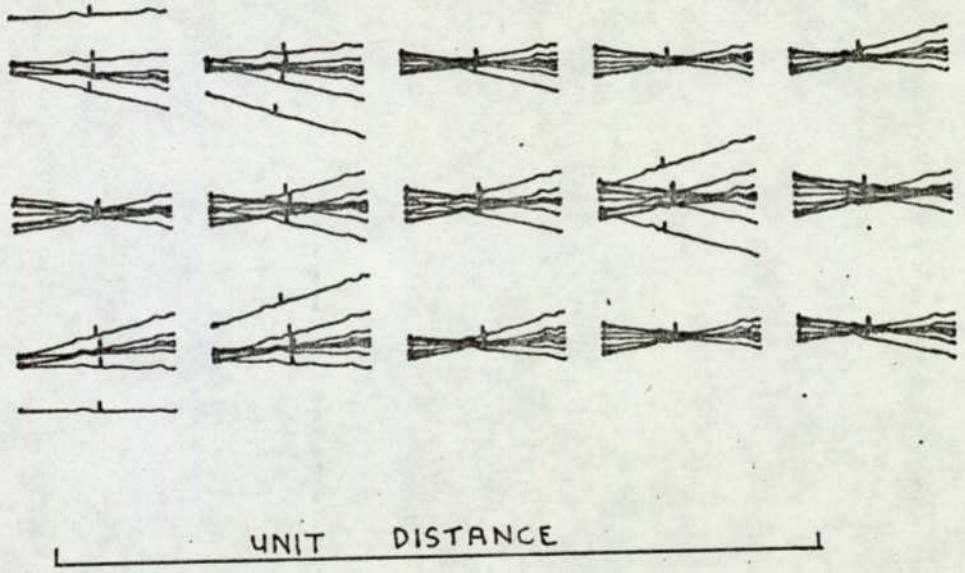

Fig.39 IMAGE FIELD OF OPTIMISED SYSTEM S4: POLYSTYRENE LENSES, BROMOFORM IMAGE MEDIUM, OTHER MEDIA WATER.

plane but is frozen at an instant in time (provided that the light flash is sufficiently short). Nevertheless, for present purposes we shall assume that the short pulse (say a single sinusoidal cycle) has an effective wavelength in the object medium of Λ, this being derived from the centre-frequency of the pulse spectrum.

The longitudinal spread of an image is equal to the pulse length, but since the longitudinal magnification of the system is equal to twice the ratio of wavelengths in image and object media, the longitudinal resolution is half the pulse length. For our short pulse this is approximately equal to $0.5\,\Lambda$.

The transverse resolution is determined by a criterion similar to the optical criterion - the radius R_A of the Airy disc. This gives

$$R_A = 1.2\ \Lambda/\sin\theta, \qquad (33)$$

where θ is the angle of the cone of rays from the object which pass through the system. The maximum value of θ in the optimised systems is about 55°, so that

$$R_A \sim 1.5\,\Lambda. \qquad (34)$$

With an effective wavelength of 0.75 mm (2 MHz in water) the transverse resolution limit is therefore about 1 mm. At the edges of the field of view, the cone of rays is smaller and the diffraction limit is about 2Λ (1.5 mm).

The above analysis does not take account of the following factors: firstly, attenuation and oblique incidence in the lenses, which reduce the effective apertures of the lenses; secondly, attenuation in the object (small in water but severe in tissue) which shifts the frequency spectrum of the pulse downwards and lengthens the effective wavelength. Thus the diffraction limits of resolution are, in practice, worse than indicated above.

The aberration-limited, or geometrical, resolutions of the optimised sonic systems were estimated from the ray plots (such as Figs.37-39) by measuring the dimensions (longitudinal and transverse) of the region containing 50% of the isochron points. This measure was adopted in order to be broadly consistent with the diffraction criterion, since the radius

of the Airy disc is approximately equal to the diameter of the disc containing 50% of the energy (viz. Born and Wolf 1970,p.398). The measured resolutions of the optimised systems are similar to each other: the longitudinal spreads are less than 0.005 units; the transverse resolutions range over the field of view from about 0.007 units to about 0.01 units. This is equivalent to about 40 'lines' of transverse resolution.

The absolute value of the geometrical resolution is proportional to the size of the system (proportional to the length unit), unlike the diffraction limit. If (as in Section 6.4) we base our calculations on a transverse field of 60 mm, since this might represent the minimum useful field of a medical abdominal scanner, then the length unit f_1 = 150 mm. The transverse resolution becomes approximately 1-1.5 mm, which is similar to the diffraction limits. The longitudinal geometrical resolution is about 0.75 mm - twice the fundamental limit.

The net resolution, made up of both diffraction and geometrical spreads, will be of the order of 1 mm longitudinally and 2 mm transversely for the system parameters considered above (Λ = 0.75 mm, f_1 = 150 mm, field 120 x 60 mm). Such a ratio of field size to wavelength appears to be near the optimum because the geometrical and diffraction spreads are about equal. If field size and wavelength are increased (or decreased) together in proportion, then the resolution changes in proportion too, while the number of resolvable lines across the field stays constant at about 120 longitudinally and 30 transversely.

The conclusion of this paper study is that a DUVD sonic system can be designed using simple (spherical surface) plastic lenses so as to obtain resolution comparable with the diffraction limits over a useful field of view in water or biological tissue. The field represents a longitudinal section of the object, of longitudinal extent (i.e. depth into the object) twice its transverse extent; the estimated possible resolution is equivalent to about 30 transverse 'lines' and 120 longitudinal lines.

Lack of time precluded proper investigation of NDT-type systems. However, preliminary ray-plots indicated that it should be possible to achieve a geometrical resolving power in steel similar to that in water.

CHAPTER 8 - PERFORMANCE OF EXPERIMENTAL SONIC SYSTEMS OF OPTIMISED DESIGN

8.1 The practical sonic lens systems

Two optimised sonic designs were constructed: one system of polystyrene lenses in water, and one of Perspex lenses in water. Because of the limited field of view of the schlieren system, the scale of both sonic systems was arranged to give an object field of 52 x 26 mm and a corresponding image field of 104 x 37 mm, the longitudinal magnification being 2 and the transverse magnification $\sqrt{2}$. The full specifications may be obtained from Appendix 4 by inserting the value of the length unit: $f_1 = 65$ mm.

The permitted tolerance in the lens surfaces is a small fraction of the ultrasonic wavelength, and so can be taken as around 0.1 mm. They were therefore manufactured (by the University Central Workshop) using standard machining techniques without any fine polishing. The minimum thickness of the bi-concave lenses was about 1 mm. Mounting of the lenses coaxially with the transducer (see next section) was achieved in a simple and easily adjustable arrangement, illustrated in Fig.40. The system was immersed in a water tank provided with schlieren-quality glass windows.

8.2 The Transducers

In order to insonify the desired cross-section or 'slice' of the object field, a long thin rectangular transducer was used. The transverse field (the width of the slice) is determined by the larger dimension of the transducer face, whilst the thickness of the slice is determined by the smaller dimension of its face.

It has been shown in Chap.5 that the major component of the pulsed near-field of a rectangular transducer is a well-defined plane pulse, so that the field approximates to a geometrical beam of uniform amplitude. In the far-field, the amplitude falls and the beam effectively spreads out. The approximate range for the start of the transition between near and far-field like behaviour, in so far as it affects the spread of the 'beam' is $d^2/4\Lambda$, where d is the corresponding dimension of the transducer face and Λ is the effective ultrasonic wavelength.

The transverse field required is sufficiently great that the insonifying pulse can be treated as a plane wave of well-defined transverse dimension. This assumption was made in the ray-plots of the insonification process (such as Fig.36, p.82), with the aid of which a transducer dimension of 0.7 units (45 mm) was selected.

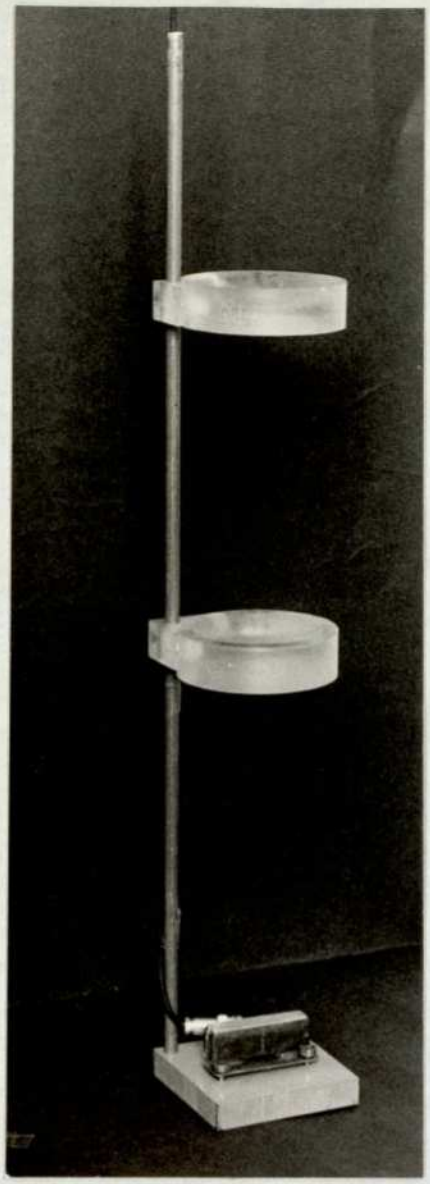

Fig.40 THE EXPERIMENTAL SONIC SYSTEM OF 2 POLYSTYRENE LENSES AND AN INSONIFYING TRANSDUCER.

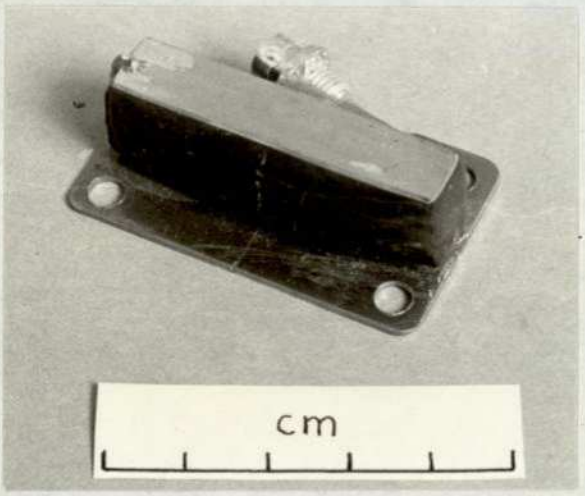

Fig.41 THE RECTANGULAR TRANSDUCER.

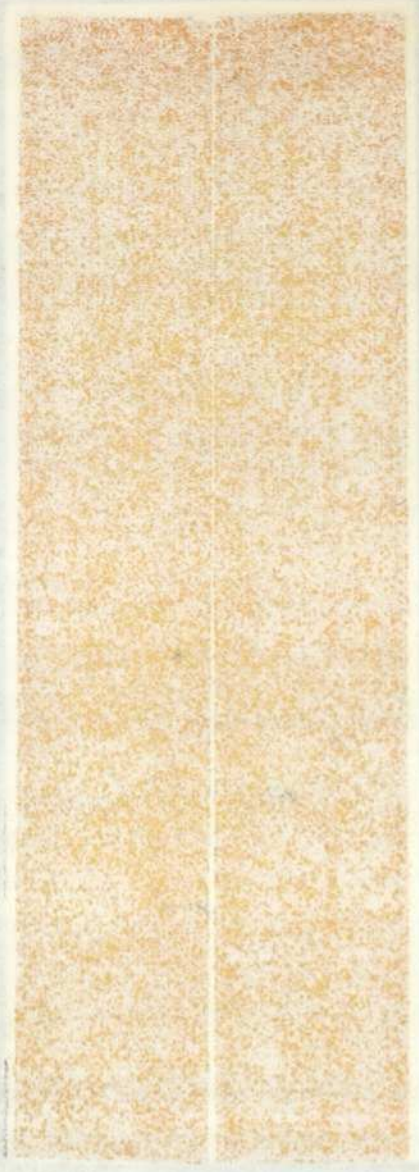

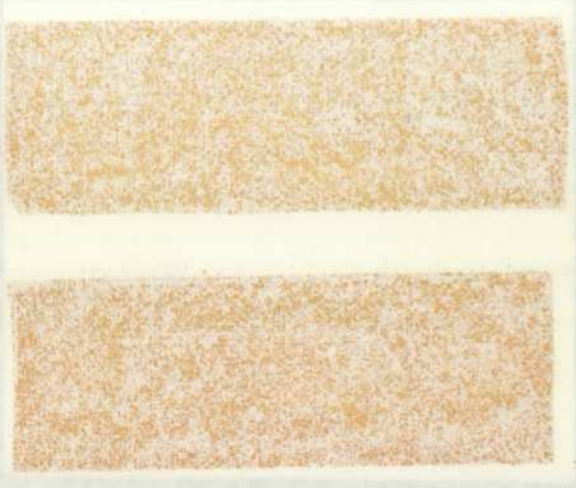

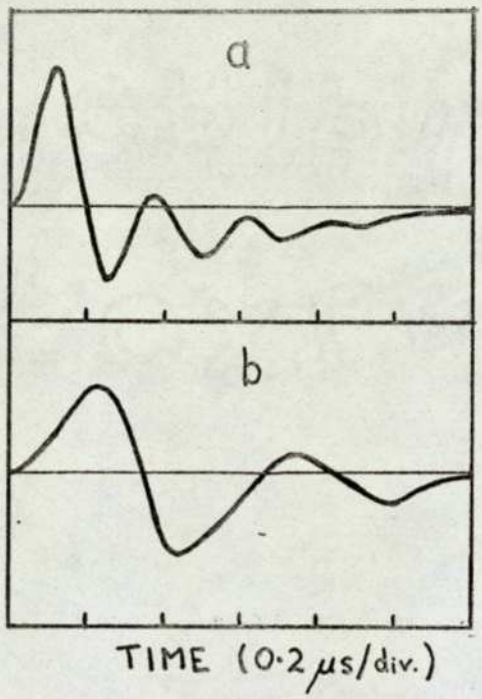

Fig.42 PRESSURE WAVEFORMS EMITTED BY (a) THE 4 MHz RESONANT FREQUENCY TRANSDUCER, (b) THE 2 MHz TRANSDUCER.

It is desirable that the thickness of the slice insonified is small, and therefore diffraction effects must be considered. In practice, a compromise has to be struck between a transducer of large thickness dimension (i.e. the smaller side of its rectangular face), giving a well-defined thick beam, and a narrow transducer, giving a narrow beam close to the transducer and a diffuse beam further away. A similar compromise is commonly made in the design of pulse-echo transducers. It should however, be remembered that, in the type of DUVD system considered here, it is not the transducer but its sonic image which is in 'contact' with the defect and the above diffraction arguments should be treated with caution. Experimental observations of the behaviour of an 'image transducer' are presented in the next section.

Two transducers were used, consisting of rectangular plates of PZT of 2 MHz and 4 MHz resonant frequencies respectively, backed by tungsten--powder-loaded epoxy. Each transducer face measured 45 x 9 mm, so that the smaller dimension of the image transducer in the object space was about 6.5 mm. The calculated approximate lengths of the near-fields in the object space were thus 27 mm (at 4 MHz) and 14mm (at 2MHz), compared with the total longitudinal field of 52 mm.

Fig.41 is a photograph of a transducer complete with its mounting plate. A spring-loaded screw adjustment enabled accurate alignment of the transducer face perpendicular to the sonic axis, as illustrated in Fig.40.

The acoustic pressure waveforms produced by the transducers are shown in Fig.42. Each pulse approximates to a single cycle at a frequency slightly less than the resonant frequency of the transducer, although some unwanted ringing is also evident.

8.3 Schlieren observations of the mechanism of sonic image formation

The entire process of image formation was observed for the system of two polystyrene lenses in water, using the 2 MHz transducer for insonfication. The light flash delay was adjusted so as to follow the pulse from its departure from the transducer to the formation of a focused image of a small object. Owing to the limited field of view of the schlieren system, the entire sonic system had to be moved to follow the pulse through differen parts of the system.

Fig.43 is a composite photograph showing the insonifying pulse travelling through the system. This is a front view (as seen from the normal direction of viewing). The lenses and transducer are indicated in their

correct positions and to scale. The pulse is initially plane (position 1 on the figure), becomes concave (3) after proceeding through the sonic lens L2, passes through a focal region (4) at the point of coincident foci of the lenses, emerges from the lens L1 as a plane pulse again, and strikes the small object O to produce a circular reflected wave-front (8).

These observations confirm that the transverse dimension of the transducer is sufficiently large that the pulse emitted can be considered a plane pulse of well-defined transverse dimension. The pulse propagates through the lens system just as predicted by ray--plotting in Fig.36, p.82. (That plot is actually for Perspex lenses, but the plot for polystyrene lenses is very similar).

Fig.44 gives a side view of the insonifying pulse in order to show the thickness of the beam. The plane and edge wave components are visible close to the transducer (1,2). It should be borne in mind that the edge waves are over-emphasised and the beam-spreading is exaggerated in this figure, firstly because the brightness of the plane pulse is in saturation, and secondly because it is impossible to reproduce photographically the range of brightnesses appreciated by the eye. If reduced ultrasonic power had been used, then the photographs would not have revealed the full structure of the pulses.

Owing to the smallness of the narrower side of the transducer face, the behaviour of the pulse in this side view is in complete contrast with that observed in the front view (Fig.43). The pulse spreads out and exhibits far-field structure (3), and no focal spot is visible between the lenses. An image of the transducer with a distinct plane front is formed (8) in a position very close to that calculated from the paraxial properties of the system. The structure of the pulse in the object field (9,10) appears similar to that expected if a real transducer occupied the position of the transducer image (8); this is clearly demonstrated by a comparison of the pulses at (3) and (10), which are at similar ranges (taking the magnifications of the system into account) from the transducer and image transducer respectively.

Fig.45 is the continuation of Fig.43; it shows the formation of the sonic image of a thin brass rod aligned parallel to the direction of viewing. At (1) the plane insonifying pulse and the cylindrical reflected pulse are seen. The pulse is made plane (3) by the action of the object lens L1

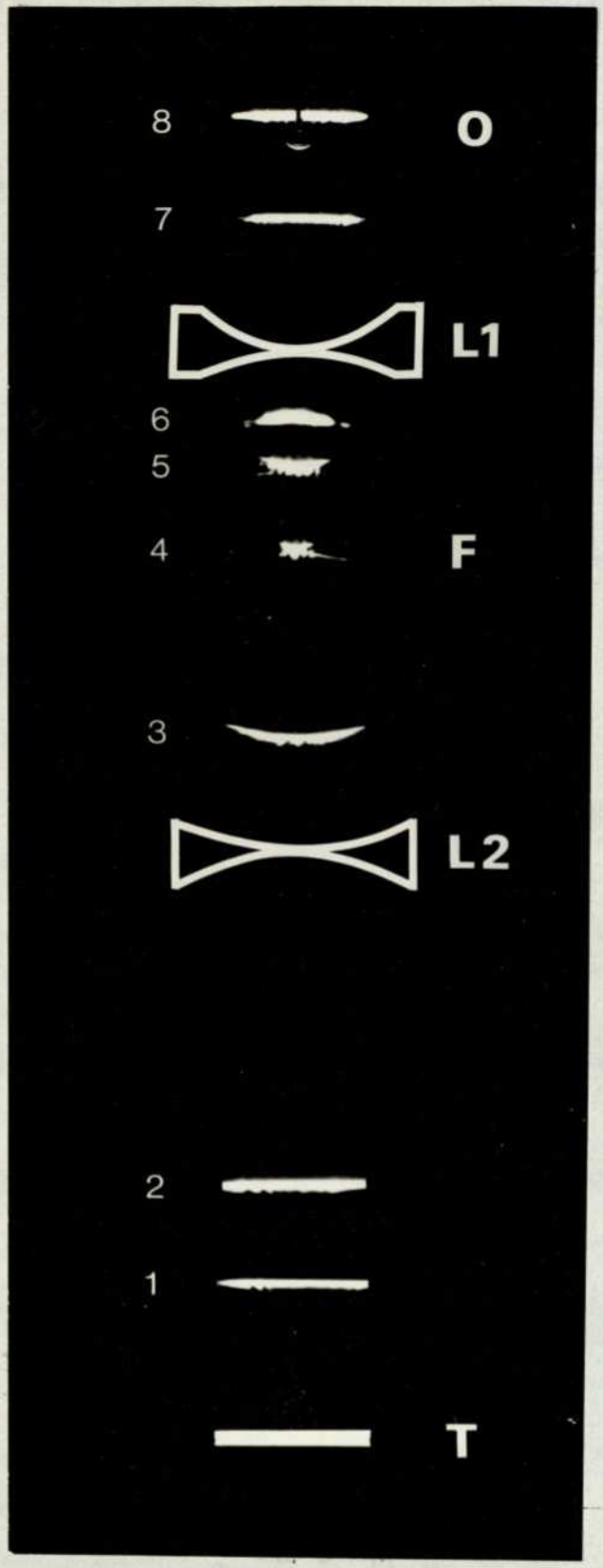

Fig.43 SCHLIEREN IMAGES OF THE INSONIFYING PULSE TRAVELLING UPWARDS THROUGH A DUVD SYSTM OF POLYSTYRENE LENSES IN WATER (indicated diagrammatically). FRONT VIEW, i.e. FROM NORMAL DIRECTION OF VIEWING. SCALE $\frac{1}{2}$ ACTUAL SIZE.
T, transducer; L1,L2, lenses; F,coincident focus of lenses; O, reflecting object.

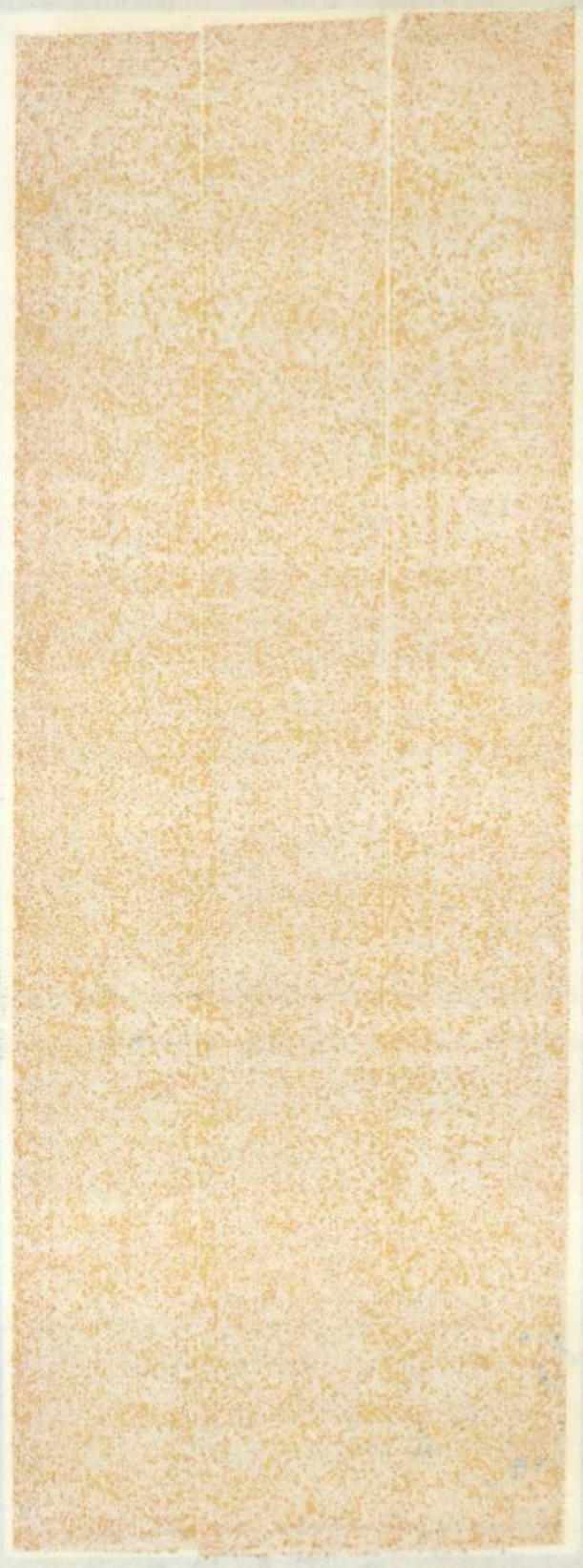

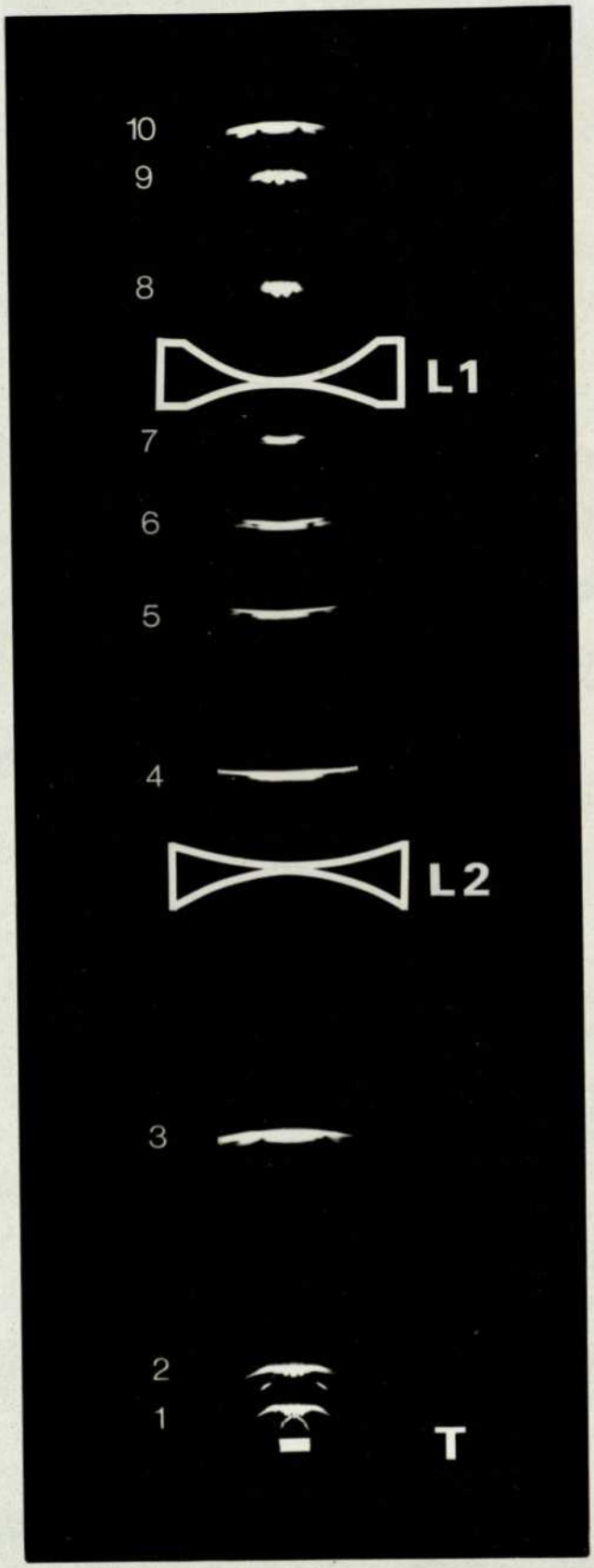

Fig.44 SIDE VIEW OF THE INSONIFYING PULSE (travelling upwards).

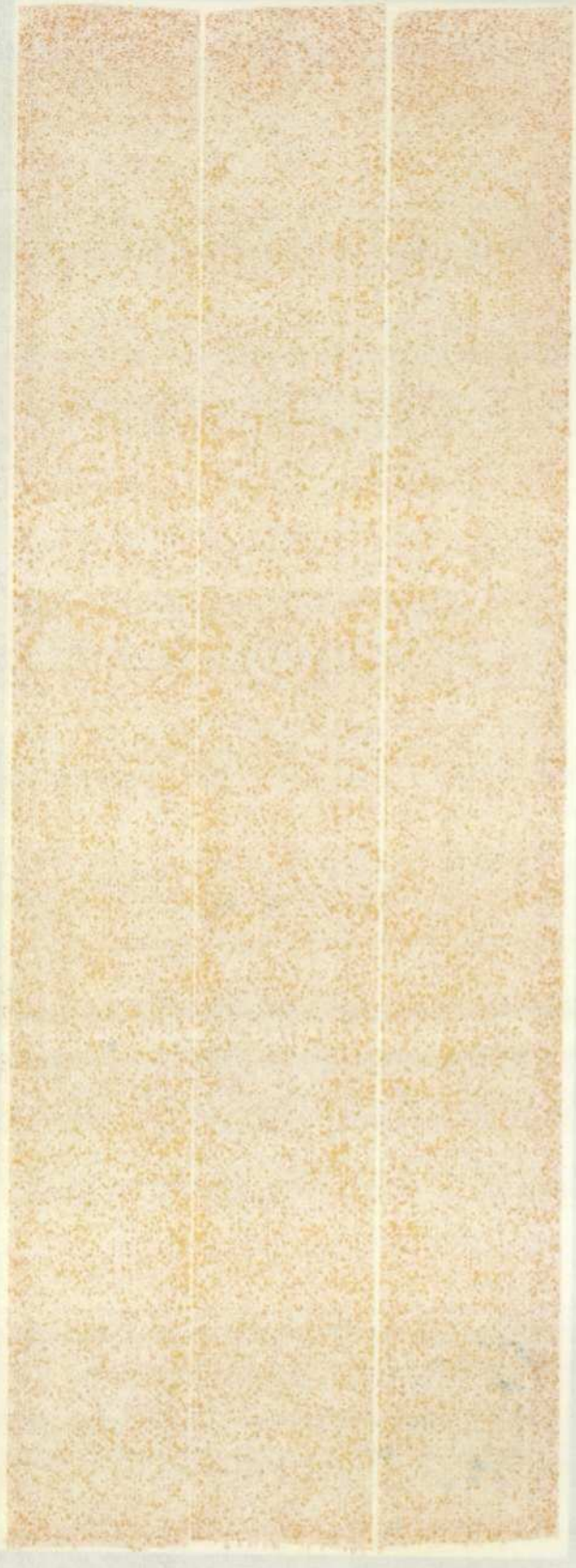

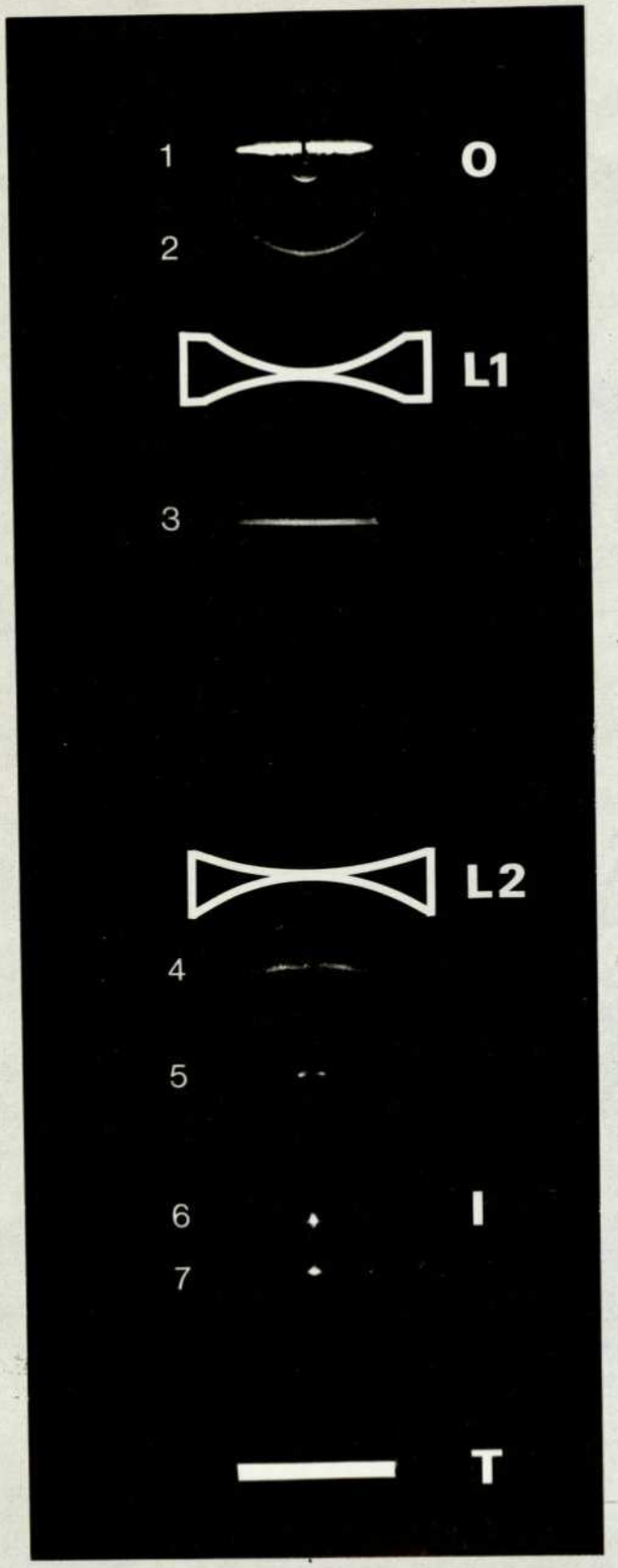

Fig. 45 FOCUSING OF THE PULSE REFLECTED DOWNWARDS FROM A THIN ROD O, ALIGNED PARALLEL TO THE DIRECTION OF VIEWING, TO GIVE THE DUVD IMAGE I. FRONT VIEW, AS IN FIG.43.

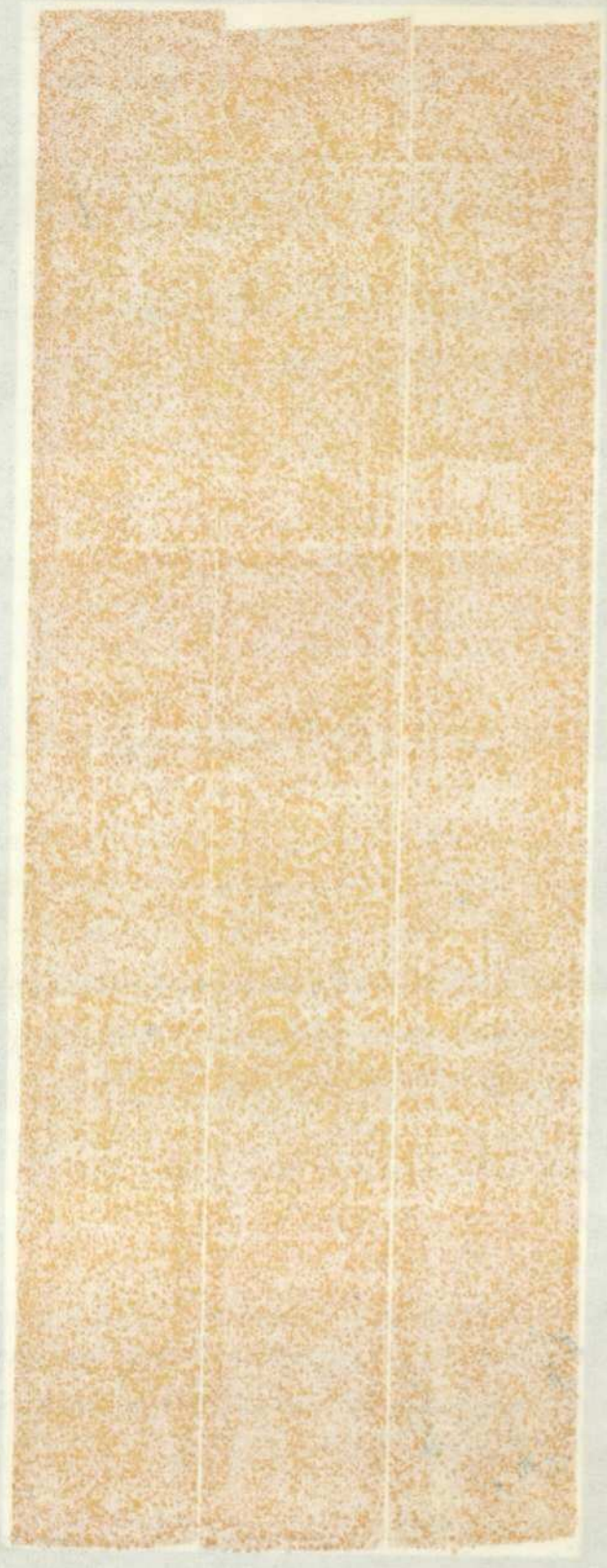

(since the reflecting object is near the focal point of this lens), and is then brought to a focus (6) by the image lens L2; this focus is the sonic image. Positions (5) and (7) show the appearance of the sonic image when the light flash delay is too short and too long, respectively.

The observations presented in this section depict clearly the mechanism, and demonstrate the principles, of the DUVD method of ultrasonic imaging. They also show that the practical lens system focuses short pulses in the expected fashion and that the 'image transducer' appears to simulate the action of a real insonifying transducer.

8.4 Acoustic energy losses

Four DUVD systems were assembled by permuting the two lens systems and the two transducers. The acoustic losses inherent in these systems were found by comparing the strength of the plane pulse generated by the transducer (position 1 in Fig.43) with the image of a plane brass reflector placed at the centre of the object field and perpendicular to the sonic axis. The pulse strength was expressed in 'dB above threshold' by observing the schlieren image of the pulse (on a TV screen), and measuring the attenuation of the excitation voltage applied to the transducer required to reduce the pulse brightness to the threshold of visibility - a rapid technique of sufficient precision for this exercise.

The measured losses in each system were as follows:
Polystyrene lenses, 2 MHz transducer: 6dB
Polystyrene lenses, 4 MHz transducer: 6dB
Perspex lenses, 2 MHz transducer: 9dB
Perspex lenses, 4 MHz transducer: 11dB.

Since the brightest parts of the pulses were measured, the above represent minimum losses due to rays passing through the thinnest ($\sim$1 mm), central parts of the lenses at normal incidence.

The calculated losses due to impedance mismatching are 2.5 dB for the system of polystyrene lenses, and 4.3 dB for the Perspex; the calculated attenuation losses are smaller, the largest being 2dB for Perspex at 4 MHz. With a total go-and-return path of 0.7 m, the attenuation in water is significant at 4 MHz ($\simeq$2.5 dB). Thus, for example, the total losses for the Perspex lens/4 MHz transducer system are about 9 dB, compared with the measured 11 dB. In each system the observed losses were greater by about 2 dB than the calculated values - this may be due to a diffraction effect.

The main point is that, as expected, the system of polystyrene lenses exhibited lower energy losses than the Perspex lenses. At the edge of the field of view, the drop in sensitivity and the disparity between the two systems was greater (see next section). The difference between the losses observed using the 2 MHz and 4 MHz transducers was small because of the thinness of the centre of the lens; at the edge of the field the difference was greater owing to the greater attenuation at 4 MHz.

8.5 Resolution, field of view, and sensitivity

Various test objects were imaged to assess the performance of the systems. In order to obtain the full benefit of the expected good geometrical resolution of the optimised lens systems, as described in Section 7.6, the shorter 4 MHz pulse should theoretically be used. However, tests showed that the drop in sensitivity at the edge of the field was more severe using the 4 MHz pulse (about 10 dB relative to the sensitivity at the centre). Therefore, so as to demonstrate the performance over the widest possible field of view, all the photographs reproduced in this report were obtained using the 2 MHz transducer and the system of polystyrene lenses.

The theoretical transverse resolution of the system (see Section 7.6) is as follows:
geometrical resolution ~ 0.007-0.01 units ~ 0.5-0.7 mm
diffraction-limited resolution ~ 1.5-$2\,\Lambda \sim 1$-1.5 mm.
The photographs to be presented show the actual sizes of the sonic images. It should be remembered that the magnifications of the sonic system from object to image are 2 longitudinally and $\sqrt{2}$ transversely.

Fig.46 shows a test object consisting of an array of parallel 0.8 mm diameter brass rods and the DUVD image obtained when the rods' axes were aligned in the direction of viewing. The central rods, whose spacing is 1.25 mm, are resolved easily, so the predicted transverse resolution is attained. The outermost pair of rods are at the edge of the transverse design field, and it can be seen that the sensitivity and resolution fall off there, the drop in sensitivity being about 10 dB. The number of resolvable lines across the field is approximately 25.

The test object in Fig.47(a) is an array of rods in the shape of a 'Z'. The images seen with the object at two different orientations, (b) and

(a)

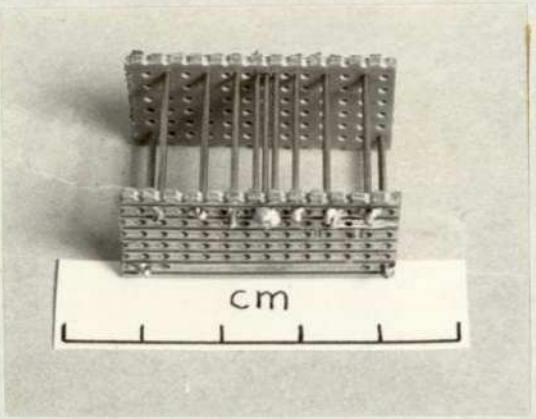

(b)

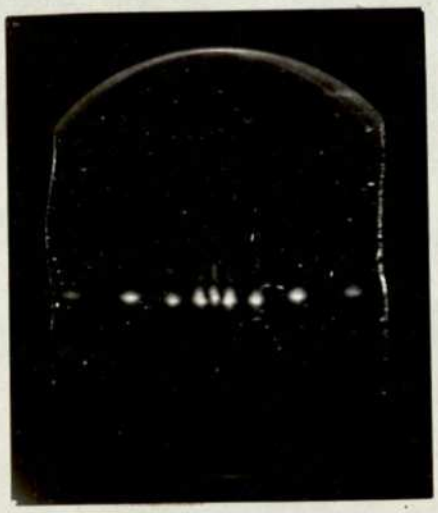

Fig.46 DUVD IMAGE OF A TEST OBJECT IN WATER, PRODUCED BY THE EXPERIMENTAL SONIC SYSTEM:
(a) THE OBJECT, AN ARRAY OF PARALLEL RODS;
(b) THE IMAGE OBTAINED WITH THE AXES OF RODS ALIGNED IN THE DIRECTION OF VIEWING. BOTH OBJECT AND IMAGE ARE SHOWN AT APPROXIMATELY ACTUAL SIZE.

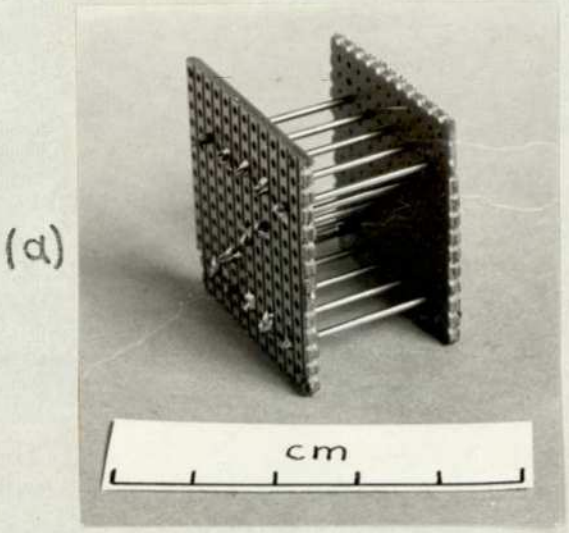

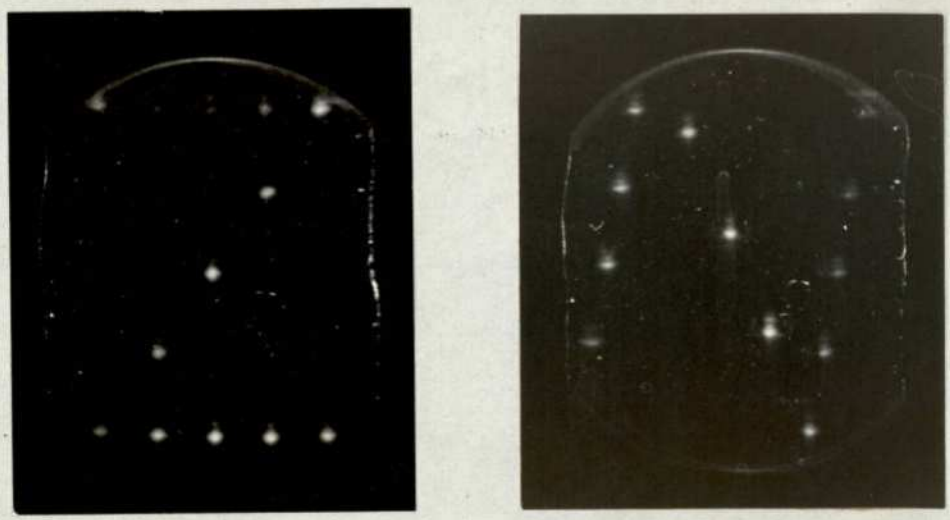

Fig.47 (a) A TEST OBJECT CONSISTING OF A Z-SHAPED ARRAY OF RODS. (b) & (c) DUVD IMAGES OBTAINED WITH THE OBJECT AT TWO DIFFERENTENT ORIENTATIONS (but with the axes of the rods parallel to the direction of viewing). SCALE: APPROXIMATELY ACTUAL SIZE. NOTE THE LONGITUDINAL MAGNIFICATION (up-and--down) OF 2, AND THE TRANSVERSE MAGNIFICATION OF 1.4 .

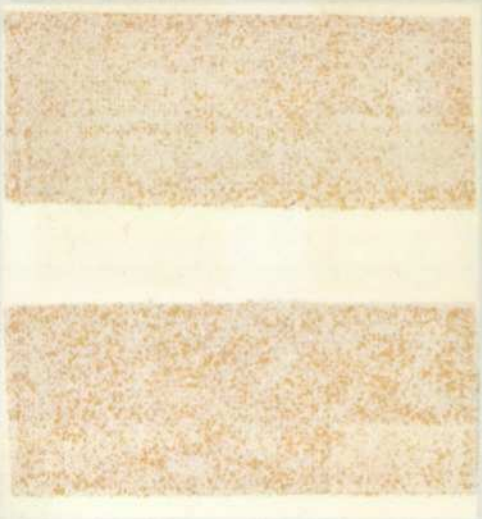

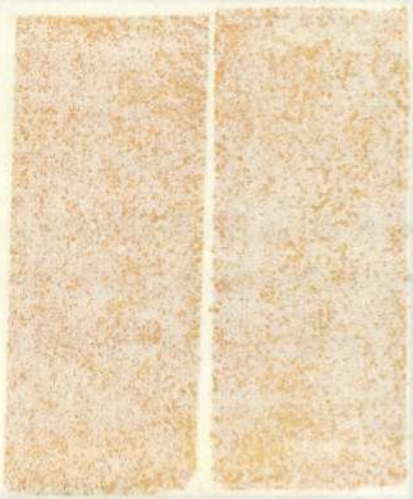

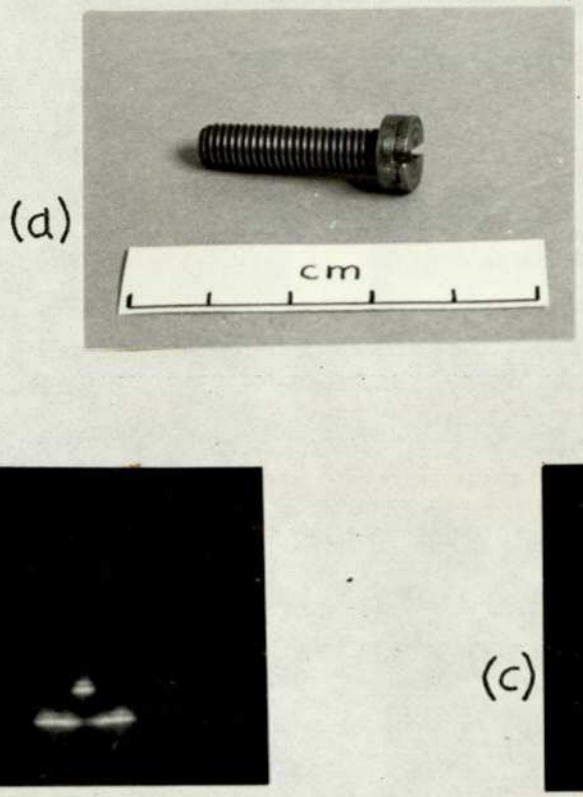

Fig.48 IMAGES OF THE HEAD OF A BOLT:
(a) THE BOLT; (b) THE IMAGE SEEN WITH THE HEAD POINTING DOWNWARDS AND THE SLOT ALIGNED IN THE DIRECTION OF VIEWING; (c) THE IMAGE SEEN WITH THE SLOT PERPENDICULAR TO THE DIRECTION OF VIEWING. SCALE: APPROXIMATELY FULL SIZE.

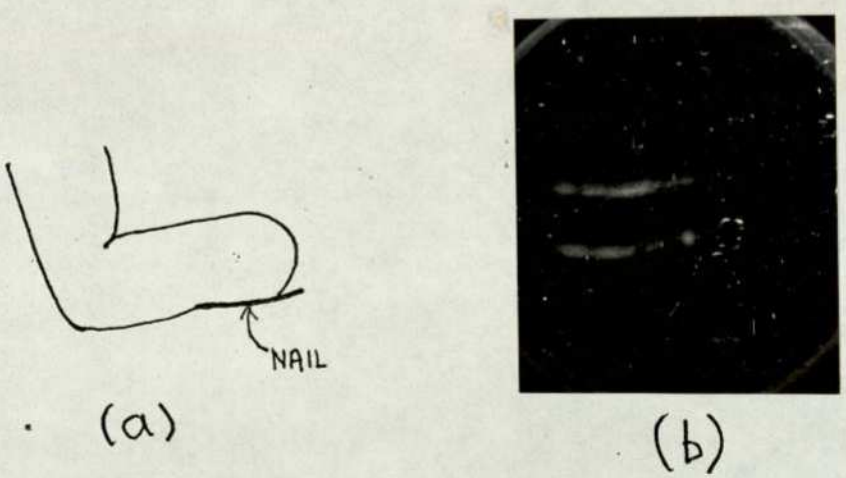

Fig.49 IMAGE OF A FINGER: (a) DIAGRAM TO SHOW THE ORIENTATION OF THE FINGER (b) THE IMAGE (approximately full size).

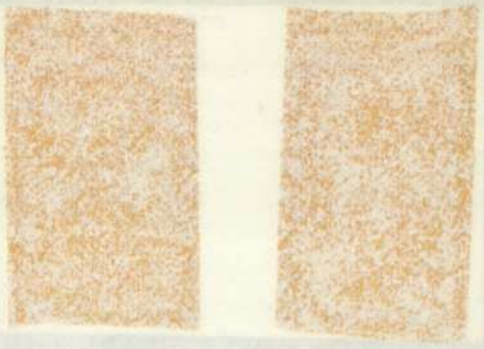

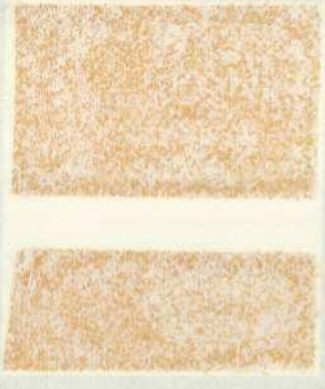

(c) demonstrate that good resolution and linearity can be obtained over an extended field. The reduction in sensitivity towards the edge of the field is again apparent. In these images, the total transverse design field is seen, but the longitudinal field is limited by the schlieren field of view.

The total longitudinal spread in the images is about 2 mm, corresponding to a resolution of 1 mm in the object field. The appearance of the image of each rod is a bright spot followed by faint spots, which are caused by the 'ringing' of the acoustic pulse. If the ultrasonic power is reduced then only the bright spot is seen and the resolution is improved. In addition, some longitudinal blurring is caused by the finite length of the light flash. This shortcoming could be readily eliminated by employing a light source giving a shorter flash; the Strobotac lamp was used only for convenience.

An undesirable feature is visible in Fig.46(b) - faint secondary images separated by a few mm longitudinally from (i.e. above) the main images. Theoretically, multiple reflections in the lenses cannot be the cause since the reflection coefficient at a water-polystyrene interface is -12dB, and hence the first multiple reflection is 24 dB down on the main pulse - too weak to be visible in these images. A possible explanation is that the insonifying pulse is reflected transversely from one of the rods making up the object, on to its neighbour, and thence back into the sonic system. This is not unlikely considering the large diameters of the rods relative to their separation, as shown in Fig.46(a). An alternative possible cause is the diffracted waves, known as creeping waves, which travel around cylindrical objects, and which could give delayed returning waves.

Another object imaged was the head of a bolt (Fig.48). The image shown in (b) was produced with the bolt vertical and the slot parallel to the direction of viewing, and the slot and head are clearly resolved. In (c) the bolt was rotated through 90° to bring the slot perpendicular to the viewing direction; because the thickness of the cross-sectional slice insonified was sufficient to include the whole bolt-head, images of both the slot and head were obtained, with the slot image appearing weaker as a result of its small thickness in the direction of viewing.

The images presented so far are of metal objects in water, which are very good acoustic reflectors. Other materials were not imaged so

successfully because of the limited sensitivity of the system. The measured sensitivity at the centre of the field in terms of the strength of the image of a perfect plane reflector was about 21 dB above threshold.

Fig.49 shows the image of one of the author's fingers. The lower interface seen represents the nail and nearer surface of the bone, the upper interface presumably a further bone surface. The sensitivity was insufficient to reveal any structural details in soft biological tissues.

8.6 Summary

The performance of the experimental sonic systems of optimised design, comprising plastic lenses in water, was in good agreeement with the theoretical expectations. Schlieren observations provided direct evidence that a sonic lens system focused short pulses in the manner predicted by Hanstead's paraxial analysis, and as predicted in more detail by the ray-plots (Chap.7) used to design the system.

It was confirmed that polystyrene lenses were more suitable than Perspex due to lower acoustic energy losses. The total losses with a system of polystyrene lenses were about 6 dB at the centre of the field, but greater towards the edge. It seems reasonable to conclude that the average losses in a system with a larger, more practicable, field would be at least 10 dB.

The system of polystyrene lenses with a 2 MHz transducer exhibited linearity over a field of view of about 25 x 25 mm, and diffraction limited resolution of about 1 mm both longitudinally and transversely. There was a rapid drop in sensitivity near the transverse edge of the field.

The principal disadvantage of the DUVD imaging technique - lack of sensitivity - was evident and the most impressive images obtained were of metal objects in the water. The maximum sensitivity, in terms of the strength of the image of a flat perfect reflector, was about 20 dB above the threshold of visibility.

Nevertheless, compared to the performance of Hanstead's experimental system (1973), and in particular his images of rods in water, the field of view, resolution, and sensitivity were all much improved.

CHAPTER 9 DISCUSSION

The potential performance of a DUVD imaging system is estimated in this chapter. It is then compared with other methods of producing an ultrasonic cross-sectional image and the feasibility of DUVD for various categories of applications is considered.

9.1 Feasible performance of a DUVD system

The resolution, sensitivity and field of view of an ultrasonic imaging system are closely interrelated. For a given longitudinal field, or penetration into the object, a compromise usually has to be made between resolution and sensitivity, and the most important decision is the choice of wavelength. If a small wavelength is used, then the resolution is good but the attenuation is high and hence the sensitivity to weak reflections is poor. A larger wavelength gives poorer resolution but better sensitivity. The performance is also fundamentally limited by the ratio of acoustic power transmitted to the detection sensitivity of the system.

When comparing different methods of imaging it is therefore necessary to consider all the parameters of performance and to remember that they are interdependent.

The most promising form of DUVD system known to be feasible is that developed to the point of experimental tests, as described in previous chapters. The sonic system consists of two polystyrene lenses in water; the transducer is placed in the image space so that the object is effectively insonified by an 'image transducer', and the acoustic image is visualised by a schlieren system. Thus the system is coupled to the object by water and the image is formed in water.

There are two possible improvements to this basic arrangement which have not yet been demonstrated in practice. Firstly, it has been shown that the use of a more sensitive visualising liquid would increase sensitivity by a worthwhile amount. Since the practical problems do not appear insurmountable, the potential gain in sensitivity will be taken account of in the estimates of performance. The second possible improvement, the astigmatic defocusing of the acoustic image in the direction of viewing, has not been investigated and the potential gains are uncertain; it is therefore ignored in the estimates.

The performance of DUVD systems will be estimated assuming a field of view of about 120 x 60 mm and a wavelength of the order of 1 mm, since this is similar to the wavelength used in conventional pulse-echo examination over a comparable field. The size of the image transducer face will be taken as 70 x 14 mm. The above dimensions are approximately double those of the experimental system described in the previous chapter.

The sensitivity of the system depends principally upon the visualisation sensitivity of the schlieren technique, the acoustic power output of the transducer and the acoustic losses in the system.

The threshold sensitivity of schlieren visualisation in water has been shown (in Chap.4) to be about 1 mW, where this refers to the power in a square beam. In certain other liquids, such as bromoform, the sensitivity is about 10 dB better, i.e. 0.1 mW.

The peak acoustic intensity radiated (see Chap.5) is proportional to the square of the excitation voltage applied to the transducer, provided that the rise time of the voltage pulse is less than the acoustic transit time across the transducer. In the experimental work (described in Chap.8) a Smiths Mk.7 excitation source was employed and the voltage pulse applied to the 2 MHz transducer had 700V amplitude. More powerful pulses could be generated by a specially-built excitation source.

Taking into account the larger transducer area, and hence greater capacitance, to be driven in the practical system envisaged here, and the mechanical limitations of a PZT piezoelectric plate (Wyatt 1977), the maximum feasible voltage will be taken as 1000 V for both a 2 MHz transducer (used to image water velocity materials) and a 5 MHz transducer (used for imaging in metals). The corresponding intensities radiated into water, calculated from the manufacturer's data, are as follows:

15 $W.cm^{-2}$ from a 2 MHz transducer

100 $W.cm^{-2}$ from a 5 MHz transducer

The acoustic energy losses in the system (see Chaps.6 and 8) will be taken as 10 dB over the whole acoustic path, i.e. 5 dB on each of the go and return paths.

The resolution depends upon the design of the sonic lens system, the ultrasonic pulse length and the duration of the lightflash with which the sonic image is 'frozen'.

Suitable short ultrasonic pulses, consisting substantially of a single cycle can be obtained by using a well-backed transducer, as demonstrated in Chap.8. Sources of suitable light flashes are also available (e.g. Wyatt 1974).

The longitudinal resolution is equal to half of the pulse length (see Chap.7) and is better than the effective wavelength of a short pulse. A ray-tracing exercise (described in Chap.7) and the performance of the experimental system (Chap.8) have shown that diffraction-limited transverse resolution of about 2 wavelengths can be obtained over a useful field in a water-velocity medium by employing a sonic system of spherically-surfaced lenses. Similar resolution is doubtless possible when imaging materials of higher velocity, such as metals, if necessary with the aid of more complex lens curvatures.

The system parameters which have been discussed above, and which will be used in the feasibility studies of Section 9.3, are summarised in Table 10.

TABLE 10. DUVD SYSTEM PARAMETERS ASSUMED IN FEASIBILITY STUDIES

Field of view	120 x 60 mm
Dimensions of image transducer	70 x 14 mm
Schlieren visualisation sensitivity	0.1 – 1 mW
Peak intensity radiated from transducers) 2 MHz into water) 5 MHz	15 $W.cm^{-2}$ 100 $W.cm^{-2}$
Losses in sonic system	10 dB
Longitudinal resolution	$< \Lambda$
Transverse resolution	2Λ

9.2 Pulse-echo imaging methods

The chief limitation of DUVD compared with pulse-echo techniques using piezoelectric transducers is its poor sensitivity. The threshold sensitivity of a piezoelectric receiver is of the order of 10^{-11} $W.cm^{-2}$ (Jones 1973) and since most practical transducers have an area of around 1 cm^2, the sensitivity can be taken as 10^{-11}W. Comparing this with the 10^{-4} W threshold of schlieren viewing in the most sensitive media, the vast difference, of the order of 70 dB, clearly indicates the relative difficulty of obtaining images by DUVD.

Various ultrasonic imaging methods have been described in Chap.1. The performance of the most important methods of producing a longitudinal

cross-section will now be summarised; the development of medical imaging systems is considerably more advanced than N.D.T. systems, presumably because the wide variety of N.D.T. applications requires specially tailored systems.

The dynamic range of a pulse-echo system, i.e. the ratio of the maximum echo from a flat reflector to the minimum echo detectable, is typically about 100 dB. Part of this range is needed to allow for attenuation, and in medical imaging automatic attenuation compensation is provided by the use of swept gain: the gain of the receiver increases with time so that echoes which come from further away, and are therefore attenuated more, are amplified more. The longitudinal resolution of a pulse-echo system is of the order of a wavelength; the transverse resolution depends on the aperture of the system and the amount of focusing employed, if any.

The transverse resolution of a B-scan system is limited by diffraction to about 10 wavelengths, and the time taken to produce an image is of the order of 30 seconds. The technique is in routine use for medical diagnosis, but is not yet widely used in N.D.T.

Existing real-time scanners based on multi-element transducer arrays have similar resolution to single-transducer B-scan devices; only medical systems have been produced so far. There are many interesting possibilities for the development of such arrays because focusing can be performed electronically by introducing time delays between the elements, and the focusing can be adjusted in synchrony with the received echoes so that the whole field is correctly focused.

It seems feasible that better transverse resolution of, say, less than 5 wavelengths over the whole field, will be achieved by the use of more elements simultaneously, which gives a larger effective aperture (Whittingham & Evans 1975). There is, indeed, no bar in principle to approaching a resolution of about 2 wavelengths. In practice the parallel processing of echoes in a large number of elements, and the switching between blocks of elements, would require complicated and costly electronics.

A transverse resolution of approximately two wavelengths can theoretically be attained by a synthetic focus technique. The computing time involved is a major drawback here, but by suitable pre-processing of the ultrasonic echoes, and by using microprocessors, it is possible that an image could be produced in about one second (Hanstead 1977).

9.3 The feasibility of DUVD in various applications

The following calculations are based on the DUVD system parameters presented in Table 10.

9.3.1 Imaging objects in water

The peak intensity transmitted by the 2 MHz transducer into water (in the image space) is 15 $W.cm^{-2}$, and the dimensions of the transducer face required to insonify the field are about 100 x 20 mm. Thus the power in a square beam of the same width as the transducer in the direction of viewing is approximately 60 W . The square-beam power in the image of a plane reflecting object is reduced to 6 W owing to the 10 dB losses in the system. Now the threshold of visualisation sensitivity in water is 1 mW, so that the dynamic range of the system is about 38 dB. Using a more sensitive visualising liquid, the dynamic range is about 10 dB greater, say 50 dB. These estimates should be compared with the typical 100 dB dynamic range of pulse-echo systems.

The sensitivity for detection of a small reflector in the form of a flat-ended cylinder of area 1 mm^2 will now be estimated. Because of the transverse magnification of the sonic system, the area of the insonifying beam is halved and its intensity is doubled in the object space. Taking account also of the 10 dB system losses, the effective intensity incident on the target is 3 $W.cm^{-2}$. Assuming that most of the incident energy is reflected back into the sonic system, since the target is larger than a wavelength, the power in the image is approximately 30 mW. This is easily visible, and in fact such a target was successfully imaged by the experimental system. There appears to be ample sensitivity to image highly reflecting objects of more complex shape, provided their characteristic dimensions are greater than a millimetre.

9.3.2 Medical imaging

The principle of medical ultrasonic imaging is that, as the ultrasonic pulse travels through the tissues, reflections arise at interfaces between tissues of different acoustic impedance and at acoustic inhomogeneities inside the tissues. In this way the biological structures are outlined and information about their internal state obtained. The difficulties are that attenuation is high and the variations in acoustic impedance are small, so that the echoes are very small.

Before proceeding with sensitivity calculations, it is necessary to check that the acoustic intensity incident on the tissues is acceptable from the point of view of safety. The 15 W/cm^2 emitted by the transducer is increased to 30 W/cm^2 at the object by the magnification of the system; it also suffers 5 dB loss so that the peak incident intensity is about 10 $W.cm^{-2}$. Assuming a single-cycle 2 MHz pulse 0.5 uS long and a pulse repetition frequency of 200, then the time-averaged intensity is 1 $mW.cm^{-2}$. This is of the order encountered in commercial pulse-echo equipment and is regarded as acceptable.

The feasibility of imaging biological structures by DUVD can be estimated using pulse-echo data. Wells (1969, p.93) gives typical values of the echo amplitudes from biological structures, expressed in dB relative to the echo from a perfect reflector at the same range in a lossless medium. The data were obtained with a 1.5 MHz, 20 mm diameter transducer. Some values are reproduced in Table 11.

TABLE 11 - TYPICAL ECHO AMPLITUDES FROM BIOLOGICAL STRUCTURES
(After Wells 1969)

Structure	Range, mm	Echo amplitude, dB
Foetal skull, 30 weeks gestation	80	-50
Posterior heart surface	100	-50
Brain mid-line	70	-60
Normal liver structures	80	-65
Anterior mitral valve leaflet (heart)	70	-70

Now a DUVD system collects echos over a greater solid angle than the pulse-echo transducer with which these results were obtained. Typically, the fan of rays accepted is 45°, compared with about 10° for the pulse-echo transducer. Thus the solid angle is greater by about 20 times and sensitivity is greater by about 13 dB.

Against this must be set the acoustic losses of 10 dB in the DUVD system and the greater attenuation encountered at 2 MHz than at 1.5 MHz.

It seems reasonable to conclude that the values in Table 11 represent the order-of-magnitude echo amplitudes which would be obtained in a DUVD system. In the previous sub-section it was estimated that the minimum echo

detectable by a DUVD system, expressed relative to the echo from a plane reflector is of the order of -40 dB using water as the visualising medium and -50 dB using a more sensitive liquid. The system therefore appears insufficiently sensitive for imaging biological structures.

The above estimates are based on a frequency of 2 MHz. At a lower frequency, the attenuation losses are reduced. According to Wells (1969,p.85) the average attenuation in human tissue is proportional to frequency and the go-and-return loss is around 0.13 dB. MHz^{-1} per mm of penetration. Thus at 2 MHz and a penetration of 100 mm, attenuation losses are approximately 25 dB. If a frequency of 1 MHz is used in the DUVD system, the attenuation falls by about 12 dB; together with a reduction in attenuation in the sonic system of around 3 dB, the sensitivity is thus improved by approximately 15 dB. The echo amplitudes from Table 11 are effectively increased to lie in the range -35 to -55 dB, compared with the DUVD threshold of -40 to -50 dB. Further reduction in frequency, to below 1 MHz, is found not to offer worthwhile gains in sensitivity.

Thus a DUVD system operating at 1 MHz, with a transverse resolution of about 3 mm, appears capable of detecting some biological structures. However, a practical imaging device should be capable of easily imaging these structures and should have sufficient sensitivity in hand to detect weaker echoes in order to present a complete image.

The conclusion is therefore that DUVD is not a feasible technique for diagnostic medical imaging.

9.3.3 Non-destructive testing of metals

The aim of ultrasonic imaging of metals (Krautkramer 1969) is to find faults, such as cracks and voids, and estimate their size. The defects are good acoustic reflectors; the problem is that they can be small and positioned or shaped unfavourably for reflection back to the detector. Attenuation varies a great deal between different materials and different states of the same material. It can however be small over a range of around 100 mm in some metals, and examination of a material of negligible attenuation will be assumed in what follows.

The example of imaging in steel will be used. Because of the high acoustic velocity in metals compared to water, a higher frequency is required to obtain good resolution: as in previous calculations, the frequency will be taken as 5 MHz ($\lambda \simeq 1.2$ mm in steel).

The peak intensity emitted by the transducer is (from Table 10), 100 $W.cm^{-2}$. The losses in the sonic system reduce the effective intensity by 10 dB. Since the transverse magnification is about 0.35, the beam is spread out at the object and the intensity is reduced by a further 10 dB. The large impedance mismatch between the steel object and the water which couples it to the sonic system introduces a large transmission loss of approximately 10 dB on both go and return. Hence the effective intensity in the steel is reduced by 40 dB altogether, to about 10 $mW.cm^{-2}$.

If the defect is a flat-bottomed hole of area 1 mm^2 and all the incident energy is reflected back into the detection system, then the defect is just detectable using the most sensitive visualising liquid (threshold ~ 0.1 mW). A real defect at an unfavourable orientation would have to be considerably larger than 1 mm to register.

There may be certain applications where an ability to detect defects effectively larger than a 1 mm disc reflector would be acceptable, but if greater sensitivity than this is needed then DUVD is ruled out.

9.3.4 Other NDT applications

Because of its lack of sensitivity, the most feasible application of DUVD is in imaging defects of favourable geometry, i.e. flat defects perpendicular to the sonic axis. Bar-Cohen has imaged delaminations at small ranges in glass-fibre-reinforced plastic, and an account of his work is about to be published (Bar-Cohen 1977).

However, equal or better resolution can be obtained by a B-scan employing a shorter wavelength, except when the grain or fibre size in the material limits the minimum wavelength. The main advantage of DUVD is instantaneous imaging, which might be valuable for rapid inspection of materials. Real-time images can also be produced by an electronically switched multi-element array, but DUVD offers greater flexibility in some ways. The simplest sonic system consists of just two easily-manufactured lenses and a transducer, immersed in water, so that a variety of systems for the examination of diverse materials and fields of view can be readily constructed. On the other hand the bulk and lack of manoevrability of a DUVD system probably restrict it to the inspection of materials which are brought to it.

9.4 Summary

The feasible applications of a DUVD system are very restricted because of its extreme lack of sensitivity, compared with conventional ultrasonic techniques. General-purpose imaging of human tissues for medical diagnosis and of defects in metals are ruled out. The technique seems most likely to be useful for rapid inspection of materials where great sensitivity is not needed because the faults give very strong ultrasonic echoes.

CHAPTER 10 CONCLUSIONS

The sensitivity of a DUVD imaging system is principally limited by the sensitivity of the schlieren technique of visualising ultrasound. The visualisation sensitivity is greater in liquids than in solids, and the best liquids have a factor of 10 advantage over water, in terms of detectable acoustic power. However, the maximum sensitivity is still several orders of magnitude inferior to that of piezoelectric methods of detection.

The main problems in the development of a practical system are associated with the sonic focusing system. An arrangement of two plastic lenses in water exhibits low acoustic losses, is easily manufactured and is convenient to use; the object under inspection is water-coupled to the system and the sonic image is formed in water. Polystyrene is the best readily available lens material.

Difficulties involved with the possible use of a more sensitive visualising liquid remain to be solved, but are not insuperable. Any further development might include a wider search for suitable lens materials and liquids.

Lens aberrations are not a limitation. Employing a system of plastic lenses, diffraction-limited transverse resolution of about two wavelengths, with longitudinal resolution of about one wavelength, can be obtained over a useful field. Simple lenses of spherical surface suffice for examining a material of similar acoustic velocity to water, and probably also for materials of higher velocity, such as metals. Computer-aided ray tracing is a valuable aid in achieving an optimum sonic design.

Practical developments of the technique included the following: the introduction of a practicable method of insonification; increased sensitivity resulting from the insonification method and the use of polystyrene lenses; a considerable improvement in resolution through optimising the sonic system design; and a larger field of view and improved sensitivity in the compact schlieren system by employing a 'Z' arrangement of mirrors.

The lack of sensitivity of the DUVD technique precludes general applications in medical diagnosis and the non-destructive testing of

metals. The method may be useful for rapid inspection of materials where great sensitivity is not needed, for example because the defects being searched for are large, or are flat and perpendicular to the ultrasonic beam. In such applications DUVD has the advantage over other techniques that a sonic system for a particular task could be developed readily and at low cost.

Further general development of DUVD does not appear to be justified. Rather, it should be directed towards specific feasible applications.

An improved understanding of the propagation of short ultrasonic pulses has been obtained in the course of the project. A schlieren system is a powerful tool in such studies, and the observations made not only confirm recent theoretical descriptions of the pulsed field but show the non-ideal behaviour of real transducers. These results are of interest in the wider field of ultrasonics and acoustics, particularly with respect to techniques using very short pulses, such as ultrasonic spectroscopy.

APPENDIX 1 - BACKGROUND ILLUMINATION IN A SCHLIEREN SYSTEM

The same idealised schlieren system is considered here as in Chap.3, using the same notation. As in Equ.(5), the free-field diffraction pattern in the stop plane is given by

$$g(y) = \sin \alpha / \alpha \qquad \text{(a1)}$$

where $\alpha = kAy/f$. (a2)

Hence the brightness of the image field when a knife-edge stop obstructs all the light between α_1 and $-\infty$ is:

$$\left[h(z)\right]^2 = \left[\text{const.} \int_{\alpha_1}^{\infty} (\sin\alpha/\alpha) e^{ik\alpha z/f} \, d\alpha\right]^2 . \qquad \text{(a3)}$$

This expression has been evaluated by Rayleigh (1920) and plotted by Speak and Walters (1954). As shown in Fig.A1 the illumination is fairly constant over a large central part of the field and increases steeply to give a very bright edge. For a knife-edge which cuts off everything below the axis and the whole of the central maximum of the diffraction pattern ($\alpha_1 = \pi$) the illumination in the centre of the field is about a hundredth of the free-field illumination. In practice, as described in Chap.4, the dark field illumination can be less than a thousandth of the free-field. It is therefore of interest to calculate the cutoff necessary to achieve this.

We will consider only the brightness B in the centre of the field ($z = 0$), so that, ignoring constant factors from now on,

$$B = \left[h(0)\right]^2 = \left[\int_{\alpha_1}^{\infty} \sin\alpha/\alpha \, d\alpha\right]^2$$

$$= \left[Si(\infty) - Si(\alpha_1)\right]^2 \qquad \text{(a4)}$$

where, as usual,

$$Si(\alpha) = \int_0^{\alpha} \sin\alpha/\alpha \, d\alpha \quad . \qquad \text{(a5)}$$

The full illumination in the absence of a stop, B_o, is found by putting $\alpha_1 = -\infty$, and, knowing that

$$Si(\pm\infty) = \pm\pi/2 \quad , \qquad \text{(a6)}$$

we get $$B_o = \pi^2 . \qquad \text{(a7)}$$

If the knife-edge is on axis ($\alpha_1 = 0$) then

$$B/B_o = (\pi/2)^2/\pi^2 = 1/4 . \qquad \text{(a8)}$$

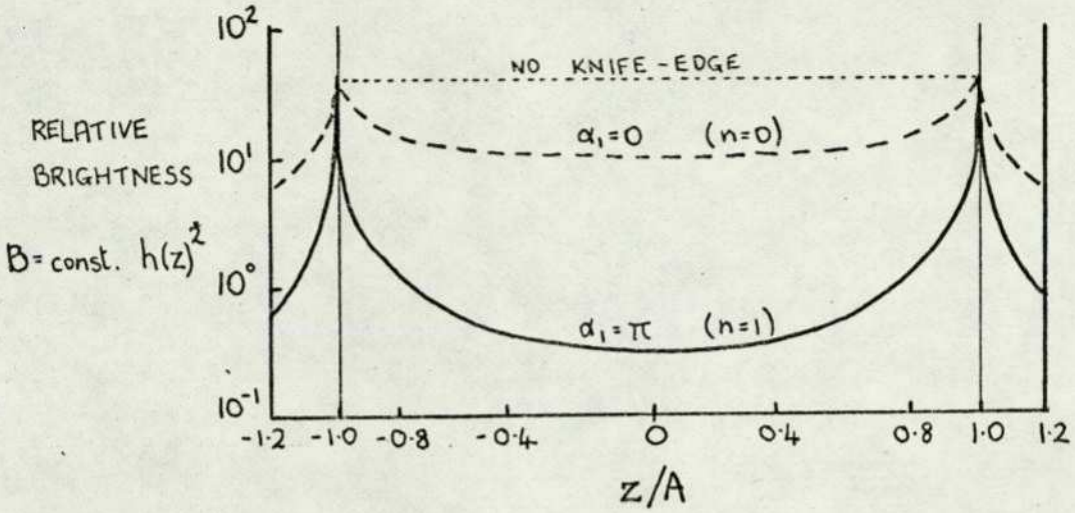

Fig.A1 BACKGROUND ILLUMINATION OF THE SCHLIEREN IMAGE FIELD, FOR VARIOUS DEGREES OF CUT-OFF BY A KNIFE-EDGE STOP (after Speak and Walters 1954).

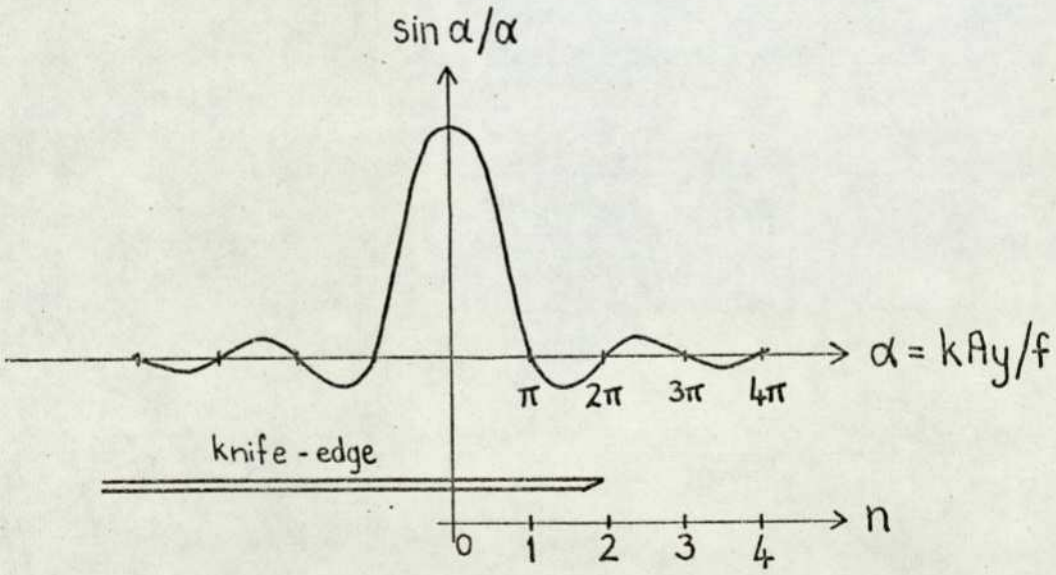

Fig.A2 NOTATION USED TO DENOTE THE POSITION OF THE KNIFE-EDGE STOP.

For larger degrees of cut-off, the following infinite series quoted by Rayleigh (1920) can be used:

$$\mathrm{Si}(\alpha) = \frac{\pi}{2} - \cos\alpha \cdot \left[\frac{1}{\alpha} - \frac{1.2}{\alpha^3} + \frac{1.2.3.4}{\alpha^5} - \cdots \right] - \sin\alpha \cdot \left[\frac{1}{\alpha^2} - \frac{1.2.3.4}{\alpha^4} + \cdots \right] \qquad (a9)$$

Our task is simplified by considering only knife-edge positions coinciding with the zeros of the diffraction pattern.

$$\text{i.e.} \quad \alpha = \pm n\pi \quad , \; n = 1,2,3\ldots \qquad (a10)$$

As Fig.A2 shows, n expresses distance in units of $\lambda f/2A$, the half-width of the central diffraction band. Thus, in Equ. a9, $\cos\alpha = \pm 1$ and $\sin\alpha = 0$; in addition the second and higher terms in the bracketed series can be neglected for present purposes. Equ. a4 then becomes

$$B \simeq (\pi/2 - \pi/2 + {}^{1}/_{n\pi})^2 = (1/n\pi)^2, \qquad (a11)$$

and hence

$$B/B_o \simeq 1/n^2\pi^4 \simeq {}^{1}/_{100\, n^2} . \qquad (a12)$$

If the pattern up to the fourth zero is cut off (n=4), then $B/B_o \simeq 6\times10^{-4}$ which is comparable with practical background levels.

It is interesting to compare this central background brightness with the total light energy passing the knife-edge, which is given by

$$L = \int_{\alpha_1}^{\infty} (\sin^2\alpha/\alpha^2)\, d\alpha . \qquad (a13)$$

Integrating by parts, we get

$$L = \left[\mathrm{Si}(2\alpha) - (\sin^2\alpha)/\alpha \right]_{\alpha_1}^{\infty}$$

$$L = \pi/2 - \mathrm{Si}(2\alpha_1) - (\sin^2\alpha_1)/\alpha_1 . \qquad (a14)$$

The total energy L_o in the diffraction pattern, obtained by putting $\alpha_1 = -\infty$, is

$$L_o = \pi . \qquad (a15)$$

Again only values $\alpha_1 = n\pi$ will be calculated, and just the first term of the series for Si used, so that

$$L \simeq \pi/2 - \pi/2 + {}^{1}/_{2n\pi} \simeq {}^{1}/_{2n\pi} \qquad (a16)$$

$$\text{and} \quad L/L_o \simeq {}^{1}/_{2\, n\pi^2} \simeq {}^{1}/_{20n} . \qquad (a17)$$

By the conservation of energy, $L_o = 2AB_o$, and therefore the ratio of central dark-field illumination B to total light energy passing the knife-edge is

$$B/L \simeq {}^{1}/_{10}\, An. \qquad (a18)$$

This demonstrates that the larger the cut-off, the smaller the proportion of light energy which contributes to the central background, and hence the greater which concentrates in the bright diffraction rim to the field.

The above results for a knife-edge stop can easily be extended to the case of a small strip stop which is symmetrical about the axis. Since the diffraction pattern is symmetrical about the axis, to the above integrals over ∞ to α_1 must be added an equal symmetrical integral below the axis. The amplitude of the central background is therefore doubled and its intensity is quadrupled. Similarly the total energy passing the knife-edge is doubled. The following expressions are obtained:

$$B/B_o = 1/25\ n^2 \qquad (a19)$$

$$L/L_o = 1/10\ n \qquad (a20)$$

$$B/L = 1/5 An \qquad (a21)$$

The theory so far applies only to the idealised infinitely thin line source. The finite source used in practice can be considered as an array of incoherent line sources, the diffraction pattern due to each of which is cut off to a slightly different extent. An approximate expression for B/B_o as the average of the values for all the elementary lines can be obtained by assuming the theory above to apply to non-integer values of $n > 1$ i.e. by ignoring the fluctuations at non-integer values of n. Thus, if a knife-edge stop is used and the cut-offs of the elementary diffraction patterns range from values of $n=n_1$ to $n=n_1+m$, where m represents the width of the source, by using Equ.a12 we obtain

$$\frac{B}{B_o} \simeq \frac{1}{m} \int_{n_1}^{n_1+m} \frac{1}{100\ n^2}\ dn \qquad (a22)$$

$$\simeq \frac{1}{100\ n_1(n_1+m)} .$$

In order to see what this means in practice, we must express the source width in units of $\lambda f/2A$, the half-width of the central band of the diffraction pattern. Using the same figures as in Chap.3 (λ = 0.5mm, f/A = 20), $\lambda f/2A = 5\mu m$ so that for a practical slit width of 0.5 mm, m = 100. A very dark background of $B/B_o = 10^{-4}$ can then be obtained with a cutoff of $n_1=1$ which corresponds to the knife edge extending 5 μm beyond the geometrical image of the source. The image of a finite source is seen to be cut off with almost geometrical sharpness, as asserted in Chap.3. The same general conclusion holds if a strip stop is employed.

APPENDIX 2 - THE SPHERICAL ABERRATION AND ASTIGMATISM OF A SPHERICAL MIRROR

A.2.1 SPHERICAL ABERRATION (from first principles)

When a bundle of rays parallel to the axis is incident upon a spherical mirror, the rays at larger distances from the axis are deviated more than according to paraxial optics. Fig.A3 shows an extreme ray RS incident upon a mirror of diameter d and focal length f whose centre of curvature is at C. We first calcuate the separation of the actual focus T and the paraxial focus F : this is the longitudinal aberration.

Triangle CST is isosceles and CS = 2f, so

$$CT = f/\cos\psi ,$$

also $\sin\psi = (d/2) / 2f$.

Using the small-angle approximation, we get

$$CT = f\,(1 + d^2 / 32\,f^2)$$

The longitudinal aberration L_s is given by

$$L_s = CT-f = d^2 / 32\,f \qquad (a22)$$

The transverse aberration T_s, i.e. the total spread of the image formed in the paraxial focal plane, is given by

$$T_s = L_s\, d/f = d^3 / 32\,f^2 \qquad (a23)$$

or

$$T_s = d / 32\,N^2 \qquad (a24)$$

where N is the f-number (f/d).

A.2.2 ASTIGMATISM

When a parallel bundle of rays is inclined to the horizontal optical axis at a vertical angle of obliquity ϕ, then the reflected rays in the vertical or tangential plane cross at T and those in the horizontal or sagittal plane cross at S. As shown in Fig.A4, the locus of T is a parabaloid and that of S is a plane. The image at T is a horizontal line and that at S is a vertical line. In a schlieren system, T and S are the best positions for a horizontal and vertical knife-edge respectively.

Jenkins and White (1957) have given equations for the location of the two images. For incident parallel light these become.

$$A\,T = f\cos\phi$$

and

$$A\,S = f/\cos\phi ,$$

as quoted by Speak and Walters (1954). Their longitudinal separation L_a, after using the small angle approximation, is

$$L_a = f\,\phi^2 \qquad (a25)$$

Thus when one astigmatic image is in focus the transverse aberration

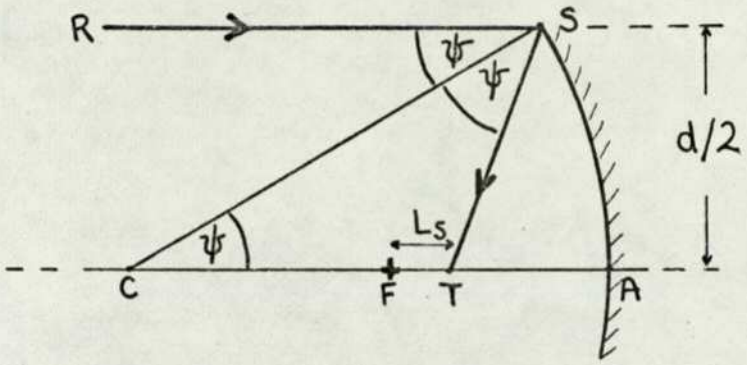

Fig.A3 GEOMETRY FOR THE CALCULATION OF THE SPHERICAL ABERRATION OF AN EXTREME RAY AT A SPHERICAL MIRROR

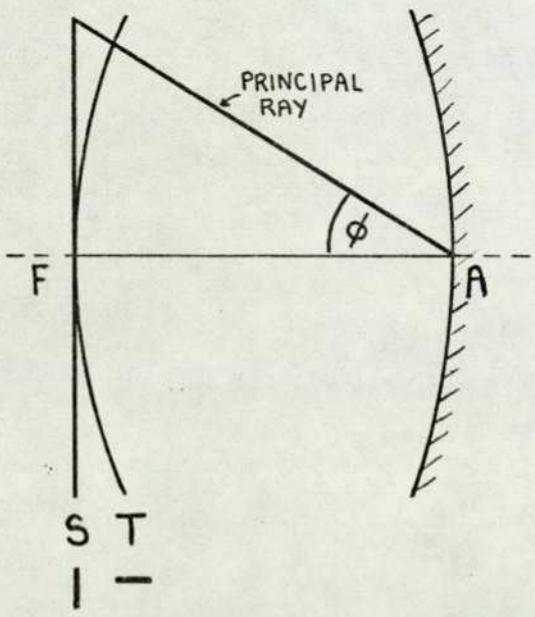

Fig.A4 LOCATIONS OF THE SAGITTAL (S) AND TANGENTIAL (T) ASTIGMATIC IMAGES AT A SPHERICAL MIRROR (after Jenkins and White 1957).

of the other is given by

$$T_a = \frac{d}{f} L_a = d\,\emptyset^2 \qquad (a26)$$

A.2.3. ABERRATIONS OF A Z SCHLIEREN SYSTEM

The aberrations are sufficiently small that those of one mirror are added to those of the other. Thus the spherical aberration and astigmatism of a Z system of two identical mirrors, as given in Section 4.1, are just double the values calculated above.

APPENDIX 3 - OPTIMUM LENS BENDING FOR AN OBJECT AT THE FOCAL POINT

As a starting point for the optimisation of DUVD sonic systems by the method outlined in Chap.7, the lens-bending (i.e.ratio of radii of curvatures) was initially adjusted so that the aberrations were minimised for an object at the focal point of the object lens. The formulae for the radii of the lenses are derived here.

Fig.A5 shows the 2 lenses of the sonic system and defines the symbols used. The equation linking the possible radii of curvature of a lens and one of its focal lengths (Hanstead 1974a,Equ.16) gives for the first sonic lens

$$\frac{f_1}{R_2} = \frac{1}{V_1/V_L - V_1/V_2} + \frac{f_1}{R_1}\left(\frac{1-V_L/V_1}{1-V_L/V_2}\right), \qquad (a27)$$

and it can be applied to the second lens by simple substitution of the appropriate corresponding symbols.

The only aberration present for an axial object is spherical aberration. By a standard optical result (Longhurst 1967, p.364) the spherical aberration of a thin lens is a minimum when the two faces share the deviation of the rays equally. Strictly, this theorem holds only when the media adjacent to the lens are the same, but it will be applied here to the more general case of two different media in the expectation that the results will not be far from those obtained by more rigorous analysis.

The object to be considered is at the focal point O. As shown in Fig.A6, the paraxial ray from O emerges from the lens parallel to the axis. The total angular deviation of the ray is h/f_1, where h is its height above the axis. Thus we require the deviation at each surface to be $h/2f_1$. The deviation at the first surface is the difference between the angles of refraction, r, and incidence, i, so that, applying Snell's law

$$h/2f_1 = r - i = (V_L/V_1 - 1)\, i ,$$

and since

$$i = h/R_1 - h/f_1$$

we get

$$\frac{R_1}{f_1} = \frac{2\,(V_L/V_1 - 1)}{2\,V_L/V_1 - 1} \qquad (a28)$$

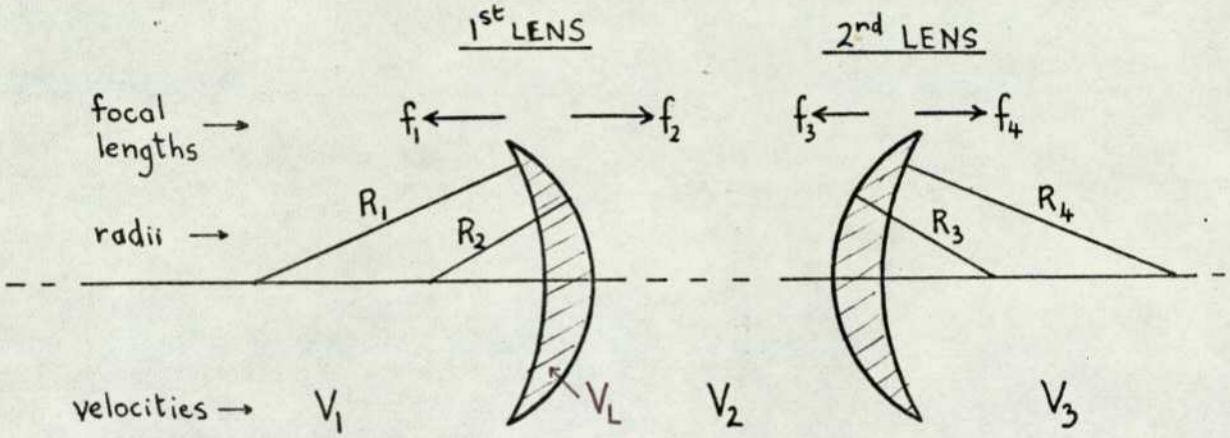

Fig.A5 SYMBOLS FOR THE DESIGN OF THIN SONIC LENSES.

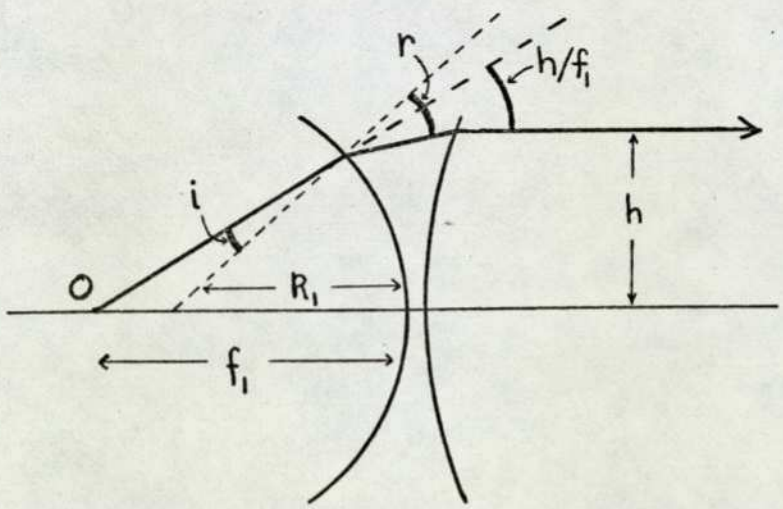

Fig.A6 GEOMETRY OF A PARAXIAL RAY INCIDENT UPON A THIN LENS FROM A FOCAL POINT.

substitution in Equ.a27 gives the second radius

$$\frac{R_2}{f_1} = -2\,(V_L/V_B - 1) \qquad (a29)$$

The radii of the second lens are governed by similar equations because paraxial rays from O are parallel between the lenses and come to a focus at the focal point of the second lens. Since $f_4 = \sqrt{2} f_1$, the radii are given by

$$R_3 = \sqrt{2}\, R_2 \qquad (a30)$$

$$\frac{R_4}{f_1} = \sqrt{2} \cdot \frac{2\,(V_L/V_3 - 1)}{2\,V_L/V_3 - 1} \qquad (a31)$$

APPENDIX 4 SPECIFICATIONS OF OPTIMISED SONIC SYSTEMS

The table below gives the full specifications of the sonic systems whose designs were optimised by the method described in Chap.7. All the systems consist of two plastic lenses in liquid media. Systems S1 and S2 were experimentally demonstrated (see Chap.8).

The symbols have been defined in Fig.32 (P.77) and Fig.A5 (P.124). All lengths are expressed in units of f_1, the first focal length of the first (object) lens. The design field of view has dimensions 0.8 x 0.4 units and is centred on the focal point of the first lens (1.0 units distant from the first lens), as shown in Fig.33.

System	S1	S2	S3	S4
1st medium	water	water	water	water
2nd medium	water	water	water	bromoform
3rd medium	water	water	bromoform	polystyrene
Lens material	Perspex	polystyrene	Perspex	polystyrene
1st lens R_1	0.73	0.60	0.73	0.60
1st lens R_2	-1.26	-0.92	-1.26	-0.92
1st lens diameter	0.9	0.85	0.9	0.85
2nd lens R_3	1.78	1.29	1.78	1.29
2nd lens R_4	-1.03	-0.85	-1.22	-1.14
2nd lens diameter	1.0	1.0	1.0	1.0
Lens separation D	2.16	2.16	1.77	1.77
Longitudinal mag. M_L	$\frac{2}{\sqrt{2}}$	$\frac{2}{\sqrt{2}}$	1.23	1.23
Transverse mag. M_T			0.87	0.87
Transducer length	0.7	0.7	0.45	0.45

REFERENCES

Bar-Cohen,Y., M.Sc.Thesis, Racah Institute of Physics, The Hebrew University of Jerusalem (1977).

Beaver,W.L. 'Sonic Nearfields of a Pulsed Piston Radiator', J.Acoust.Soc. Am. 56, 1043-1048 (1974).

Born,M. and Wolf,E. Principles of Optics, (Pergamon, Oxford, 1970).

Brandrup,J. and Immergut,E.H. (Eds.) Polymer Handbook, (J.Wiley & Sons, New York, 1975).

Brown,P.H. et.al. 'A High Resolution, Sensitive Ultrasonic Image Converter', Ultrason. Int.1975 Conf.Proc.73-79, (IPC Science and Technology Press, London, 1975).

Bucaro,J.A. et.al. 'Image Profiles in Schlieren Observations of Acoustic Wave Fronts', J.Acoust.Soc.Am.60, 1079-1084 (1976).

Carome,E.F., Parks,P.E. and Mraz,S.J. 'Propagation of Acoustic Transients in Water', J.Acoust.Soc.Am.36, 946-952 (1964).

Christie,D.G. 'The Distribution of Pressure in the Sound Beams from Probes used with Ultrasonic Flaw Detectors', Materials Research 1, 86-97 (1962).

Coffey,J.M. and Wickham,G.R. (CEGB., Timpson Road, Manchester M23 9LL), 'An Improved Theory of Ultrasonic Shear-Wave Probes', Conf.on Evaluation and Calibration of Ultrasonic Transducers, London (May 1977).

CRC Handbook of Chemistry and Physics, edited by Weast,R.C. (CRC Press, Cleveland, Ohio, 1974).

Duck,F.A. (Institute of Cancer Research, Sutton, Surrey), Private Communication (1977), (to be published).

Duck,F.A. et.al. 'Digital Image Focussing in the Near Field of a Sampled Acoustic Aperture', Ultrasonics 15, 83-88 (1977).

Ernst,P.J. 'Ultrasonic Lenses and Transmission Plates', J.Sci. Instr. 22, 238-243 (1945).

Folds,D.L. 'Experimental Determination of Ultrasonic Wave Velocities in Plastics, Elastomers, and Syntactic Foam as a Function of Temperature', J.Acoust.Soc.Am. 52, 426-7 (1972).

Folds,D.L. 'Focusing Properties of Solid Ultrasonic Cylindrical Lenses', J.Acoust.Soc. Am. 53, 826-834 (1973).

Freedman,A. 'Farfield of a Pulsed Rectangular Acoustic Radiator', J.Acoust.Soc. Am. 49, 738-748 (1971).

Fukumoto ,A. and Watanabe, A. 'Liquid Materials and their Figures of Merit as Acoustooptical Detector', Jap.J.App.Phys.9, 662-665 (1970).

Greguss,P. 'Holography and Acoustics', in Acoustics and Vibration Progress, edited by Stephens, R.W.B.,and Leventhall,H.G.,Vol.2,pp.1-54 (Chapman and Hall, London, 1976).

a. Hanstead,P.D. 'Three-dimensional Imaging of Ultrasound: Direct Ultrasonic Visualisation of Defects', Nature, Sept.29, 273-274 (1972).

b. Hanstead,P.D. 'Computer-aided Optimisation of Schlieren Sensitivity', C.E.G.B. Report SSD/SW/M.409 (1972).

Hanstead,P.D. 'Direct Ultrasonic Visualisation: A New Method for Materials Inspection', Ph.D.Thesis, The City University, London (1973).

a. Hanstead,P.D. 'A New Ultrasonic Focusing System for Materials Inspection', J.Phys.D: Appl.Phys. 7, 226-245 (1974).

b. Hanstead,P.D. 'Direct Ultrasonic Visualisation: A New Inspection Method', Brit.J. Non-Destructive Testing, 16, 34-44 (1974).

Hanstead,P.D. 'The Sensitivity of Schlieren Systems for Viewing Ultrasound', Proc.8th World Conf. on Non-destructive Testing, Cannes (1976), (to be published).

Hanstead,P.D. (C.E.G.B., Portishead, Bristol) Private Communication (1977).

Hartmann,B. and Jarzynski,J. 'Ultrasonic Hysteresis Absorption in Polymers', J.Appl.Phys.43, 4304-4312 (1972).

Holder,D.W. and North,R.J. Schlieren Methods: Notes on Applied Science No.31, D.S.I.R., N.P.L. (H.M.S.O., London, 1963).

Jenkins,F.A. and White,H.E. Fundamentals of Optics (McGraw-Hill, London, 1957), pp.94-96.

Jones, H.W. 'Some Aspects of Ultrasonic Imaging at Frequencies of 1 to 100 MHz', Ultrason.Int.1973 Conf. Proc. 257-264 (IPC Science and Technology Press, London, 1975).

Kaye G.W.C. and Laby T.H. Tables of Physical and Chemical Constants (Longmans,London, 1972).

Kisslo,J., Von Ramm, O.T. and Thurstowe, F.L. 'A Phased Array Ultrasound System for Cardiac Imaging', in Ultrasonics in Medicine, edited by Kazner et.al., pp.67-74 (Excerpta Medica, Amsterdam, 1975).

Kozina,O.G. and Makarov,G.I. 'Transient Processes in the Acoustic Fields Generated by a Piston Membrane of Arbitrary Shape', Akust.Zh.7, 53-58 (1961). (English transl.: Soviet Phys.-Acoust. 7, 39-43 (1961)).

Krautkramer,J. and H. Ultrasonic Testing of Materials (George Allen & Unwin, London, 1969).

Longhurst,R.S. Geometrical and Physical Optics (Longmans,London,1967).

Marsh,D.M. 'Methods of Visualising Ultrasound', in Research Techniques In Non-Destructive Testing, Vol.2., edited by Sharpe,R.S., pp.317-367 (Adademic Press, London and New York, 1973).

Mason,P.W. and McSkimin, H.J. 'Mechanical Properties of Polymers at Ultrasonic Frequencies', Bell Syst.Tech.J. 31, 122-171 (1952).

Mayer,W.G. 'Energy Partition of Ultrasonic Waves at Flat Boundaries', Ultrasonics 3, 62-68 (1965).

McDicken,W.N., Bruff,K., and Paton,J.S. 'An Ultrasonic Instrument for Rapid B Scanning of the Heart', Ultrasonics 11, 269 (1974).

Nomoto,O. 'Theory of the Visualisation of Ultrasonic Waves,(1) Theory of the Schlieren Method for Visualising Ultrasonic Waves', J.Phys. Soc. Japan 9, 267-278 (1954).

Oschepkov.P.K., Rozenberg,L.D., Semennikov, Iu.B. 'An Electronic--Acoustical Transducer for the Visualisation of Sound Images', Soviet Phys.-Acoust. 1, 362 (1955).

Otani,T. 'Contributions à la Theorie du Sonar à Onde Pulsée', Ph.D.Thesis, The University of Provence, Aix-Marseille (1972).

Raman, C.V. and Nath,N.S.N. 'The Diffraction of Light by High Frequency Sound Waves: Part 1', Proc. Indian Acad.Sci.2, 406-412 (1935).

Raman,C.V. and Venkataraman,K.S. 'Determination of Adiabatic Piezo--optic Coefficient of Liquids', Proc.Roy.Soc.171, 137-147 (1939).

Rayleigh, J.W. Strutt,Lord, 'On Methods for Detecting Small Optical Retardations and on the Theory of the Foucault Test', Scientific Papers Vol.6, 455-470 (Cambridge University Press,1920).

Rayleigh, J.W. Strutt, Lord. Theory of Sound (Dover, New York, 1945), Vol.2, Chap.14.

Redwood,M. 'A Study of Waveforms in The Generation and Detection of Short Ultrasonic Pulses', Appl. Mat.Res.2, 76-84 (1963).

Riley,W.A. and Klein,W.R. 'Piezo-optic Coefficients of Liquids', J.Acoust.Soc.Am.42, 1258-1261 (1967).

Robinson,D.E., Lees,S. and Bess,L. 'Near Field Transient Radiation Patterns for Circular Pistons', IEEE Trans.Acoust., Speech and Signal Processing, ASSP-22, 395-403 (1974).

Schafer,H.J. 'Physical Optic Analysis of Image Quality in Schlieren Photography', J.Soc.Motion Picture Engineers 53, 524-544 (1949).

Smith,T.M. and Korpel,A. 'Measurement of Light-Sound Interaction Efficiencies in Solids', IEEE J.Quantum Electronics, QE-1, 283-284 (1965).

Smyth,C.N., Poynton,F.Y., and Sayers,J.F. 'The Ultrasound Image Camera', Proc. IEE, 110, 16-28 (1963).

Sokolov,S., USSR Patent No.49 (31.8.36). 'Improvements in and relating to the Detection of Faults in Solid, Liquid and Gaseous Bodies'. British Patent No. 477139 (1937).

Speak,G.S. and Walters,D.J. 'Optical Considerations and Limitations of the Schlieren Method', Ministry of Supply, Aeronautical Research Council Reports and Memoranda (H.M.S.O., London, 1954).

Stepanishen,P.R. 'Transient Radiation from Pistons in an Infinite Planar Baffle', J.Acoust.Soc.Am.49, 1629-1638 (1971).

Szilard, J. and Kidger,M. 'A New Ultrasonic Lens', Ultrasonics 14, 268-272 (1976).

Tupholme,G.E. 'Generation of Acoustic Pulses by Baffled Plane Pistons' Mathematika 16, 209-224 (1969).

Uchida,N. 'Elastooptic Coefficient of Liquids Determined by Ultrasonic Light Diffraction Method', Jap.J.App.Phys.7,1259-1266 (1968).

Uchida,N. and Niizeki,N. 'Acoustooptic Deflection Materials and Techniques', Proc.IEEE, 61, 1073-1092 (1973).

Weight,J.P. 'Instrumentation Associated with the Development of Wide Band Ultrasonic Techniques (Ultrasonic Spectroscopy)', M.Phil.Thesis, The City University, London (1975).

Weight,J.P. and Hayman,A.J. 'Observations of the Propagation of Very Short Ultrasonic Pulses and their Reflection by Small Targets', J.Acoust.Soc.Am.(to be published 1978).

Weinberg,F.J. Optics of Flames (Butterworths, London, 1963), pp.116-149.

Wells,P.N.T. Physical Principles of Ultrasonic Diagnosis (Academic Press, London and New York, 1969).

Whittingham,T.A. 'A Hand-held Electronically Switched Array for Rapid Ultrasonic Scanning', Ultrasonics 14,29-33 (1976).

Whittingham,T.A. and Evans J.A. 'Ultrasonic Visualisation of the Heart', Ultrason.Int.1975 Conf.Proc.182-189, (IPC Science and Technology Press, London, 1975).

Wyatt,R.C. 'A Simple Method for Displaying the True Acoustic Waveform of a Repetitive Ultrasonic Pulse', C.E.G.B. Report SSD/SW/M.443 (1972).

Wyatt,R.C. (C.E.G.B., Portishead, Bristol), Private Communication (1973).

Wyatt,R.C. 'A Compact Stroboscopic Spark Light Source with Short Flash Duration and Low Time Jitter', J.Phys.E: Sci.Instr. 7, 437-440 (1974).

Wyatt,R.C. 'Imaging Ultrasonic Beams in Solids', Brit.J.Non-Destructive Testing, 17, 133-140 (1975).

Wyatt,R.C. (address above), Private Communication (1977).

Zemanek,J. 'Beam Behaviour within the Nearfield of a Vibrating Piston', J.Acoust.Soc.Am. 49, 181-191 (1971).